AMERICAN MUSEUM NOVITATES

Number 4051, 55 pp. February 27, 2026

Phylogeny and divergence time estimation of relictual Asian scorpion family suggests Early Cretaceous connections between Burma Terrane and Eurasia, and corrects placement of Chinese taxon

LORENZO PRENDINI,[1] QIANG XUAN,[2] SHIYU DU,[3] CHENGBIN WANG,[4] VALENTIN L. EHRENTHAL,[5] AND STEPHANIE F. LORIA[6]

ABSTRACT

The ancient, relictual Asian scorpion family Pseudochactidae Gromov, 1998, has a disjunct distribution. Five genera and seven species of living pseudochactids are assigned to one epigean subfamily, Pseudochactinae Gromov, 1998, from Central Asia and southern China, and two hypogean subfamilies, Troglokhammouaninae Prendini et al., 2021, and Vietbocapinae Lourenço, 2012, from caves of the Khammouan-Phong Nha-Kẻ Bàng Karst in the northern Annamite (Trường Sơn) Mountains of Laos and Vietnam. The extinct subfamily Chaerilobuthinae Lourenço and Beigel, 2011, comprises one genus and 15 species, hypothesized to be endogean, from mid-Cretaceous Burmese amber. The discovery and uncertainty regarding the phylogenetic placement of *Qianxie solegladi* Tang, 2022, from South China, together with the discovery that the Cretaceous amber Chaerilobuthinae, from the Burma Terrane, is the sister group of the extant pseudochactid subfamily

[1] Arachnology Lab and Scorpion Systematics Research Group, Division of Invertebrate Zoology, American Museum of Natural History, New York.

[2] State Key Laboratory of Palaeobiology and Stratigraphy, Nanjing Institute of Geology and Palaeontology, and Center for Excellence in Life and Palaeoenvironment, Chinese Academy of Sciences, Nanjing, China; University of Chinese Academy of Sciences, Beijing, China.

[3] College of Life Sciences, Nanjing Normal University, Nanjing, China.

[4] Engineering Research Center for Forest and Grassland Disaster Prevention and Reduction, Mianyang Normal University, Mianyang, China.

[5] Department of Biology, School of Biological Sciences, University of Oklahoma, Norman, OK; Arachnology Lab and Scorpion Systematics Research Group, Division of Invertebrate Zoology, American Museum of Natural History, New York.

[6] Department of Biology, College of Math and Sciences, University of Central Oklahoma, Edmond, OK; Arachnology Lab and Scorpion Systematics Research Group, Division of Invertebrate Zoology, American Museum of Natural History, New York.

 ISSN 0003-0082

Vietbocapinae provided an opportunity to revisit the phylogeny and biogeography of Pseudochactidae, and their adaptation to subterranean habitats in Southeast Asia. In the present contribution, pseudochactid phylogeny is reanalyzed using three mitochondrial markers (12S rDNA, 16S rDNA, Cytochrome *c* Oxidase Subunit I), three nuclear markers (18S rDNA, 28S rDNA, Internal Transcribed Spacer) and 143 morphological characters, for all extant pseudochactid taxa and seven exemplar species of the extinct Chaerilobuthinae. Divergence time and ancestral range estimation are conducted and the evolution of troglomorphic characters investigated to reassess how this lineage of "living fossils" dispersed and diversified. Recent changes to the systematics of Pseudochactidae are confirmed. The four subfamilies, genera, and species were monophyletic with high support and the following scheme of relationships: (Pseudochactinae (Troglokhammouaninae (Chaerilobuthinae + Vietbocapinae))). Phylogenetic analyses, reinforced by a multivariate morphometric analysis and pairwise genetic distances, confirm the validity of the monotypic, epigean Chinese genus, *Qianxie* Tang, 2022, which formed a monophyletic group with the epigean Central Asian genus, *Pseudochactas* Gromov, 1998, rather than the hypogean Southeast Asian genus, *Troglokhammouanus* Lourenço, 2007. *Qianxie solegladi* is transferred to Pseudochactinae. A revised time tree of Pseudochactidae suggests that the Burmese Chaerilobuthinae diverged from the Indochinese subfamilies, Troglokhammouaninae and Vietbocapinae, in the Early Cretaceous (ca. 117 Ma), consistent with Early Devonian rifting of the Burma Terrane.

INTRODUCTION

The scorpion family Pseudochactidae Gromov, 1998, currently comprising four subfamilies, six genera, and 22 species, 15 known only from mid-Cretaceous Burmese amber (Prendini et al., 2021; Tang, 2022; Xuan et al., 2025), has a disjunct distribution in Central and Southeast Asia (table 1; fig. 1). Among the living pseudochactid taxa, one epigean genus, *Pseudochactas* Gromov, 1998, inhabits arid valleys near the Tajik Depression and north Pamir Mountains of Central Asia (fig. 1), another inhabits river valleys in southern China, and three hypogean genera are restricted to the Khammouan-Phong Nha-Kẻ Bàng Karst in the northern Annamite (Trường Sơn) Mountains of Southeast Asia (Prendini et al., 2021; Loria et al., 2022; Tang, 2022).

Pseudochactidae represent an ancient, relictual lineage that was once more widespread (Loria et al., 2022). These scorpions are considered "living fossils" due to their distinctive morphology, which includes a unique configuration of carapacial sutures and a unique pattern of pedipalp trichobothria, among other characters (Soleglad and Fet, 2003a; Fet et al., 2004; Prendini et al, 2006, 2021; Lourenço, 2007; Loria et al., 2022). The phylogenetic position of the family has been extensively debated. Three alternative hypotheses were initially proposed (Coddington et al., 2004; Prendini et al., 2006, 2021): (1) sister to all Recent (extant) scorpions; (2) sister to Buthidae C.L. Koch, 1837; or (3) sister to Chaerilidae Pocock, 1893. Fet (2000) suggested that the family might be closely related to Buthidae or Chaerilidae based on trichobothrial pattern whereas Lourenço (2000) placed it in superfamily Chaeriloidea Pocock, 1893, implying a sister-group relationship with Chaerilidae. Soleglad and Fet (2001) and Prendini et al. (2006) suggested a close relationship to Buthidae based on trichobothria and other characters, including the reproductive system. Morphological phylogenetic analyses (Soleglad and Fet, 2003a, 2003b) placed *Pseudochactas ovchinnikovi* Gromov, 1998, the only pseudochactid known at the time, sister to all Recent scorpions, supporting Gromov's (1998) original opinion. Phylogenomic analyses initially placed two of the Southeast Asian species of Pseudochactidae sister to an exemplar species of Chaerilidae (Sharma et al., 2015a, 2015b), apparently confirming the Chaeriloidea hypothesis of Lourenço (2000), but

TABLE 1. Subfamilies, genera, and species of the relictual Asian scorpion family Pseudochactidae Gromov, 1998, with known countries of occurrence, based on Prendini et al. (2021), Tang (2022), and Xuan et al. (2025).

Subfamily	Species	Distribution
†Chaerilobuthinae Lourenço and Beigel, 2011		
	†*Chaerilobuthus barbarae* (Lourenço and Velten, 2025)	Myanmar
	†*Chaerilobuthus brigittemuellerae* (Lourenço and Velten, 2020)	
	†*Chaerilobuthus birmanicus* Lourenço, 2015	
	†*Chaerilobuthus brandti* Lourenço, 2022	
	†*Chaerilobuthus bruckschi* Lourenço, 2015	
	†*Chaerilobuthus complexus* Lourenço and Beigel, 2011	
	†*Chaerilobuthus enigmaticus* Lourenço, 2015	
	†*Chaerilobuthus gigantosternum* Lourenço, 2016	
	†*Chaerilobuthus hansgeorgmuelleri* Lourenço, 2019	
	†*Chaerilobuthus knodelorum* Lourenço, 2018	
	†*Chaerilobuthus longiaculeus* Lourenço, 2013	
	†*Chaerilobuthus meggeri* Lourenço, 2021	
	†*Chaerilobuthus schmidti* (Lourenço and Velten, 2024)	
	†*Chaerilobuthus schwarzi* Lourenço, 2015	
	†*Chaerilobuthus serratus* Lourenço, 2016	
	†*Chaerilobuthus staxi* Lourenço, 2024	
Pseudochactinae Gromov, 1998		
	Pseudochactas mischi Soleglad et al., 2012	Afghanistan
	Pseudochactas ovchinnikovi Gromov, 1998	Tajikistan, Uzbekistan
	Qianxie solegladi Tang, 2022	China
Troglokhammouaninae Prendini et al., 2021		
	Troglokhammouanus steineri Lourenço, 2007	Laos
	= *Troglokhammouanus louisanneorum* Lourenço, 2017	
Vietbocapinae Lourenço, 2012		
	Aemngvantom lao (Lourenço, 2012)	Laos
	Aemngvantom thamnongpaseuam Prendini et al., 2021	
	Vietbocap canhi Lourenço and Pham, 2010	Vietnam
	= *Vietbocap thienduongensis* Lourenço and Pham, 2012	
	= *Vietbocap auriantiacus* Lourenco et al., 2018	
	= *Vietbocap quinquemilia* Lourenco et al., 2018	

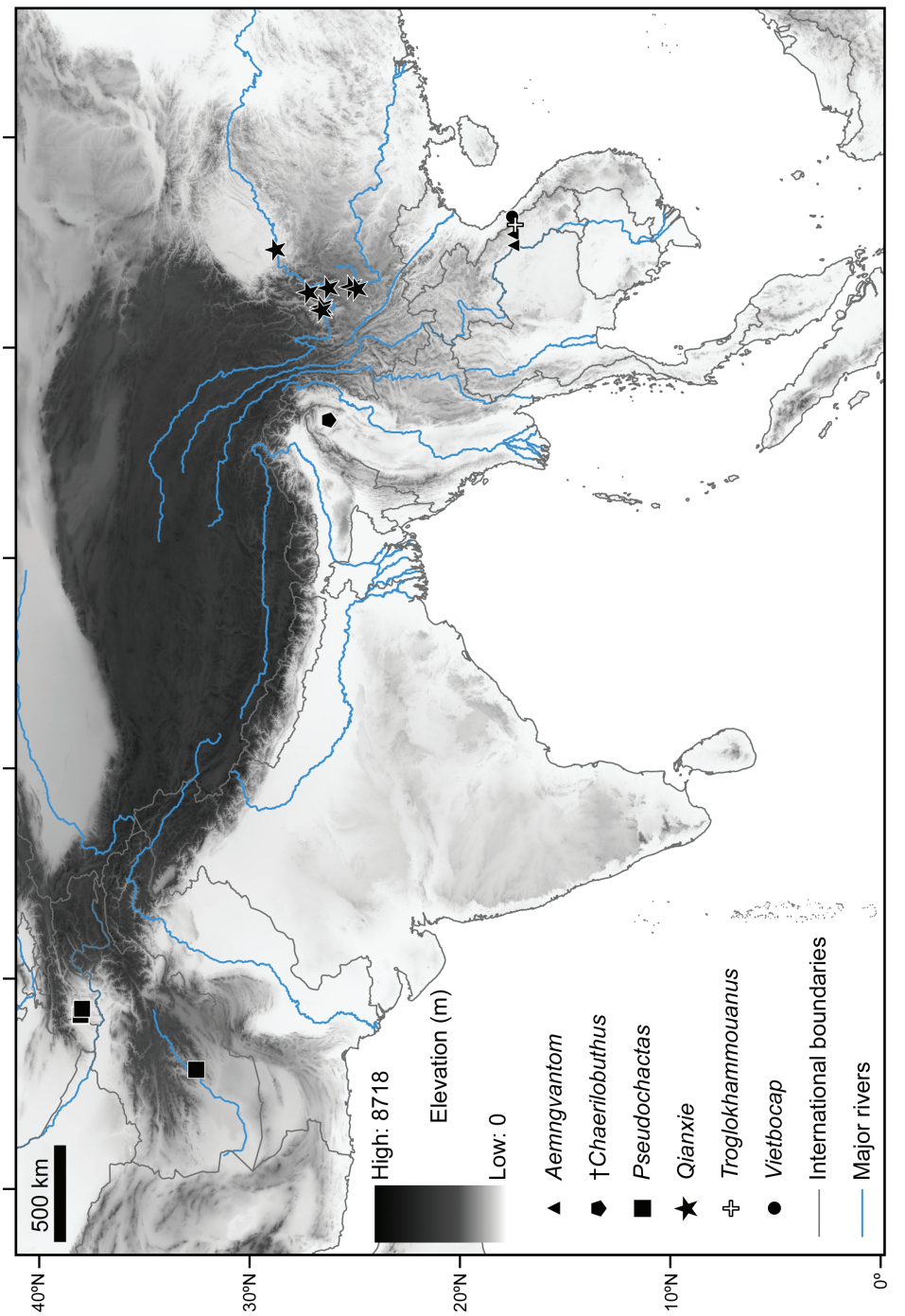

FIGURE 1. Distribution of subfamilies and genera of the relictual Asian scorpion family Pseudochactidae Gromov, 1998: Chaerilobuthinae Lourenço and Beigel, 2011: *Chaerilobuthus* Lourenço and Beigel, 2011; Pseudochactinae Gromov, 1998: *Pseudochactas* Gromov, 1998, *Qianxie* Tang, 2022; Troglokhammouaninae Prendini et al., 2021: *Troglokhammouanus* Lourenço, 2007; Vietbocapinae Lourenço, 2007: *Aemngvantom* Prendini et al., 2021, *Vietbocap* Lourenço and Pham, 2010.

subsequent analyses placed the family sister to a clade comprising Buthoidea and Chaeriloidea (Du et al., 2024).

Prendini et al. (2021) presented the first integrative systematic revision of Pseudochactidae. The subfamilies, genera and species were revised following a phylogenetic analysis of 140 morphological characters and 8608 nucleotide base pairs (bp) of concatenated DNA sequence from two nuclear and three mitochondrial gene loci for all species known at the time, and a multivariate statistical analysis of 22 ratios and 8 counts recorded from 60 specimens. Three subfamilies, four genera and six species were recognized in the family following the synonymy of four species and the description of a new subfamily, genus and species (Lourenço and Pham, 2010, 2012; Lourenço, 2012, 2017; Lourenço et al., 2018; Prendini et al., 2021): Pseudochactinae Gromov, 1998, accommodating two species of *Pseudochactas*; Vietbocapinae Lourenço, 2012, accommodating two species of *Aemngvantom* Prendini et al., 2021, and the monotypic *Vietbocap* Lourenço and Pham, 2010; and Troglokhammouaninae Prendini et al., 2021, accommodating the monotypic *Troglokhammouanus* Lourenço, 2007. The following scheme of phylogenetic relationships was recovered: (Pseudochactinae (Troglokhammouaninae + Vietbocapinae)).

Subsequently, Tang (2022) described the first pseudochactid from China, and placed it in a new monotypic genus, *Qianxie* Tang, 2022. Tang (2022) suggested *Qianxie* is closely related to *Troglokhammouanus* and assigned it to Troglokhammouaninae, a move considered plausible by Loria et al. (2022).

In a recent morphological phylogenetic analysis, based in part on an extensive new collection of Burmese amber fossils, Xuan et al. (2025) demonstrated that the extinct family Chaerilobuthidae Lourenço and Beigel, 2011, comprising one genus and 16 species (after synonymizing two monotypic genera), forms a monophyletic group with the extant pseudochactid subfamily Vietbocapinae, justifying its transfer to Pseudochactidae (as Chaerilobuthinae) and indicating that the minimum age of Pseudochactidae is more than 99 Ma. The Bayesian analysis of Xuan et al. (2025) placed *Qianxie* sister to *Troglokhammouanus*, supporting Tang's (2022) assignment to Troglokhammouaninae. However, Troglokhammouaninae was rendered paraphyletic by the placement of *Qianxie* sister to all other Pseudochactidae, except *Troglokhammouanus*, in the maximum likelihood analysis of Xuan et al. (2025). The multivariate morphometric analysis presented by Xuan et al. (2025) suggested that *Qianxie* is more closely related to *Pseudochactas* than to *Troglokhammouanus*.

The two Central Asian species of *Pseudochactas* Gromov, 1998, are lapidicolous (Prendini, 2001) with an affinity for humid microhabitats (hygrophily), occurring under stones or in mud cracks along riverbanks in semiarid mountainous areas (Prendini et al., 2006; Soleglad et al., 2012). The Chinese species, *Quanxie solegladi* Tang, 2022, also appears to be lapidicolous and was collected in riparian habitats, again suggesting an ecological requirement for humidity (Tang, 2022). The three Southeast Asian genera, *Aemngvantom*, *Troglokhammouanus*, and *Vietbocap*, occur below ground in limestone caves, and were collected along walls, under stones or in cracks in rock or mud, and in the case of *Troglokhammouanus*, close to a river (Prendini et al., 2021). Although the three Southeast Asian genera are exclusively subterranean, records of their distance from the surface environment vary. *Troglokhammouanus steineri* Lourenço, 2007 was collected from the twilight zone of the cave to ca. 3 km from the downstream entrance, whereas *Vietbocap canhi* Lourenço and Pham, 2010, and the two species of *Aemngvantom* were recorded from 200 m to 5 km from the cave entrance. This variation in ecology among pseudochactid genera is reflected in their morphology. *Pseudochactas*, *Qianxie*, and *Troglokhammouanus* exhibit well-developed ocelli and pigmentation, and no noticeable attenuation of the appendages, whereas *Aemngvantom* and *Vietbocap* are markedly troglomorphic, lacking ocelli and pigmentation, and exhibiting marked attenuation of the appendages, among other troglomorphic charac-

ters (Prendini et al., 2021). The difference in ecology and morphology among pseudochactid genera led Prendini et al. (2021) and Loria et al. (2022) to classify *Pseudochactas* and *Qianxie* as epigean; *Troglokhammouanus* as a hypogean troglophile; and *Aemngvantom* and *Vietbocap* as hypogean troglobites.

Although the habitat of the 15 extinct species of subfamily Chaerilobuthinae is unknown, these scorpions exhibit several apparent troglomorphies (e.g., absence of the median ocelli and attenuation of the legs and pedipalps), consistent with a subterranean habitus (Prendini, 2001; Prendini et al., 2021; Xuan et al., 2025), which must be reconciled with the presence of pollen and sporangia preserved together with the scorpions in the amber. Xuan et al. (2025: 50) hypothesized that *Chaerilobuthus* Lourenço and Beigel, 2011, "were endogean/humicolous like the extant species of *Troglotayosicus* Lourenço, 1981 which also lack median ocelli but possess lateral ocelli and do not exhibit other pronounced troglomorphies."

Considering their disjunct distribution and variable levels of troglomorphic adaptation, Pseudochactidae represent a model system for historical biogeography and comparative analysis of the origins and evolution of cave organisms (Loria et al., 2022). The presence of relictual taxa in caves or subterranean habitats is often explained by the "Climate Relict" model, according to which caves acted as "museums" or refugia when environmental stresses resulted in extinction of their epigean relatives (Barr, 1968; Howarth, 1973; Romero and Green, 2005; Wessel et al., 2007; Niemiller et al., 2008; Assmann et al., 2010; Juan et al., 2010; Bryson et al., 2014; Loria et al., 2022).

Several biogeographical hypotheses have been suggested to account for the distribution of Pseudochactidae. Soleglad and Fet (2003a) proposed that the family originated on Pangaea in the Permian/Triassic. Fet et al. (2004) hypothesized that the ancestor of Pseudochactidae inhabited littoral forests on islands in the Tethys Sea, near the modern-day Tajik Depression, during the Cretaceous and that these forested islands were elevated by orogeny when the Indian subcontinent collided with Eurasia in the Tertiary, shielding these populations from Eocene aridification which followed the collision. Prendini et al. (2006) suggested that a more recent divergence might be plausible if Pseudochactidae were the sister group of Buthidae, but, after *T. steineri* was discovered in Southeast Asia, a Pangaean origin for the family in the Permian/Triassic had to be reconsidered because the old Asia core, dating to the Paleozoic, represented the only land connection between Central Asia and Laos (Lourenço, 2007). A dated phylogenomic analysis of scorpions, calibrated using fossil scorpions and other arachnids under an autocorrelated lognormal model, proposed an even earlier divergence between Pseudochactidae and Chaerilidae, ca. 329 Ma in the Carboniferous (Sharma et al., 2015a), whereas a second analysis, applying an uncorrelated gamma rates model, placed this divergence much later, at ca. 198 Ma in the Jurassic (Sharma et al., 2018). Although Sharma et al. (2018) preferred the results of the autocorrelated lognormal model because of its better performance, no biogeographical hypotheses were proposed to explain either of these divergence dates.

Loria et al. (2022) presented the first quantitative biogeographical analysis of Pseudochactidae, based on the dataset of Prendini et al. (2021), in which divergence time and ancestral range estimation analyses were conducted and the evolution of troglomorphic characters investigated. Consistent with the "Out of Eurasia" hypothesis, Loria et al. (2022) proposed that Pseudochactidae originated in Eurasia, probably near the Tajik block, during the Carboniferous. After the collision of the Cimmerian continent and Indochina with Eurasia during the Late Jurassic, pseudochactids dispersed across Southeast Asia, colonizing caves between the Late Cretaceous and the Miocene. The onset of aridification in Southeast Asia during the Late Miocene resulted in the extinction of epigean pseudochactids, but hypogean members of the family survived in caves in the limestone massifs of the Annamite Mountains, consistent with the "Climate Relict" hypothesis.

The analyses of Loria et al. (2022) preceded discovery of the Chinese pseudochactid, *Q. solegladi*. However, in a note added in proof, Loria et al. (2022: 17) remarked that "the discovery of this new species supports the biogeographical hypotheses presented herein as the area in which it occurs was formerly part of the South China block, suggesting that the ancestor of the Southeast Asian pseudochactid subfamilies (Troglokhammouaninae + Vietbocapinae) dispersed from the Tajik–north Pamir region of proto-Eurasia into Indochina via the north and south China blocks."

The discovery of *Q. solegladi*, from South China, and uncertainty regarding its phylogenetic placement (Tang, 2022; Loria et al., 2022; Xuan et al., 2025), together with the discovery that the Cretaceous amber Chaerilobuthinae, from the Burma Terrane, is the sister group of the extant pseudochactid subfamily Vietbocapinae (Xuan et al., 2025), provided an opportunity to revisit the phylogeny and biogeography of Pseudochactidae, and their adaptation to subterranean habitats in Southeast Asia. In the present contribution, pseudochactid phylogeny is reanalyzed using three mitochondrial markers (12S rDNA, 16S rDNA, Cytochrome Oxidase *c* Subunit I), three nuclear markers (18S rDNA, 28S rDNA, Internal Transcribed Spacer) and 143 morphological characters, for all living pseudochactid taxa and seven exemplar species of Chaerilobuthinae. Divergence time and ancestral range estimation analyses are conducted and the evolution of troglomorphic characters investigated to reassess how this unique, relictual scorpion lineage dispersed and diversified.

MATERIALS AND METHODS

Material Examined. Material examined for the present study is deposited in the following collections (appendix 1): Alexander V. Gromov Private Collection (AGPC), Almaty, Kazakhstan; American Museum of Natural History (AMNH), New York, including the Ambrose Monell Cryocollection (AMCC); Institute of Ecology and Biological Resources (IEBR), Vietnamese Academy of Sciences, Hanoi; Museum National d'Histoire Naturelle (MNHN), Paris; Nanjing Institute of Geology and Palaeontology (NIGP), Chinese Academy of Sciences, Nanjing; Phong Nha-Kẻ Bàng National Park (PNKB), Bố Trạch, Vietnam.

Microscopy, Terminology, and Primary Homology. Specimens were examined, and measurements and other meristic data recorded with Nikon SMZ1500 and Leica MZ16 stereo dissecting microscopes. Sexual maturity of males and females was assessed based on total length, coloration, sclerotization, granulation, and carination of the tegument (including the presence of a pale, raised, triangular surface on the posteroventral margin of mesosomal sternite V, more pronounced in the adult male). Although not always significantly smaller in total length, the tegument of immature stages is typically paler and less sclerotized, with less surface granulation and less-pronounced carinae. A pale, raised, triangular surface is absent from the posteroventral margin of mesosomal sternite V in immature stages. Morphological terminology and primary homology assessment follows Prendini et al. (2006, 2021) and Xuan et al. (2025).

Taxon Sampling. The dataset comprised 35 terminals, 33 representing the ingroup (all extant pseudochactid taxa and seven extinct pseudochactid taxa) and two representing the outgroup (*Chaerilus sejnai* Kovařík, 2005, representing Chaerilidae, and *Buthus atlantis* Pocock, 1889, representing Buthidae). The tree was rooted on *B. atlantis*. Ingroup terminals were represented by both morphological and molecular data except for *Pseudochactas mischi* Soleglad et al., 2012, and the seven terminals of Chaerilobuthinae, which lack molecular data. *Pseudochactas ovchinnikovi* was represented by three terminals from Dikhana Canyon, near the type locality in the Babatag Mountains, Uzbekistan; *Qianxie solegladi* by a single terminal from Ningnan County in Sichuan Province, China; *Troglokhammouanus steineri* by five terminals from the type locality, Tham Xe

TABLE 2. Distribution of morphological characters used for phylogenetic analysis of the relictual Asian scorpion family Pseudochactidae Gromov, 1998. First two taxa are outgroups. Numbers following terminal taxon names correspond to samples from which DNA was extracted and sequenced (appendix 1, table 3). Character states scored 0–5, inapplicable (-) or unknown (?). Character descriptions in appendix 6.

***Buthus atlantis* 3489**
0010002000 0000020000 ---0000000 0000021110 1010011000 0010001110 1100000000
1000000010 0101010110 0000000001 -200--0010 1100000200 0000000011 0000101000 100

***Chaerilus sejnai* 3685**
1130111101 0001101010 ---1000111 0001000001 1101201201 1101100000 1101?11001
0221200101 000002010- 1323322100 01110-0101 0011-00-51 2000211011 11102-1000 001

†*Chaerilobuthus bruckschi*
??????0111 1001001110 ---1101110 2111021010 0111100011 0010011001 0?10?01110
0001011110 2010300011 ?3?????0?0 ??12111??? ??001??04? 200??10000 0?11010??? ?01

†*Chaerilobuthus complexus*
??????0111 1001001110 ---1101110 2111021010 0111100011 0010011001 0?10?01110
0001011110 2010300011 ?33????020 1012111??? ??001??04? 200??10000 0?11010??? ?01

†*Chaerilobuthus enigmaticus*
??????0111 1001001110 ---1101110 2111011010 0111100011 0010011001 0?10?01?10
0001011110 2010300011 ???????020 1012111??? ??001??04? 200??10000 0?11010??? ?01

†*Chaerilobuthus gigantosternum*
????????111 1001001110 ---1101110 2111031010 0111100011 0010011001 0?10?01?10
0001011110 2010300011 ???????020 1012111??? ??001??04? 200??10000 ??11010??? ?01

†*Chaerilobuthus hansgeorgmuelleri*
??????0??1 1001001110 ---1101110 2111011010 0111100011 0010011001 0010?01110
0001011110 2010300011 ???????020 1012111??? ??001??04? ??0??10000 0?110?00?? ???

†*Chaerilobuthus knodelorum*
??????0111 1001001110 ---1101110 2111021010 ??????00?11 0010011001 0010?01110
0001011110 2010300011 ?33????020 1012111??? ??001??04? 200??10000 0?110??1?? ?01

†*Chaerilobuthus serratus*
??????0111 1001001110 ---1101110 2111021010 0111100011 0010011001 0010?01110
0001011110 2010300011 ?33????020 1012111??? ??001??04? 200??10000 0?110?01?? ?01

Pseudochactas mischi
0002100111 0001201011 ?011100110 1111011010 0111110111 0020011001 0010111110
0001000010 2010101011 ?334333000 1001101??? ??001?222? ??1??10021 1?10010?0 ?11

***Pseudochactas ovchinnikovi* 2303A–2303C**
0131100111 0001211011 0001100110 1111011010 0111110111 0020011001 0010111110
0001000010 2010101011 1333333000 1001101100 0000102221 1110210011 0110010000 011

***Qianxie solegladi* 20856**
0120100111 2001211011 1011100110 0111011010 0111110111 0010011001 0010111110
0111010010 2010101011 1333322020 0102101??? ??00102222 ??00210021 0110010100 ?11

***Troglokhammouanus steineri* 11271–11275**
1122100111 2101201011 1011100110 0000011010 0111110111 0010011001 0010111110
0111110010 2010102011 1323222020 0102101100 0000101311 2000211022 2110011100 011

***Aemngvantom lao* 11349 11350 15570 15591**
0002100111 2201201111 200111-110 0000021010 0111110111 0010011001 0010101110
0001010010 1020301011 0111111010 1112111100 0000112311 2001110021 2010011101 001

***Aemngvantom thamnongpaseuam* 11351**
0002100111 2201201111 200111-110 0010021010 0111110111 0010011001 0010?01110
0001010010 1020301011 ?111111010 1112111??? ??001?231? ??1??10121 0?11010?1? ?01

***Vietbocap canhi* 11270 16750 16751**
0002100110 2212200101 212111-110 1110131010 0111110111 0010011001 0010001110
0001010010 2010201011 0222222010 1112111100 0000102131 2010?10111 0110010111 001

***Vietbocap canhi* 11348 16533–16537**
0002100110 2212200111 212111-110 1110131010 0111110111 0010011001 0010001110
0001010010 2010201011 0333333010 1112111100 0000102131 2010?10111 0110010111 001

Bang Fai; *Aemngvantom lao* (Lourenço, 2007) by four terminals from the type locality, Tham Nam Lot; *Aemngvantom thamnongpaseuam* Prendini et al., 2021, by the holotype; and *Vietbocap canhi* by nine terminals from two caves: three from the type locality, Tiên Sơn, and six from Thiên Đường. *Pseudochactas mischi* was represented by the subadult female holotype from Uruzugan Province, Afghanistan, scored from the original description. Chaerilobuthinae was represented by terminals representing seven species of *Chaerilobuthus* Lourenço and Beigel, 2011, scored from Xuan et al. (2025): *Chaerilobuthus bruckschi* Lourenço, 2015; *Chaerilobuthus complexus* Lourenço and Beigel, 2011; *Chaerilobuthus enigmaticus* Lourenço, 2015; *Chaerilobuthus gigantosternum* Lourenço, 2016; *Chaerilobuthus hansgeorgmuelleri* Lourenço, 2019; *Chaerilobuthus knodelorum* Lourenço, 2018; and *Chaerilobuthus serratus* Lourenço, 2016.

Morphometrics and Multivariate Statistical Analysis. Thirty-seven measurements (mm) and eight counts were recorded from a female specimen of *Q. solegladi*, following Prendini et al. (2006, 2021), to which corresponding data for the holotype female were added from the original description (Tang, 2022; appendix 2). Twenty-two morphometric ratios, calculated from the measurements, were then added, along with the eight counts (appendix 3) for both specimens of *Q. solegladi*, to corresponding data for another 40 specimens, representing all genera and species of Pseudochactidae, from Prendini et al. (2021) (appendices 4, 5). Nonmetric multidimensional scaling (NMDS) was conducted on the data, i.e., 22 ratios and eight counts for 42 female specimens (no male specimens of *Q. solegladi* have thus far been collected), using the programs vegan (Oksanen et al., 2020) and ggplot2 (Wickham, 2016) in R ver. 4.3.1 (R Core Team, 2023).

Morphological Dataset. The morphological character matrix developed by Prendini et al. (2021) and modified by Xuan et al. (2025), incorporating characters from previously published matrices (Lamoral, 1980; Stockwell, 1989; Prendini, 2000, 2004; Soleglad and Sissom, 2001; Soleglad and Fet, 2001, 2003a), augmented by observations in Prendini et al. (2006), was updated to comprise 143 characters (table 2, appendix 6) scored for the 33 terminals. Most characters pertain to the adult stage: coloration and infuscation, 4 (3%); chelicerae, 5 (3.5%); carapace, 26 (18%); pedipalps, 62 (43%); coxosternum, 5 (3.5%); legs, 5 (3.5%); genital operculum, 1 (1%); male and female reproductive anatomy, 4 (3%); pectines, 10 (7%); tergites, 1 (1%); sternites, 3 (2%); metasoma, 11 (8%); telson, 6 (4%). The breakdown of morphological characters by character system is as follows: trichobothria, 39 (27%); surface macrosculpture, 34 (24%); shape and size, 14 (10%); pectines, 10 (7%); ocelli, 8 (6%); surface topography, 8 (6%); pedipalp finger dentition, 6 (4%); genitalia, 5 (3.5%); leg setation and spination, 5 (3.5%); cheliceral dentition, 4 (3%); color patterns, 4 (3%); serrula, 2 (1%), sutures, 2 (1%); respiratory spiracles (stigmata), 1 (1%); venom glands, 1 (1%). Forty-two (29%) multistate characters were treated as unordered/nonadditive (Fitch, 1971) to avoid a priori character state transformations, and 54 (38%) characters were uninformative. The matrix was prepared using WinClada ver. 1.00.08 (Nixon, 2002) and deposited in Morphobank (https://www.morphobank.org/permalink/?P5979).

Molecular Dataset. The molecular dataset presented by Loria et al. (2022), comprising three mitochondrial loci, 12S rDNA (hereafter, 12S), 16S rDNA (16S), and Cytochrome *c* Oxidase Subunit I (COI), and three nuclear loci, 28S rDNA (28S), 18S rDNA and Internal Transcribed Spacer (18S-ITS2), was updated to include data for *Q. solegladi*. Lab methods of DNA extraction, PCR and sequencing follow Loria et al. (2022). Primers are listed in appendix 7. Sequences are deposited in Genbank (https://www.ncbi.nlm.nih.gov/genbank; table 3). The 18S-ITS2 locus was partially sequenced for one terminal of *P. ovchinnikovi* and *Q. solegladi* but completely sequenced for one terminal each of *T. steineri*, *A. lao*, and *A. thamnongpaseuam*, and two terminals of *V. canhi*. The 28S locus was partially sequenced for three terminals of *P. ovchinnikovi* and *Q. solegladi*.

TABLE 3. Tissue samples and GenBank accession codes for DNA sequences used for phylogenetic analysis of the relictual Asian scorpion family Pseudochactidae Gromov, 1998. Sequences of the 18S rDNA (18S), Internal Transcribed Spacer (ITS2), 28S rDNA (28S), 12S rDNA (12S), 16S rDNA (16S), and Cytochrome *c* Oxidase Subunit I (COI) loci. Tissue samples deposited in the Ambrose Monell Collection for Molecular and Microbial Research (AMCC) at the American Museum of Natural History, New York. Asterisks denote partial sequences. Specimen collection data in appendix 1.

Species	AMCC	Country	18S/18S-ITS2	28S	12S	16S	COI
Buthidae C.L. Koch, 1837							
Buthus atlantis Pocock, 1889	LP 3489	Morocco	MZ041717	MZ041765	MZ041686	MZ041735	MZ032877
Chaerilidae Pocock, 1893							
Chaerilus sejnai Kovařík, 2005	LP 3685	Malaysia	MZ041718	MZ041766	MZ041687	MZ041736	MZ032878
Pseudochactidae Gromov, 1998							
Pseudochactas ovchinnikovi Gromov, 1998	LP 2303A	Uzbekistan	MZ041759*	MZ041767*	MZ041688	MZ041737	MZ032879
	LP 2303B		MZ041719	MZ041768*	MZ041689	MZ041738	MZ032880
	LP 2303C		MZ041720	MZ041769*	MZ041690	MZ041739	MZ032881
Qianxie solegladi Tang, 2022	LP 20856	China	PV915734*	PV915735	PV915732	PV915733	PV915784
Troglokhammouanus steineri Lourenço, 2007	LP 11271	Laos	MZ041760	MZ041770	MZ041691	MZ041740	MZ032882
	LP 11272		MZ041721	MZ041771	MZ041692	MZ041741	MZ032883
	LP 11273		MZ041722	MZ041772	MZ041693	MZ041742	MZ032884
	LP 11274		MZ041723	MZ041773	MZ041694	MZ041743	MZ032885
	LP 11275		MZ041724	MZ041774	MZ041695	MZ041744	MZ032886
Aemngvantom lao (Lourenço, 2012)	LP 11349		MZ041761	MZ041775	MZ041696	MZ041745	MZ032887
	LP 11350		MZ041725	MZ041776	MZ041697	MZ041746	MZ032888
	LP 15570		MZ041726	MZ041777	MZ041698	MZ041747	MZ032889
	LP 15591		MZ041727	MZ041778	MZ041699	MZ041748	MZ032890
Aemngvantom thamnongpaseuam Prendini et al., 2021	LP 11351		MZ041762	MZ041779	MZ041700	MZ041749	MZ032891
Vietbocap canhi Lourenço and Pham, 2010	LP 11270	Vietnam	MZ041763	MZ041780	MZ041701	MZ041750	MZ032892
	LP 16750		MZ041733	MZ041787	MZ041708	MZ041757	MZ032899
	LP 16751		MZ041734	MZ041788	MZ041709	MZ041758	MZ032900
	LP 11348		MZ041728	MZ041781	MZ041702	MZ041751	MZ032893
	LP 16533		MZ041764	MZ041782	MZ041703	MZ041752	MZ032894
	LP 16534		MZ041729	MZ041783	MZ041704	MZ041753	MZ032895
	LP 16535		MZ041730	MZ041784	MZ041705	MZ041754	MZ032896
	LP 16536		MZ041731	MZ041785	MZ041706	MZ041755	MZ032897
	LP 16537		MZ041732	MZ041786	MZ041707	MZ041756	MZ032898

Sequence length was calculated using the gc_calculator.py script in Biopython (Cock et al., 2009). Sequences of the COI locus were length invariant (1078 bp). The number of haplotypes was calculated using DNACollapser (https://users-birc.au.dk/palle/php/fabox/dnacollapser.php) in FaBox (Villesen, 2007). The 18S-ITS2, 16S, and COI loci each comprised 13 haplotypes, 12S comprised 11, and 28S nine (table 4).

Sequence Alignment and Genetic Distances. Sequences were aligned with MAFFT ver. 7.471 (Katoh et al., 2002; Katoh and Standley, 2013) on the CIPRES Science Gateway (https://www.phylo.org; Miller et al., 2015). The Q-INS-i alignment strategy was used for the 12S, 16S, 28S, and 18S-ITS2 loci and the G-INS-i alignment strategy for the COI locus. The aligned sequence lengths were as follows: 12S (370 bp), 16S (500 bp), COI (1078 bp), 28S (2251 bp), 18S-ITS2 (4505 bp). Aligned sequences were checked in Mesquite ver. 4.0 (Maddison and Maddison, 2025) and concatenated in BBedit ver. 15.1.1. The combined length of the concatenated alignments was 8704 bp.

MEGA ver. 11.0.13 (Tamura et al., 2004, 2013, 2021; Kumar et al., 2018) was used to calculate mean nucleotide composition as well as number of parsimony-informative (PI) sites and variable positions (VP) for each locus and the concatenated molecular dataset. Mean GC content was higher (table 4) for the nuclear 28S (59%) and 18S-ITS2 (51%) loci than for the mitochondrial COI (37%), 12S (28%), and 16S (28%) loci, whereas the proportions of VP and PI sites were higher for the mitochondrial 12S (60% and 42%, respectively), 16S (50% and 35%), and COI (37% and 30%) loci than for the nuclear 18S-ITS2 (25% and 11%) and 28S (18% and 7%) loci. The third codon position of the COI locus possessed the highest proportion of VP (27%) and PI sites (25%), followed by the first (7% and 5%) and second (2% and 1%) codon positions.

The ingroup dataset was aligned separately using the methods described above and MEGA used to calculate the mean uncorrected pairwise genetic distances (*p*-distances) of all loci within and between the species of Pseudochactidae (Kumar et al., 2018; Stecher et al., 2020; Tamura et al., 2021).

Phylogenetic Analyses. The morphological and molecular datasets were analyzed separately and simultaneously. Parsimony analyses were performed in TNT (Goloboff, 1993; Goloboff et al., 2003, 2008; Goloboff and Morales, 2023) with equal weighting and implied weighting with five values of the concavity constant (k = 1, 3, 10, 60, 100). Uninformative characters were deactivated in all analyses and gaps treated as missing data. Tree search was conducted using a script combining mixed sectorial searches, tree drift and tree fusion (Dimitrov et al., 2012, 2013; Santibáñez-López et al., 2014). Tree statistics (length, fit, retention indices, adjusted homoplasy, and consistency indices) were also calculated.

Maximum likelihood (ML) analyses were performed using RAxML-HPC ver. 8 (Stamatakis, 2006, 2014) on the CIPRES cluster. The morphological dataset and five molecular loci were treated as separate partitions. A GTRGAMMA or GTCAT model was applied to each partition in the molecular analyses. An MK model (Lewis, 2001) was applied to the morphological partition and a Multistate GAMMA or Multistate CAT model to the molecular partitions, in the simultaneous analyses. In two simultaneous analyses, an ascertainment bias, using Lewis correction, was applied to the morphological partition. A rapid bootstrap analysis (-f a) (1000 bootstrap iterations) was used to search for the tree with the best score.

Bayesian inference (BI) was performed using MrBayes ver. 3.2.7a (Ronquist and Huelsenbeck, 2003) on the CIPRES cluster. The molecular dataset was partitioned as for the ML analyses. A Lewis MK model was applied to the morphological partition. Twenty-four nucleotide substitution models were tested for each molecular locus using jModelTest2 ver. 2.1.6 (Guindon and Gascuel, 2003; Darriba et al., 2012) on the CIPRES cluster and the best model chosen using the

TABLE 4. Statistics for nuclear loci, 18S rDNA (18S), Internal Transcribed Spacer (ITS2), and 28S rDNA, and mitochondrial loci, 12S rDNA, 16S rDNA and Cytochrome *c* Oxidase subunit I (COI), in phylogenetic analysis of the relictual Asian scorpion family Pseudochactidae Gromov, 1998: number of haplotypes; length (nucleotide base-pairs) of unaligned and aligned sequences; average percent GC content; number (and percent) of variable positions (VP); number (and percent) of parsimony-informative sites (PI); and model selected for Bayesian inference using the Akaike Information Criterion (AIC).

Locus	Haplotypes	Unaligned	Aligned	GC	VP	PI	AIC
18S-ITS2	13	1760–3926	4505	51	1111 (25)	500 (11)	GTR + G
28S	9	1329–2193	2251	59	415 (18)	167 (7)	GTR + I + G
12S	11	337–344	370	28	222 (60)	156 (42)	GTR + G
16S	13	475–483	500	28	250 (50)	175 (35)	GTR + I + G
COI	13	1078	1078	37	396 (37)	323 (30)	GTR + I + G
COI 1st Codon	–	–	359	–	79 (7)	50 (5)	–
COI 2nd Codon	–	–	359	–	22 (2)	8 (1)	–
COI 3rd Codon	–	–	360	–	295 (27)	265 (25)	–

Akaike Information Criterion (AIC). The following parameters were implemented: mcmc; nchains = 4; print frequency = 1000; sample frequency = 1000; diagnosing frequency = 1000; burnin = 0.25; savebrlens = yes. Analyses ran for 25 million generations to ensure that the standard deviation of split frequencies of the two chains was below 0.01.

Divergence Time Estimation. Divergence time estimation was performed using BEAST ver. 2.7.7 (Bouckaert et al., 2019), with similar parameters to Loria et al. (2022). The molecular dataset was trimmed to one terminal per species and sequences aligned in MAFFT as described above; the morphological dataset was also trimmed to match. xml files were prepared in Beauti (Drummond et al., 2012). The morphological dataset was imported without recording variable characters only and subsequently divided into five partitions, and the molecular dataset partitioned by the five loci, resulting in 10 partitions. Whereas the tree model was linked and site models unlinked across partitions, clock models were unlinked across molecular partitions but linked across morphological partitions. The tree was rooted on *B. atlantis*, Pseudochactidae was constrained to be monophyletic and Chaerilidae to be its sister group. A Lewis MK model was applied to the morphological partitions with the gamma rate category count set to four and the gamma shape parameter linked across the morphological partitions by manually editing the xml files. A simple HKY model was applied to the molecular partitions with the gamma category count set to four and base frequencies set to estimated. A Fossilized Birth–Death model was implemented for the tree prior, and origin and diversification rates estimated by applying a uniform prior, with the initial value for the origin set to 349.4779 and the initial value for the diversification rate set to 0.01. A relaxed lognormal molecular clock was set for the clock model of each partition. Clock priors were set to the default uniform distribution for the morphological partition and a uniform distribution applied to all loci with the following parameters: ucld.min = 0.002, ucld.max = 0.5 for 12S, 16S, COI, and ucld.min = 0.0001, ucld.max = 0.01 for 28S and 18S-ITS2 (Bryson et al., 2013; Loria and Prendini, 2020; Loria et al., 2022). A normal distribution was applied to the clade comprising Chaerilidae and Pseudochactidae with $\mu = 329.3195$ Ma and $\sigma = 5$ Ma, following Loria et al. (2022). This calibration was based on Sharma et al. (2018), who recovered 329 Ma as the divergence date between Pseudochactidae and Chaerilidae based on an autocorrelated lognormal

model. The tip for each chaerilobuthine fossil was set to 98.79 Ma. A most recent common ancestor (MRCA) prior, including Chaerilobuthinae and Vietbocapinae, was configured as monophyletic. Additionally, a Sampled Ancestors MRCA prior with a uniform distribution (lower value = 98.17 Ma; upper value = 99.41) was specified for each chaerilobuthine fossil using the *Tipsonly* option. Two Markov Chain Monte Carlo (MCMC) runs were performed using different starting seed values, to test for convergence. Each analysis ran for 500 million generations on the CIPRES cluster with tracelog = 10,000 and treelog = 10,000. Convergence was assessed using Tracer ver. 1.7.2 (Rambaut et al., 2014). Trees were combined in LogCombiner by removing 25% of burnin from each run, and the maximum clade credibility tree selected using TreeAnnotator. For comparison, a second BEAST analysis was run with the same parameters described above except that only fossil tips (Sampled Ancestors MRCA prior with a uniform distribution, lower value = 98.17 Ma; upper value = 99.41) were used to calibrate the tree.

Ancestral Range Estimation. Ancestral range reconstruction was performed on the time-calibrated phylogenetic tree using the BioGeoBEARS ver. 1.1.1 package (Matzke, 2013a, 2013b, 2014) in R. As the ancestral areas of Buthidae and Chaerilidae are unknown, outgroup taxa were removed by using the *drop.tip* function from the package APE (Paradis et al., 2004). Due to poor resolution among the fossil terminals, resulting in short branch lengths in the time tree, all fossil taxa were removed, except *C. complexus*, the type species of *Chaerilobuthus*. Six biogeographical areas were defined based on the geological history of the region (Metcalfe, 2011) and the distribution of taxa: (A) the South China block; (B) Western Cimmeria, referring only to the Farah, Helmand, south-central Pamirs, Karakorum, and Band-e Bayan blocks (present-day Afghanistan and northern Pakistan) for this analysis; (C) Tajik and North Pamir blocks, defined here as northern Afghanistan and southern China, Uzbekistan, and Tajikistan, with Cimmerian areas to the west excluded (for details, see Loria et al., 2022); (D) the Indochina block, which includes the northwest (Phong Nha-Kẻ Bàng Karst, Vietnam) and northeast (Khammouan Karst, Laos) Annamite Mountains; and (E) the Burma Terrane. Each species was scored present or absent in each area. The maximum number of areas was set to five. Likelihood calculations were undertaken using GenSA. The analysis was time stratified into two periods (153–55 Ma, 55–0 Ma) to account for the collisions of Cimmeria (ca. 200 Ma) and India (ca. 55 Ma) with Eurasia (Ali and Atichison, 2008; Metcalfe, 2011, 2013). Areas allowed, areas adjacent and dispersal multiplier matrices were prepared based on paleogeographical maps from Metcalfe (2011, 2013), Li et al. (2023), and Ali and Aitchison (2008). For areas allowed, all combinations were allowed because all areas existed during each time period. For areas adjacent, all areas and connections were permitted except that, from 55–0 Ma, biotic exchange between the South China/Indochina/Burma Terrane and the Tajik and North Pamirs/Western Cimmeria was considered impossible due to orogeny of the Himalayas and the Tibetan Plateau. To account for geological distance, a dispersal multiplier matrix was prepared in which different scores of dispersal potential were assigned: 1, highest dispersal for adjacent biogeographical areas; 0.5, intermediate dispersal for biogeographical areas connected through an intermediate landmass or small ocean gap; and 0.0000001, little to no dispersal for widely separated areas between which long distance dispersal was considered unlikely (appendix 8). Four models that allow dispersal and extinction were compared in the analysis: Dispersal-Extinction-Cladogenesis (DEC), DEC*, DIVALIKE, and BAYAREALIKE. DEC allows for narrow and subset sympatry, and narrow vicariance. DIVALIKE permits narrow sympatry and narrow and widespread vicariance. BAYAREALIKE permits narrow and widespread sympatry but does not allow for vicariance (Matzke, 2014). A jump dispersal parameter (*j*), which allows founder

event speciation during cladogenesis, was tested despite recent criticisms (see Ree and Sanmartín, 2018) that were later refuted (Matzke, 2022). In all six models, *include_null_range* = *TRUE* was assigned, except for DEC* in which *include_null_range* = FALSE was assigned (Massana et al., 2015). Statistical analyses were performed to determine the log likelihood of the dataset for each model. Considering the debate regarding the positions of some areas defined in the analysis (e.g., the Burma Terrane) and to explore the effects of maximum range size on the results, a time-stratified analysis was performed with the maximum number of areas set to two and two unconstrained analyses were performed with the maximum number of areas set to two or five, respectively.

Mapping. Maps were generated with QGIS ver. 3.16 (http://www.qgis.org), by superimposing locality records and borders, coastlines and rivers from Natural Earth (https://www.naturalearthdata.com) on the global multi-resolution terrain elevation data (GTMTED2010; https://www.usgs.gov/core-science-systems/euros/coastal-changes-and-impacts/gmted2010). Palaeogeographical reconstructions were adapted from Li et al. (2023).

Ancestral State Reconstruction. Fifteen morphological characters pertaining to cave adaptation were used to reconstruct the evolution of troglomorphism in Pseudochactidae, following Prendini et al. (2021) and Loria et al. (2022). The following troglomorphic characters were scored into a morphological matrix (table 5): presence/absence of pigmentation on the carapace, tergites and legs, 4 (27%); presence/absence of the median and lateral ocelli, 6 (40%); attenuation of the pedipalps, 1 (7%); presence/absence of spurs, spinules and macrosetae on the legs, 3 (20%); and shape of the telson vesicle, 1 (7%). The extinct Chaerilobuthinae could not be scored for four characters of pigmentation. Character states were scored and summed for each species and scaled to create an ensemble index of cave adaptation so that values ranged from 1–10 (Ojanguren-Affilastro et al., 2016; Loria and Prendini, 2021, Loria et al., 2022). The preferred ML tree was chosen for this analysis due to the short branch lengths of the fossil terminals in the time tree. The ML tree was converted into an ultrametric tree using the commands *makeChronosCalib* and *chronos* in the R package, APE. Each species was reduced to a single terminal using the *drop.tip* function and the ultrametric tree with the lowest log-likelihood score selected for ancestral state reconstruction by setting the rate-smoothing parameter lambda to zero using a relaxed substitution model. Scaled scores were assigned to a troglomorphic continuum from epigean species (score = 1) to hypogean species progressively more adapted to caves (score = 10): 1–5.9 (epigean), 6–8.9 (troglophilic), 9–10 (troglobitic). Scaled scores were treated as continuous characters and ancestral state reconstruction performed on the ML tree applying Brownian motion, using the *contMap* function in the R package phytools (Revell, 2012). For comparison, the 15 discrete characters were optimized by applying a parsimony-based, node-driven method in TNT, following Ojanguren-Affilastro et al. (2016) and Ramírez and Michalik (2014), and scaled to the ensemble index following optimization. Because ambiguous characters were added for all states using this method, a second run was performed with the four pigmentation characters changed from "?" to "0" for the fossil terminals (i.e., ambiguous characters treated as absent).

RESULTS

Multivariate Statistical Analysis. Nonmetric multidimensional scaling (NMDS) of morphometric data confirmed the previous discoveries of Prendini et al. (2021) regarding the genera and species of Pseudochactidae, as well as the generic distinctiveness of *Q. solegladi*. However, *Q. solegladi* clustered more closely with the species of *Pseudochactas*, especially *P. ovchinnikovi* (fig. 2), than with *T. steineri*, suggesting that it is more closely related to the former than the latter. The NMDS score for the subadult holotype of *Q. solegladi* (x = -0.07, y = -0.04) was

TABLE 5. Distribution of 15 characters concerning morphology used to reconstruct ancestral ecomorphotypes for the relictual Asian scorpion family Pseudochactidae Gromov, 1998. Terminology follows appendix 6.

Species	Character Matrix	Score
Buthus atlantis	11000 00000 20000	[2]
Chaerilus sejnai	00000 10011 01100	[2.5]
†*Chaerilobuthus bruckschi*	????2 11011 21210	[6]
†*Chaerilobuthus complexus*	????2 11011 21210	[6]
†*Chaerilobuthus enigmaticus*	????2 11011 11210	[5.5]
†*Chaerilobuthus gigantosternum*	????2 11011 31210	[6.5]
†*Chaerilobuthus hansgeorgmuelleri*	????2 11011 11210	[5.5]
†*Chaerilobuthus knodelorum*	????2 11011 21211	[6.5]
†*Chaerilobuthus serratus*	????2 11011 21211	[6.5]
Pseudochactas mischi	11110 11011 10110	[5.5]
Pseudochactas ovchinnikovi	10000 11011 10110	[4]
Qianxie solegladi	10000 11011 10211	[5]
Troglokhammouanus steineri	00011 11111 10211	[6]
Aemngvantom lao	11112 11211 21211	[9.5]
Aemngvantom thamnongpaseuam	11112 11211 21211	[9.5]
Vietbocap canhi	11112 11211 31211	[10]

1. Tegument base coloration: brown [0]; yellowish [+1].
2. Carapace infuscation: present [0]; absent (immaculate) [+1].
3. Mesosomal tergites infuscation: present (entirely or partially infuscate) [0]; absent (immaculate) [+1].
4. Legs, femoral and patellar prolateral surfaces infuscation: present [0]; absent (immaculate) [+1].
5. Carapace median ocelli: present, pigmented [0]; present, not pigmented in some individuals [+1]; absent [+2].
6. Carapace lateral ocelli, anterolateral major (ALMa) ocelli: present, pigmented [0]; absent [+1].
7. Carapace lateral ocelli, mediolateral major (MLMa) ocelli: present, pigmented [0]; absent [+1].
8. Carapace lateral ocelli, posterolateral major (PLMa) ocelli: present, pigmented [0]; present, not pigmented in some individuals [+1]; absent [+2].
9. Carapace lateral ocelli, anterodorsal minor (ADMi) ocelli: present, pigmented [0]; absent [+1].
10. Carapace lateral ocelli, posterodorsal minor (PDMi) ocelli: present, pigmented [0]; absent [+1].
11. Pedipalps shape: segments very robust, chela manus incrassate [0]; segments moderately robust, chela manus globose [+1]; segments gracile, chela manus globose [+2]; segments gracile, chela manus elongate [+3].
12. Legs III and IV, tibial spurs: present [0]; absent [+1].
13. Legs I–IV basitarsi and telotarsi, spinules: absent [0]; short [+1]; long [+2].
14. Legs I–IV telotarsi, ventrosubmedian rows of (socketed) macrosetae: present [0]; absent [+1].
15. Telson vesicle, shape: globose [0]; elongate [+1].

similar to the scores for *P. ovchinnikovi* (x_{min} = -0.09 x_{max} = -0.06, y_{min} = -0.04, y_{max} = -0.03).

Genetic Divergence. As in the previous study by Prendini et al. (2021), uncorrected pairwise genetic distances (*p*-distances) within species were low across all loci, compared to *p*-distances between species (table 6): 12S (0%–1.13%), 16S (0%–0.99%), COI (0%–2.38%), 28S (0%–0.05%) and 18S-ITS2 (0%–0.01%). Interspecific *p*-distances were higher for the mitochondrial loci, with greatest variation in COI (12.62%–46.52%), followed by 16S (6.15%–27.92%) and 12S (4.44%–25.9%), than for the nuclear loci, in which the distances were higher for 18S-ITS2 (0.54%–5.07%) than for 28S (0.23%–3.7%). The distances between

P. ovchinnikovi and *Q. solegladi* were lower in most loci (18S-ITS2, 12S, 16S, COI) than the distances between *Q. solegladi* and the Southeast Asian genera, supporting the phylogenetic results that *Qianxie* is more closely related to *Pseudochactas*.

Phylogenetic Analyses. Separate analyses of the molecular dataset with BI, ML, and parsimony with equal or implied weighting (k = 1, 3, 10, 60, 100) recovered all subfamilies, genera, and species as monophyletic (tables 7, 8). *Qianxie solegladi* was placed sister to *P. ovchinnikovi* with high bootstrap support (BS: 100% for both GTRGAMMA and GTRCAT) in the ML analyses and high posterior probability (PP: 1) in the BI analysis. The (*P. ovchinnikovi* + *Q. solegladi*) clade received high support (BS: 100% for GTRGAMMA, 96% for GTRCAT; PP: 1) and was, in turn, sister to (Troglokhammouaninae + Vietbocapinae) with high support (BS: 91% for GTRGAMMA, 98% for GTRCAT; PP: 0.97)

Separate analysis of the morphological dataset with parsimony and equal weighting, which additionally included *P. mischi* and seven fossil species of Chaerilobuthinae, recovered all pseudochactid subfamilies, genera and species as monophyletic. In the analyses with equal weighting and implied weighting (k = 3, 10, 60, 100), *Q. solegladi* was placed sister to Troglokhammouaninae, unlike the analysis with implied weighting and k = 1, in which *Q. solegladi* was placed sister to a clade comprising the Southeast Asian genera (i.e., Chaerilobuthinae, Vietbocapinae, and Troglokhammouaninae).

Simultaneous analyses of the morphological and molecular datasets with BI, ML, and parsimony with equal and implied weighting (k = 3, 10, 60, 100) were congruent, and recovered all pseudochactid subfamilies, genera and species as monophyletic. In these analyses, *Q. solegladi* was placed sister to *Pseudochactas* with high support (BS: 93%–99% for ML; PP: 0.98 for BI); the Southeast Asian subfamilies formed a clade (Troglokhammouaninae (Chaerilobuthinae + Vietbocapinae)) with moderate support (46%–59%; PP: 0.78), sister to (*Pseudochactas* + *Q. solegladi*); and Chaerilobuthinae was placed sister to Vietbocapinae with moderate to high support (BS: 72%–91%; PP: 0.82). All relationships were similar in the parsimony analyses with implied weighting, except for the analysis with k = 1, in which Chaerilobuthinae was placed sister to all other pseudochactids. Unambiguous morphological synapomorphies were optimized on the preferred phylogeny, the ML Multistate CAT tree with Lewis correction obtained by simultaneous analysis of the morphological and molecular datasets (fig. 3).

Divergence Time Estimation. The two independent MCMC chains from the divergence time estimation analysis in BEAST2 each produced 50,000 trees. Examination of the logfiles in Tracer indicated convergence of the two chains. ESS values were above 200 for all parameters in both MCMC runs. The maximum clade credibility tree (fig. 4), produced after removing 25% burnin and combining trees from both chains, was fully dichotomous and matched the topology obtained by simultaneous analysis of the morphological and molecular datasets using BI and ML. In accordance with the calibrated node, the divergence between Chaerilidae and Pseudochactidae occurred in the Late Mississippian of the Carboniferous (328 Ma, 95% HPD: 318–338 Ma). The divergence between (Pseudochactinae + *Q. solegladi*) and the Southeast Asian subfamilies (Troglokhammouaninae (Chaerilobuthinae + Vietbocapinae)), occurred at the Jurassic-Cretaceous boundary (153 Ma, 95% HPD: 126–184 Ma), whereas the divergence between Troglokhammouaninae and (Chaerilobuthinae + Vietbocapinae) occurred in the Early Cretaceous (130 Ma, 95% HPD: 108–157 Ma). Divergence between Chaerilobuthinae and Vietbocapinae occurred towards the end of the Early Cretaceous (117 Ma, 95% HPD: 100–139 Ma), whereas divergence between Pseudochactinae and *Q. solegladi* occurred at the end of the Late Cretaceous (67 Ma, 95% HPD: 47–92 Ma). Diversification within the

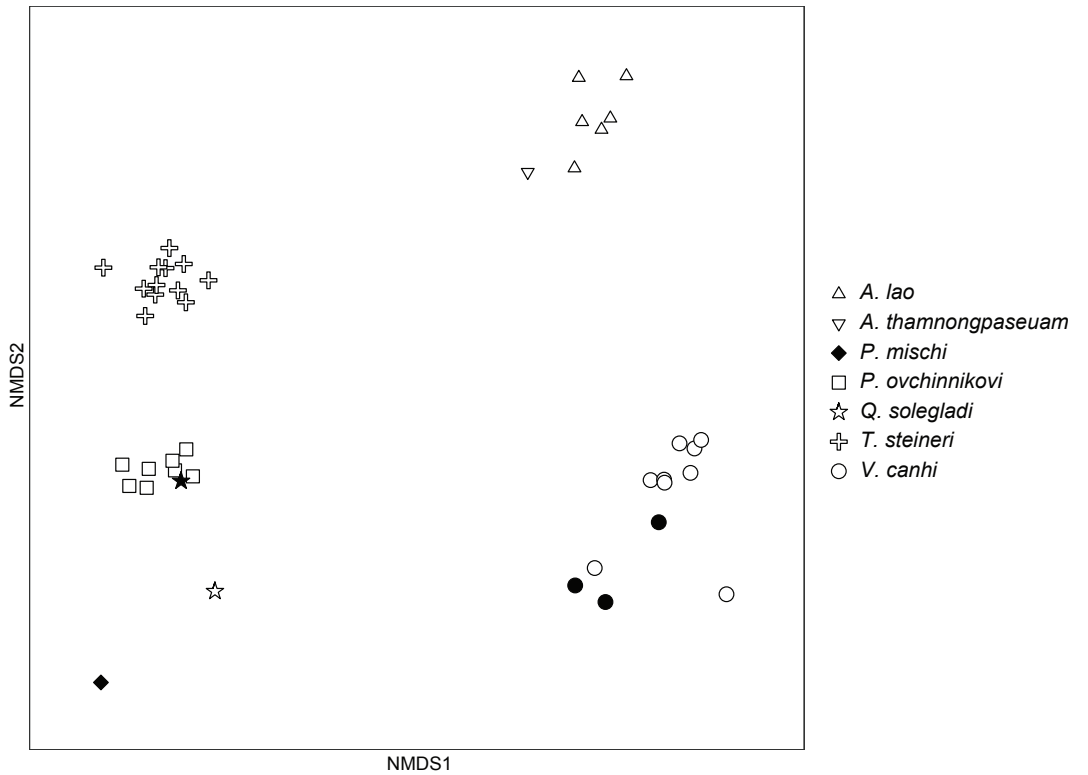

FIGURE 2. Nonmetric multidimensional scaling (NMDS) plot for females of extant species of the relictual Asian scorpion family Pseudochactidae Gromov, 1998, based on 22 morphometric ratios and eight counts, for 42 specimens (38 adults, two subadults and two juveniles; appendices 3–5). Each symbol represents an individual, empty (white) symbols represent adults, solid (black) symbols represent immatures.

subfamilies began in the Late Cretaceous, i.e., 105 Ma (95% HPD: 84–128 Ma) for the divergence between *Aemngvantom* and *Vietbocap* in Vietbocapinae, and continued into the Miocene, i.e., 19 Ma (95% HPD: 0.4–51 Ma) between *P. mischi* and *P. ovchinnikovi* in Pseudochactinae, and 18 Ma (95% HPD: 11–25 Ma) between the two troglobitic species of *Aemngvantom*, *A. lao* and *A. thamnongpaseuam*. Diversification within Chaerilobuthinae began in the Late Cretaceous (103 Ma, 99–117 Ma) although divergence times within this group were unresolved.

Ancestral Range Estimation. Based on the statistical output of the ancestral range estimation analysis in BioGeoBEARS, the DIVALIKE + *j* model had the best log likelihood and AIC scores in the time stratified analysis with the maximum number of areas (mx) set to five (tables 9, 10; fig. 5). According to this model, the ancestral range of Pseudochactidae at the Jurassic–Cretaceous boundary, was unresolved, although the probability was highest for Indochina + South China + Western Cimmeria + Tajik and North Pamir blocks. The ancestral range of highest probability for the Central Asian subfamily, Pseudochactinae, was Western Cimmeria + Tajik–North Pamir + South China, and for the Southeast Asian subfamilies (Troglokhammouaninae (Chaerilobuthinae + Vietbocapinae)), Indochina. The Burma Terrane was the ancestral range of highest probability for Chaerilobuthinae. Comparison of the corrected Akaike Information Criterion

TABLE 6. Mean intraspecific (boldface) and interspecific uncorrected pairwise (*p*) distances of three mitochondrial loci, 12S rDNA (12S), 16S rDNA (16S), Cytochrome *c* Oxidase Subunit I (COI) and two nuclear loci, 18S rDNA-Internal Transcribed Spacer (18S-ITS2) and 28S rDNA (28S), for four species of Pseudochactidae Gromov, 1998: *Pseudochactas ovchinnikovi* Gromov, 1998, *Qianxie solegladi* Tang, 2022, *Troglokhammouanus steineri* Lourenço, 2007, *Aemngvantom lao* (Lourenço, 2012), *Aemngvantom thamnongpaseuam* Prendini et al., 2021, and *Vietbocap canhi* Lourenço and Pham, 2010.

		P. ovch.	*Q. sole.*	*T. stein.*	*A. lao*	*A. tham.*	*V. canhi*
18S-ITS2	*P. ovchinnikovi*	**0**					
	Q. solegladi	0.0317	–				
	T. steineri	0.0139	0.0388	**0**			
	A. lao	0.0164	0.0507	0.0097	**0**		
	A. thamnongpaseuam	0.0384	0.1698	0.0320	0.0054	–	
	V. canhi	0.0137	0.0436	0.0088	0.0078	0.0281	**0.0001**
28S	*P. ovchinnikovi*	**0**					
	Q. solegladi	0.0178	–				
	T. steineri	0.0251	0.0155	**0**			
	A. lao	0.0228	0.0156	0.0331	**0**		
	A. thamnongpaseuam	0.0204	0.0148	0.0321	0.0023	–	
	V. canhi	0.0319	0.0262	0.0367	0.0351	0.0337	**0.0005**
12S	*P. ovchinnikovi*	**0**					
	Q. solegladi	0.1469	–				
	T. steineri	0.2362	0.2109	**0**			
	A. lao	0.2590	0.2236	0.2010	**0.0040**		
	A. thamnongpaseuam	0.2411	0.2208	0.1956	0.0444	–	
	V. canhi	0.2346	0.2217	0.1905	0.1914	0.1967	**0.0113**
16S	*P. ovchinnikovi*	**0.0028**					
	Q. solegladi	0.1284	–				
	T. steineri	0.2508	0.2634	**0**			
	A. lao	0.2429	0.2736	0.2179	**0.0031**		
	A. thamnongpaseuam	0.2457	0.2792	0.2084	0.0615	–	
	V. canhi	0.2762	0.2554	0.1977	0.1919	0.2138	**0.0099**
COI	*P. ovchinnikovi*	**0**					
	Q. solegladi	0.2187	–				
	T. steineri	0.4652	0.3776	**0.0009**			
	A. lao	0.2975	0.2447	0.3014	**0.0142**		
	A. thamnongpaseuam	0.2329	0.2633	0.2895	0.1262	–	
	V. canhi	0.3580	0.2696	0.2971	0.2517	0.2677	**0.0238**

TABLE 7. Tree statistics for phylogenetic analysis of the relictual Asian scorpion family Pseudochactidae Gromov, 1998. Length, consistency index (CI), retention index (RI), fit, and adjusted homoplasy (AH) of most parsimonious trees (MPTs) obtained by separate and simultaneous analyses of the morphological and molecular (concatenated aligned DNA sequences of two nuclear and three mitochondrial gene markers) datasets, with equal weighting (EW) and implied weighting (IW), applying five values of the concavity constant (*k*).

	Weight	MPTs	Length	CI	RI	Fit	AH
Morphology	EW	15	193	0.725	0.920	76.85–76.90	12.10–12.15
	IW: $k = 1$	6	193	0.725	0.920	66.25	22.75
	IW: $k = 3$	6	193	0.725	0.920	76.90	12.10
	IW: $k = 10$	6	193	0.725	0.920	84.36	4.64
	IW: $k = 60$	6	193	0.725	0.920	88.14	0.86
	IW: $k = 100$	6	193	0.725	0.920	88.48	0.52
Molecular	EW	1	2564	0.729	0.874	1163.3	157.7
	IW: $k = 1$	1	2564	0.729	0.874	1025.75	295.25
	IW: $k = 3$	1	2564	0.729	0.874	1163.3	157.7
	IW: $k = 10$	1	2564	0.729	0.874	1260.31	60.69
	IW: $k = 60$	1	2564	0.729	0.874	1309.70	11.31
	IW: $k = 100$	1	2564	0.729	0.874	1314.15	6.85
Simultaneous	EW	6	2763	0.727	0.878	1237.95– 1238.9	171.1–172.05
	IW: $k = 1$	11	2764	0.727	0.878	1089.83	320.17
	IW: $k = 3$	3	2763	0.727	0.878	1238.90	171.1
	IW: $k = 10$	3	2763	0.727	0.878	1344.16	65.84
	IW: $k = 60$	3	2763	0.727	0.878	1397.74	12.26
	IW: $k = 100$	3	2763	0.727	0.878	1402.57	7.43

(AICc) scores revealed the DIVALIKE model as the best fit. All results were similar except that dispersal into Burma was anagenic (along the branches) rather than a cladogenetic jump event (tables 9, 10).

BioGeoBEARS analyses using time stratified with mx = 2, time stratified with mx = 5 but null areas excluded, and unconstrained with mx = 2 and 5, yielded similar results (table 10). DIVALIKE + *j* was the model with best fit. However, when the *j* parameter was excluded, DIVALIKE was the best fit for the unconstrained analyses whereas DEC was the best fit for time stratified with mx = 2. In general, increasing the maximum number of areas a species was allowed to occupy resulted in more uncertainty in the ancestral nodes (table 10). According to Matzke (2014), when maximum range size increases, DIVA is more likely to infer more widespread ancestors at deeper nodes, and this is reflected in the analyses as the jump-dispersal parameter was higher in the mx = 2 ($j = 0.22007$ for time stratified, $j = 0.13245$ for unconstrained) than the mx = 5 ($j = 0.13828$ for time stratified, $j = 0.08537$ for unconstrained) analyses. Extinction rates (*e*) were similar with the DIVALIKE and DIVALIKE + *j* models ($e = 1e\text{-}07$) but lower compared to DEC ($e = 0.00234–0.01$) across all analyses. Similarly, excluding the null range (DEC*) had no effect on the reconstruction and results were identical to DIVALIKE + *j* in the time stratified analysis. Although results are similar across all analyses, the DIVALIKE + *j* model from the

TABLE 8. Nodal stability for selected clades and taxa in phylogenetic analysis of the relictual Asian scorpion family Pseudochactidae Gromov, 1998, based on separate and simultaneous (Simul) analyses of the morphological (Mor) and molecular (concatenated aligned DNA sequences of two nuclear and three mitochondrial gene markers, Mol) datasets using maximum likelihood (ML) with GTRGAMMA, GTRCAT, Multistate GAMMA (MS-GAMMA) or Multistate CAT (MS-CAT) models including ascertainment bias with Lewis correction (ASC), Bayesian inference (BI) and parsimony with equal weighting (EW), and implied weighting (IW) with five values of the concavity constant (*k*). Bootstraps (ML) and posterior probabilities (BI) indicated in cells. Highlighted black cells indicate clades and taxa recovered under various parameters (classification follows Prendini et al., 2021). Highlighted gray cells inapplicable due to missing data.

		Pseudochactidae	*Pseudochactas*	(*Pseudochactas* + *Q. solegladi*)	Troglokhammouninae	(*Q. solegladi* + Troglokhammouninae)	(*Q. solegladi* (Troglokhammouninae + Chaerilobuthinae + Vietbocpinae))	Vietbocapinae	Chaerilobuthinae	Chaerilobuthinae + Vietbocapinae	(Chaerilobuthinae (all other subfamilies))
Simul	ML MS-GAMMA	100	100	93	100			85	100	76	
	ML MS-CAT	95	99	98	100			93	100	91	
	ML MS-GAMMA-ASC	100	100	94	100			86	99	72	
	ML MS-CAT-ASC	96	100	99	100			94	100	91	
	BI	1	1	0.98	1			0.69	0.99	0.82	
	EW										
	IW (k = 1)										
	IW (k = 3)										
	IW (k = 10)										
	IW (k = 60)										
	IW (k = 100)										
Mol	ML GTRGAMMA	100	100	100	100			95			
	ML GTRCAT	96	100	100	100			100			
	BI	1	1	1	1			1			
	EW										
	IW (k = 1)										
	IW (k = 3)										
	IW (k = 10)										
	IW (k = 60)										
	IW (k = 100)										
Mor	EW										
	IW (k = 1)										
	IW (k = 3)										
	IW (k = 10)										
	IW (k = 60)										
	IW (k = 100)										

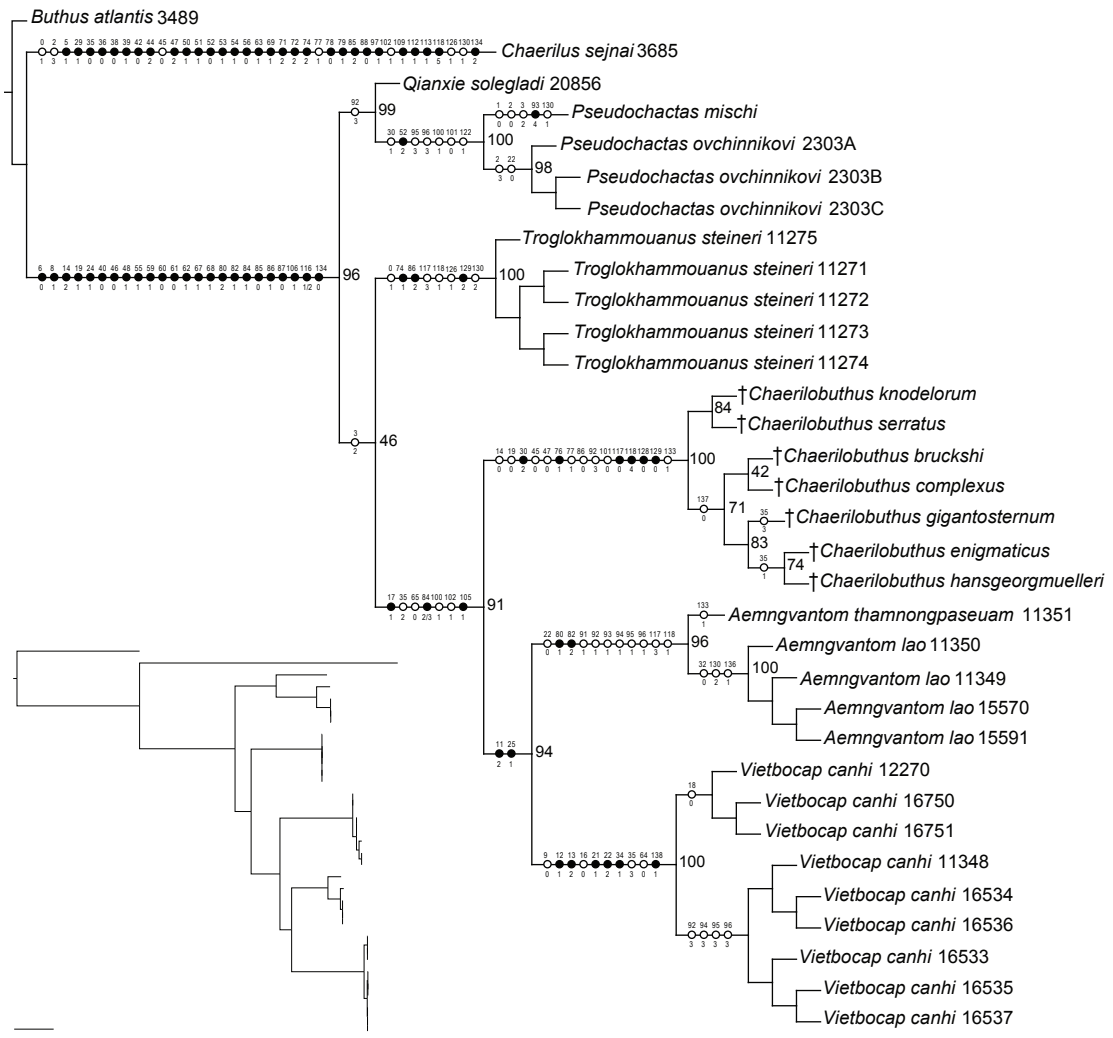

FIGURE 3. Preferred phylogeny of the relictual Asian scorpion family Pseudochactidae Gromov, 1998, based on simultaneous analysis of the morphological and molecular datasets using maximum likelihood (ML) applying a Multistate CAT model with Lewis correction. Unambiguous morphological synapomorphies optimized. Black circles indicate uniquely derived apomorphic states, white circles parallel deviations of apomorphic states. Numbers above circles indicate characters, numbers below indicate states (table 2, appendix 6). Numbers adjacent to nodes indicate bootstrap support values. Inset indicates reconstruction with branch lengths. Scale bar = 0.07 substitutions per site.

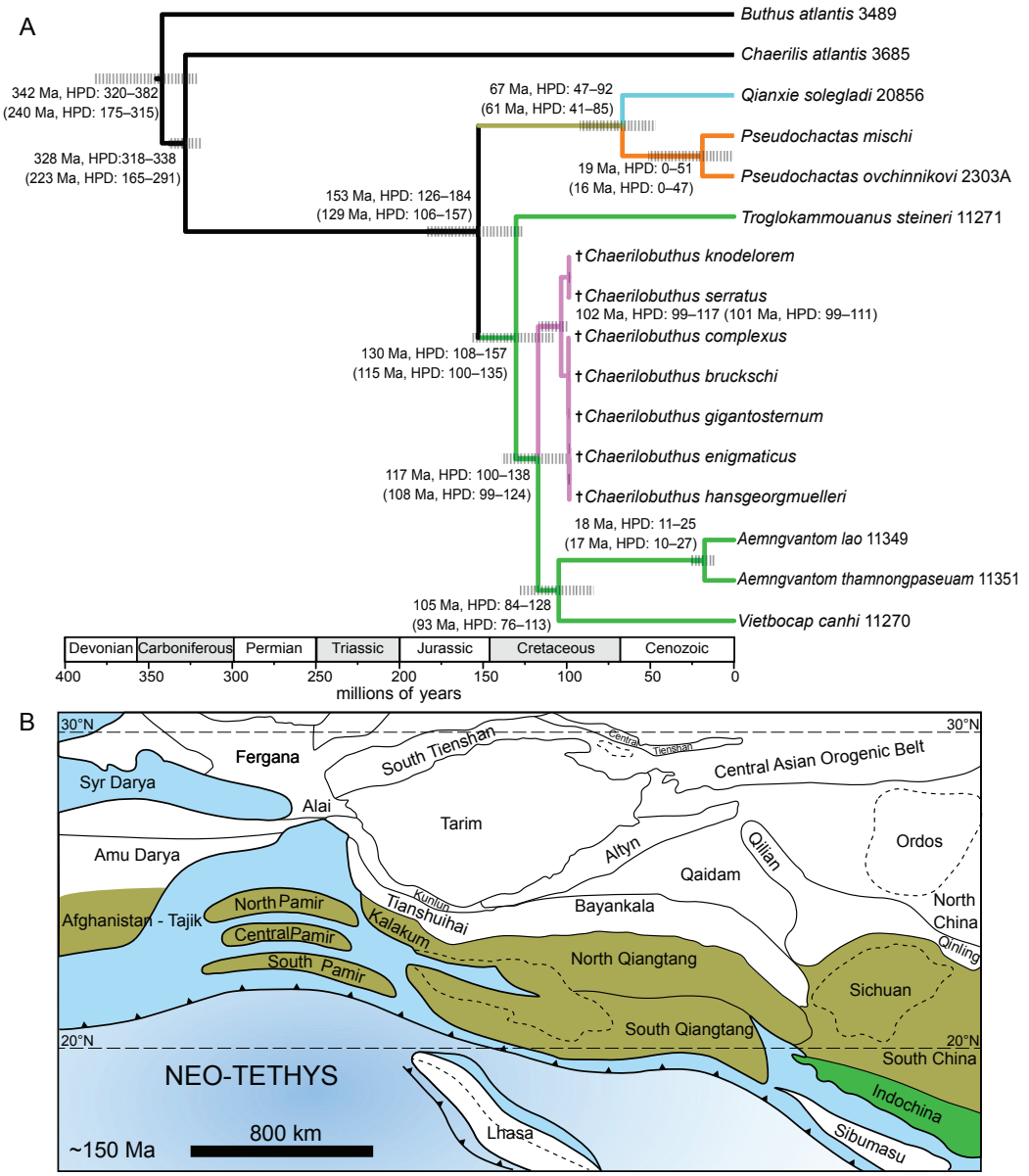

FIGURE 4. **A.** Time tree for evolution of the relictual Asian scorpion family Pseudochactidae Gromov, 1998, calibrated using 329 Ma divergence with Chaerilidae Pocock, 1893, and fossil tips. Numbers in parentheses adjacent to nodes indicate divergence times and 95% highest posterior density (HPD) values recovered from calibration using fossil tips only. Geological time periods (Devonian, Carboniferous, Permian, Triassic, Jurassic, Cretaceous, Cenozoic) and divergence ages (millions of years) indicated. **B.** Paleogeographical reconstructions indicating tectonic positions, past and present plate boundaries in Early Cretaceous (150 Ma): Following collision of Cimmerian continent with Eurasia in the Jurassic, pseudochactids disperse into Cimmeria and surrounding regions, resulting in subfamily Pseudochactinae; ancestor of Southeast Asian families originates on Indochina block. Paleogeographical reconstructions from Li et al. (2023). Following Montenat (2009) and Siehl (2017), South Pamir interpreted to include South Pamir, Farah, Helmand, Karakorum blocks; Central Pamir to include Central Pamir and Band-e Bayan blocks; and Afghanistan-Tajik to represent Tajik block.

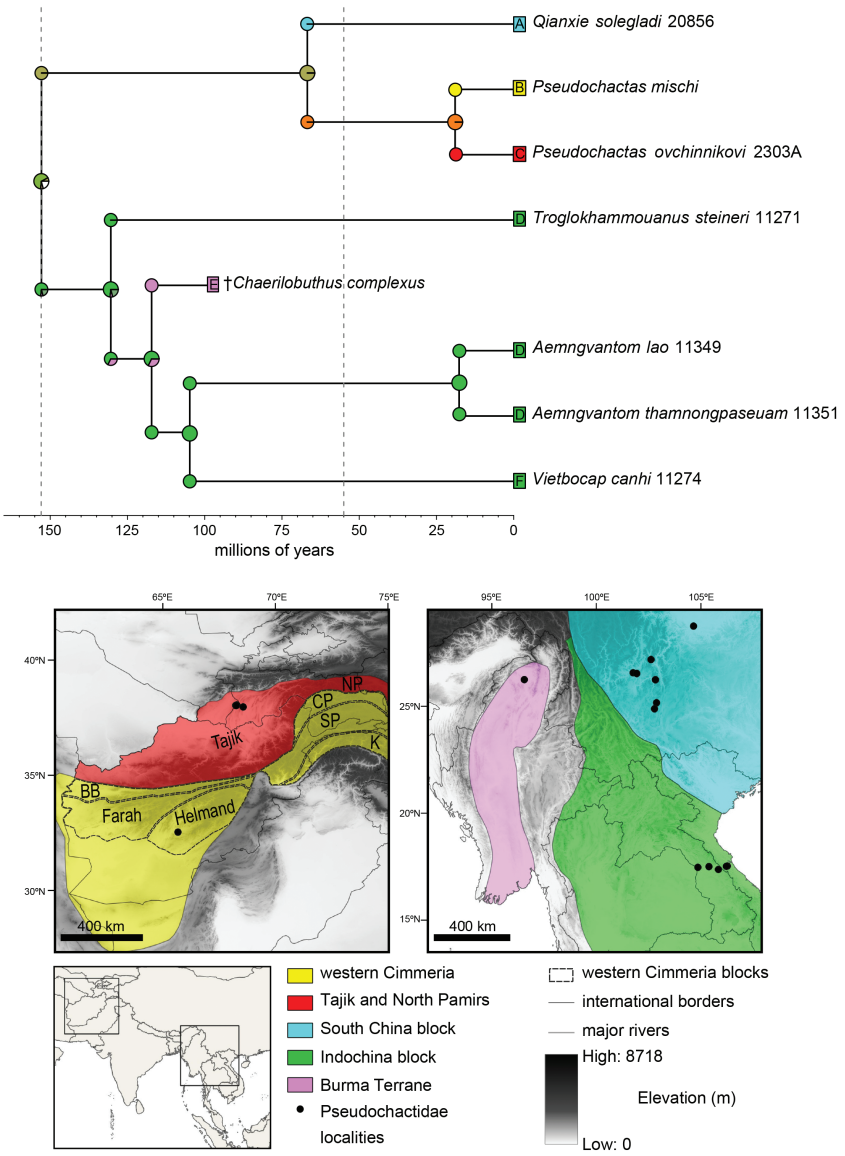

FIGURE 5. Estimation of ancestral ranges for the relictual Asian scorpion family Pseudochactidae Gromov, 1998, in five biogeographical areas according to DIVALIKE + *j* model in time-stratified analysis with maximum number of areas set to five (appendix 8): A, South China block; B, Western Cimmeria, including only Farah, Helmand, South-Central Pamirs, Karakorum and Band-e Bayan blocks (present-day Afghanistan and northern Pakistan); C, Tajik and North Pamir blocks (northern Afghanistan and southern China, Uzbekistan and Tajikistan); D, Indochina block; and E, Burma Terrane. Geological reconstructions following Montenat (2009), Collett et al. (2015), Robinson (2015), Siehl (2017), Li et al. (2020), and Nga et al. (2026).

TABLE 9. Statistics for models tested (DEC, DEC*, DIVALIKE, and BAYERLIKE) including additional founder effect (*j*) parameter in ancestral range estimation of the relictual Asian scorpion family Pseudochactidae Gromov, 1998: likelihoods (lnL), number of parameters in each model, dispersal (*d*), extinction (*e*), founder effect (*j*), Akaike Information Criterion (AIC) and corrected AICc (AICc). Models tested in four analyses: time stratified with maximum number of areas (mx) = 2; time stratified with mx = 5; unconstrained with mx = 2; and unconstrained with mx = 5.

Time Stratified, mx = 2							
Model	lnL	Parameters	*d*	*e*	*j*	AIC	AICc
DEC	-20.01	2	0.00621	0.00236	0	44.03	46.42
DEC + *j*	-16.11	3	0.00142	1e-12	0.30628	38.23	44.23
DIVALIKE	-28.31	2	0.00395	1e-12	0	60.62	63.02
DIVALIKE + *j*	-13.18	3	0.00147	1e-12	0.22008	32.35	38.35
BAYAREALIKE	-27.25	2	0.02029	0.01223	0	58.51	60.91
BAYAREALIKE + *j*	-23.13	3	0.00264	0.00334	0.9999	52.26	58.26

Time Stratified, mx = 5							
Model	lnL	Parameters	*d*	*e*	*j*	AIC	AICc
DEC	-13.95	2	0.00148	1e-12	0	31.89	34.29
DEC + *j*	-10.92	3	1e-12	1e-12	0.13584	27.84	33.84
DEC*	-13.87	3	0.00185	0.00203	0	31.74	34.14
DEC* + *j*	-10.92	2	1e-12	1e-12	0.13764	27.84	33.84
DIVALIKE	-10.91	2	0.00167	1e-12	0	25.83	28.23
DIVALIKE + *j*	-8.74	3	1e-12	1e-12	0.13828	23.47	29.47
BAYAREALIKE	-24.66	2	0.00498	0.01288	0	53.33	55.73
BAYAREALIKE + *j*	-20.95	3	0.00011	0.00414	0.43436	47.89	53.89

Unconstrained, mx = 2							
Model	lnL	Parameters	*d*	*e*	*j*	AIC	AICc
DEC	-17.35	2	0.00141	0.00074	0	38.69	41.09
DEC + *j*	-9.89	3	1e-12	1e-12	0.15973	25.78	31.78
DIVALIKE	-13.44	2	0.00130	1e-12	0	30.88	33.28
DIVALIKE + *j*	-9.14	3	1e-12	1e-12	0.13245	24.28	30.28
BAYAREALIKE	-20.96	2	0.00409	0.01073	0	45.91	48.31
BAYAREALIKE + *j*	-10.71	3	1e-12	1e-07	0.16477	27.42	33.42

Unconstrained, mx = 5							
Model	lnL	Parameters	*d*	*e*	*j*	AIC	AICc
DEC	-25.70	2	0.01	0.01	0	55.41	57.81
DEC + *j*	-9.40	3	1e-12	1e-12	0.12655	24.80	30.80
DIVALIKE	-11.34	2	0.00057	1e-12	0	26.68	29.08
DIVALIKE + *j*	-8.07	3	1e-12	1e-12	0.08537	22.13	28.13
BAYAREALIKE	-30.35	2	0.01	0.01	0	64.71	67.11
BAYAREALIKE + *j*	-10.71	3	1e-07	1e-07	0.16456	27.42	33.42

TABLE 10. Most probable ancestral areas of the relictual Asian scorpion family Pseudochactidae Gromov, 1998, its subfamilies Chaerilobuthinae Lourenço and Beigel, 2011, Pseudochactinae Gromov, 1998, Troglokhammouaninae Prendini et al., 2021, Vietbocapinae Lourenço, 2007, and major lineages based on best-fit model with and without *j* parameter for four different analyses: time stratified with maximum number of areas (mx) = 2; time stratified with mx = 5; unconstrained with mx = 2; and unconstrained with mx = 5. Abbreviations: mx = maximum number of areas allowed to occupy; DIVA = DIVALIKE. Biogeographical regions as follows: A, South China block; B, Western Cimmeria, including only Farah, Helmand, South-Central Pamirs, Karakorum and Band-e Bayan blocks (present-day Afghanistan and northern Pakistan); C, Tajik and North Pamir blocks (northern Afghanistan and southern China, Uzbekistan and Tajikistan); D, Indochina block; and E, Burma Terrane.

Model	DIVA	DEC	DIVA	DIVA	DIVA	DIVA	DIVA	DIVA
j parameter	X		X		X		X	
mx	2	2	5	5	2	2	5	5
Time Stratified	X	X	X	X				
Pseudochactidae	AB	BD	ABCD	ABCD	AD	AD	ABCD	ABCD
Chaerilobuthinae	E	E	E	E	E	E	E	E
Pseudochactinae	AB	BD	ABC	ABC	A	AB	ABC	ABC
Troglokhammouaninae	D	D	D	D	D	D	D	D
Vietbocapinae	D	D	D	D	D	D	D	D
SE Asian subfamilies	D	D	D	D	D	D	D	D

time-stratified analysis with maximum number of areas set to five is considered the most plausible biogeographical hypothesis (table 9). Output files for all BioGeoBEARS analyses are available online (https://doi.org/10.6084/m9.figshare.29565065).

Ancestral State Reconstruction. The ensemble index of troglomorphic characters identified a continuum from epigean species (score = 1) to hypogean species progressively more adapted to caves (score = 10): 1–5.9 (epigean), 6–8.9 (troglophilic), 9–10 (troglobitic). *Qianxie solegladi* and the two *Pseudochactas* were recovered as epigean (scores for *Q. solegladi*, *P. mischi*, and *P. ovchinnikovi* = 5, 5.5, and 4, respectively), *T. steineri* as troglophilic (score = 6), and the three species of Vietbocapinae, as troglobitic (scores for *A. lao*, *A. thamnongpaseuam*, and *V. canhi* = 9.5, 9.5 and 10, respectively). Although the extinct Chaerilobuthinae were recovered as epigean or troglophilic (scores = 5.5, 6, or 6.5), these scores should be interpreted with caution as four characters of pigmentation could not be scored in these taxa. The outgroup taxa, *B. atlantis* and *C. sejnai*, were recovered as epigean (scores = 2 and 2.5, respectively).

According to the reconstructions (figs. 6, 7), the ancestor of Pseudochactinae, including *Q. solegladi*, was epigean (scores = 5.1/3.5/3.5 for the three analyses including phytools, TNT with ambiguous characters as such, and TNT with ambiguous characters treated as absent, respectively); the ancestor of Chaerilobuthinae was troglophilic (scores = 6.6/7.5/6.5); and that of Vietbocapinae was troglophilic in the phytools analyses (scores = 8.6) but troglobitic in the TNT analyses (scores = 9.5/9.5). The ancestor of the clade comprising (Troglokhammouaninae (Chaerilobuthinae + Vietbocapinae)) was troglophilic (score = 6.6) in the phytools analysis but epigean in the TNT analyses (scores = 5/4), and the ancestor of Pseudochactidae was epigean in all analyses (scores = 5.6/3/2.5). Output files are available online (https://doi.org/10.6084/m9.figshare.29565065).

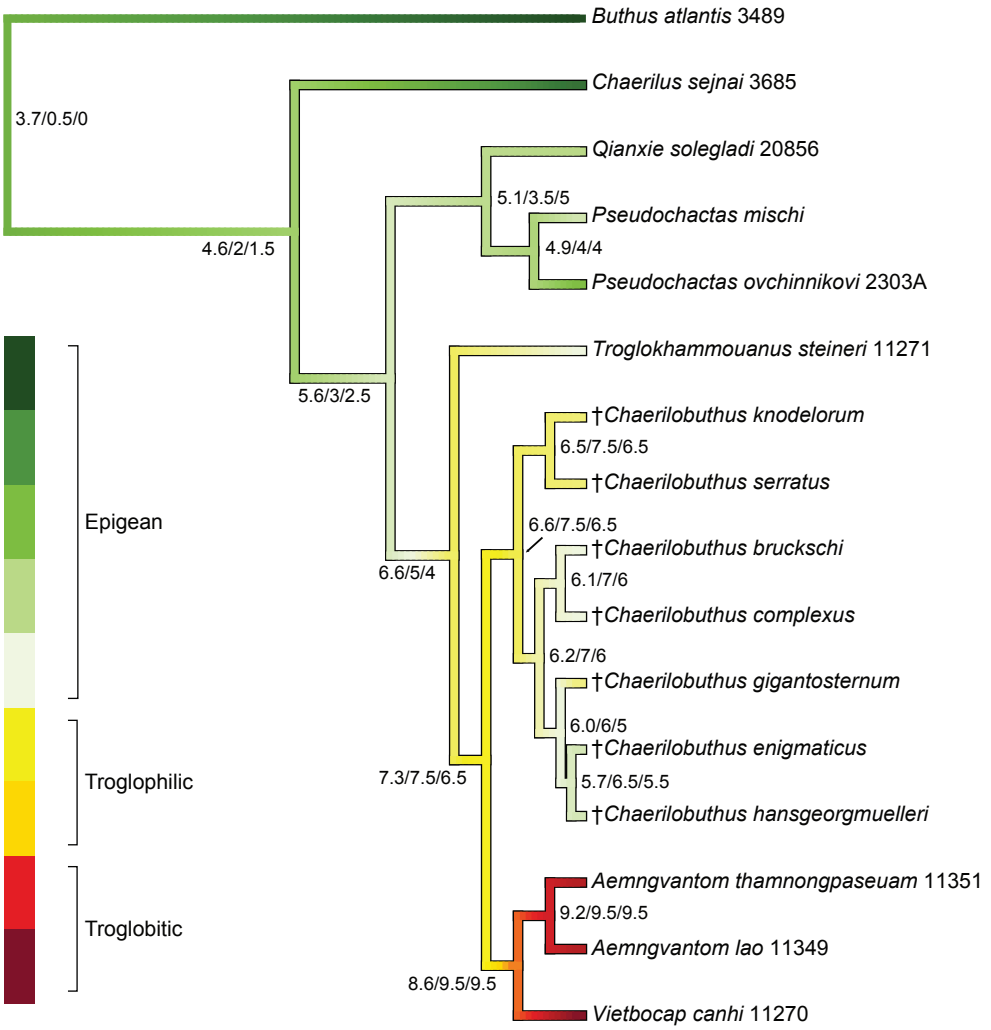

FIGURE 6. Preferred ancestral state reconstruction for the relictual Asian scorpion family Pseudochactidae Gromov, 1998, using Brownian motion of troglomorphism index (scale = 1–10) ranging from epigean (score = 1) to hypogean, troglobitic (score = 10). Ecomorphotypes classified as epigean (1–5.9); hypogean, troglophilic (6–8.9); and hypogean, troglobitic (9–10). Color scale ranges from lowest (2) for *Buthus atlantis* Pocock, 1889, to highest (10) for *Vietbocap canhi* Lourenço, 2010. Numbers adjacent to nodes represent reconstruction values from three different analyses: phytools/TNT with ambiguous characters as such/TNT with ambiguous characters absent.

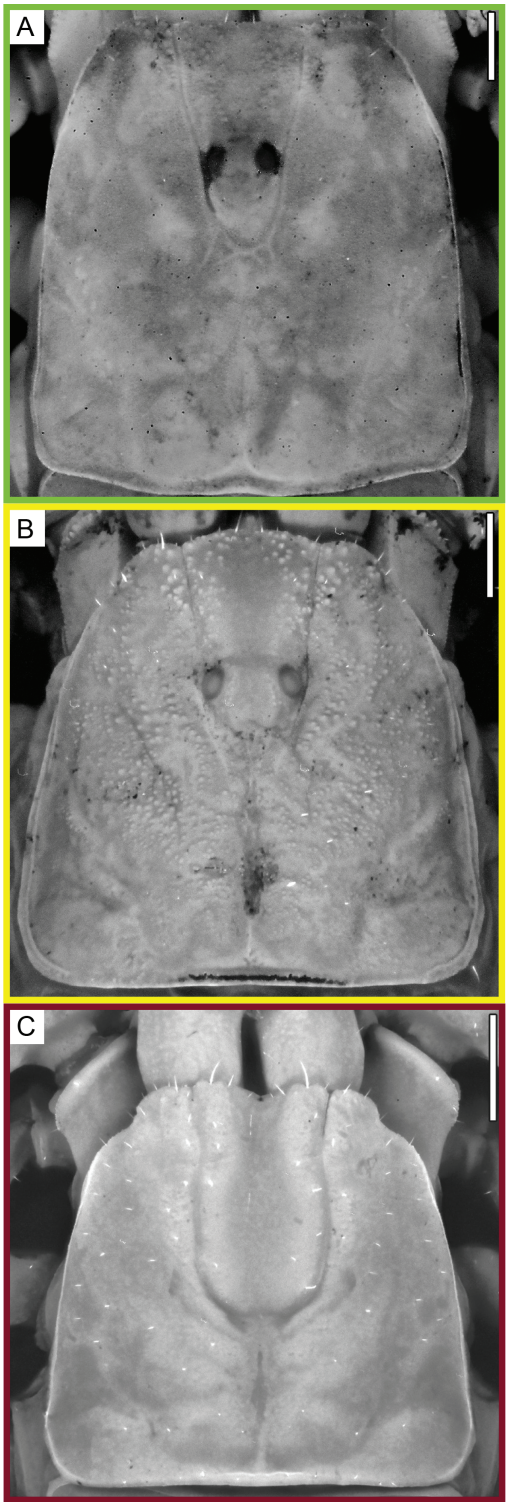

FIGURE 7. Carapaces of three pseudochactid species, representing each ecomorphotype: **A,** epigean, *Pseudochactas ovchinnikovi* Gromov, 1998; **B,** troglophilic, *Troglokhammouanus steineri* Lourenço, 2007; and **C,** troglobitic, *Vietbocap canhi* Lourenço, 2010.

DISCUSSION

Trichobothrial Patterns in Pseudochactidae

Based on comparisons with the trichobothrial patterns of buthid scorpions, particularly those that deviate from Type A orthobothriotaxy, Prendini et al. (2006) concluded that the Type D trichobothrial pattern of Pseudochactidae is homologous, fundamentally, with that of Buthidae. More similarities (i.e., potentially synapomorphic or symplesiomorphic trichobothria) than differences between the two patterns were identified, even if Soleglad and Fet's (2001) interpretation was adopted. Prendini et al. (2006) proposed a reinterpretation of the trichobothrial pattern of Pseudochactidae that was more similar to the buthid pattern than either the interpretations of Gromov (1998) or Soleglad and Fet (2001). This reinterpretation, also applied in the present contribution, is only one of several possible reinterpretations for particular trichobothria, however. Other interpretations imply more potential similarities with Buthidae. Despite recent phylogenetic reconstructions which place Pseudochactidae sister to Chaerilidae, the Type D pattern of Pseudochactidae shares few similarities with the Type B pattern of Chaerilidae, which may be more derived.

By applying modern imaging methods, such as confocal laser scanning microscopy, Xuan et al. (2025) accurately documented the trichobothrial pattern of the extinct Chaerilobuthinae, revealing that it conforms largely to the Type D pattern, previously restricted to extant Pseudochactidae, and comprising a total of 33 trichobothria: 11 trichobothria on the pedipalp femur (d_1–d_4, d_6, i_2, i_4, e_1–e_3), ten trichobothria on the patella (d_1–d_3, i_1, eb_1, eb_2, esb_1, *est*, et_1, et_2), and 12 trichobothria on the chela (*db*, *dt*, ib_1, ib_2, *it*, *eb*, *esb*, Eb_2, Eb_3, *Est*, Et_1, V_2). Previous researchers erroneously concluded that two *V* trichobothria occur on the

chela manus of chaerilobuthine scorpions by mistaking a macroseta for a *V* trichobothrium (Lourenço and Beigel, 2011; Lourenço, 2015, 2018; Lourenço and Velten, 2015, 2019, 2020, 2021, 2022). Compared to the basic Type D pattern observed in extant pseudochactids, however, Chaerilobuthinae lack the femoral trichobothrium d_5 and the chelal trichobothrium Eb_1. Additionally, femoral trichobothria d_3 and d_4 are situated closer to the midpoint of the segment and the d_3–d_4 axis is directed slightly away from the retrodorsal carina rather than parallel to it as in extant pseudochactids.

Pseudochactid Systematics

Recent changes to the systematics of Pseudochactidae implemented by Prendini et al. (2021) and Xuan et al. (2025) were confirmed by the phylogenetic analyses presented here. The four subfamilies, Chaerilobuthinae, Pseudochactinae, Troglokhammouaninae, and Vietbocapinae, were monophyletic with high support and the following scheme of relationships was recovered: (Pseudochactinae (Troglokhammouaninae (Chaerilobuthinae + Vietbocapinae))). *Pseudochactas*, *P. ovchinnikovi*, *T. steineri*, and the genera and species of Vietbocapinae, were also monophyletic across the analyses.

Prendini et al. (2021) synonymized *Vietbocap thienduongensis* Lourenço and Pham, 2012, *Vietbocap auriantiacus* Lourenco et al., 2018, and *Vietbocap quinquemilia* Lourenco et al., 2018, with *V. canhi*, falsifying the hypothesis that more than one species of *Vietbocap* inhabits the Thiên Đường and Tiên Sơn caves of Vietnam. These decisions were based on phylogenetic analyses of 8608 bp of DNA sequence from two nuclear and three mitochondrial genes (including 1078 bp of COI) and 140 morphological characters scored for nine individuals from both caves, and well as the multivariate morphometric analysis, based on 30 ratios and counts for 17 individuals from both caves. The suggestion by Duong et al. (2025: 403, 412) that more than one species of *Vietbocap* occurs in these caves, based on analysis of 628 bp of COI, is rejected. Consistent with the findings of Prendini et al. (2021), the phylogenetic and multivariate morphometric analyses presented herein, confirmed that the populations of the two caves are conspecific and there is no morphological or molecular justification for their recognition as distinct species or subspecies.

Tang (2022) hypothesized that *Qianxie* is closely related to the hypogean Southeast Asian genus, *Troglokhammouanus*. This initial taxonomic placement is not surprising given the superficial resemblance between these genera, supported by parsimony analysis of the morphological dataset, which placed them as sister taxa, due to the presence of homoplastic characters. The simultaneous analyses of morphological and molecular data demonstrated that *Qianxie* forms a monophyletic group with the epigean Central Asian genus, *Pseudochactas*, however. These results were reinforced by the multivariate morphometric analysis and pairwise genetic distances, both of which suggest that *Qianxie* is more closely related to *Pseudochactas* than to *Troglokhammouanus*, consistent with the multivariate morphometric analyses of Xuan et al. (2025). Based on the available evidence, *Q. solegladi* is transferred to Pseudochactinae (table 1).

Lourenço and Velten (2025: 2–5) criticized the work of Prendini et al. (2021) and Xuan et al. (2025), reinstated Chaerilobuthinae to the rank of family, revalidated *Chaeriloiurus* Lourenço, 2020, and *Serratochaerilobuthus* Lourenço, 2024, synonymized Troglokhammouaninae with Pseudochactidae, newly elevated Vietbocapinae to the rank of family, synonymized *Aemngvantom* with *Vietbocap*, and claimed the validity of *Qianxie* to be "*dubius*." Lourenço and Velten (2025) also claimed to newly elevate Pseudochactidae Gromov, 1998, to the rank of superfamily, as Pseudochactoidea Gromov, 1998, although this superfamily was previously recognized by others, e.g., Santibáñez-López et al. (2019, 2023). No data, analyses or argumentation justified the decisions of Lourenço and Velten (2025), which contradict the extensive data and analy-

ses of Prendini et al. (2021), Loria et al. (2022), Xuan et al. (2025), and the present contribution. Consequently, the classification of Prendini et al. (2021) and Xuan et al. (2025) is restored (table 1). Specifically, Chaerilobuthidae Lourenço and Beigel, 2011 = Pseudochactidae Gromov, 1998, syn. nov.; Vietbocapidae Lourenço, 2012 = Pseudochactidae Gromov, 1998, syn. nov.; Chaerilobuthinae Lourenço and Beigel, 2011, stat. rev.; Troglokhammouaninae Prendini et al., 2021, stat. rev.; *Aemngvantom* Prendini et al., 2021, stat. rev.; *Chaeriloiurus* Lourenço, 2020 = *Chaerilobuthus* Lourenço and Beigel, 2011, syn. nov.; *Serratochaerilobuthus* Lourenço, 2024 = *Chaerilobuthus* Lourenço and Beigel, 2011, syn. nov.; *Chaerilobuthus barbarae* (Lourenço and Velten, 2025), comb. nov.

Origins and Diversification

Based on the time stratified, mx = 5 analysis, the selection of the DIVALIKE + *j* model over other models in the BioGeoBEARS analysis implies that the paleogeographical history of Pseudochactidae was driven by dispersal-vicariance, jump-dispersal and sympatric speciation events caused by plate tectonics and climatic changes in the region. The addition of *Q. solegladi* from South China and Chaerilobuthinae from the Burma Terrane requires revision of the biogeographical hypothesis proposed by Loria et al. (2022), however.

At the time of its diversification (ca. 150 Ma), the ancestor of Pseudochactidae was epigean and widespread across Indochina + South China + Western Cimmeria + Tajik–North Pamir (fig. 5). Given the large geographical distance between Western Cimmeria/Tajik–North Pamir and South China/Indochina, Pseudochactidae were likely present in the intervening areas, including parts of Eastern Cimmeria, broadly defined here as Lhasa, South Qiantang, Sibumasu (including the Baoshan and Tenchong blocks), and the North Qiangtang-Kalakum block (fig. 4). Loria et al. (2022) proposed that Pseudochactidae originated in Eurasia and this hypothesis remains plausible as Pseudochactidae could have originated in Eurasia, perhaps near Tajik, and dispersed to Western Cimmeria, South China, and Indochina when these landmasses connected at the Triassic–Jurassic boundary (ca. 200 Ma). Unlike other arachnid orders, scorpions have an extensive Paleozoic record with most fossils occurring in the Northern Hemisphere (Dunlop and Penney, 2012). The geographical distribution of Paleozoic fossils, combined with the phylogenetic position of Pseudochactidae as one of the earliest diverging Recent scorpion lineages and the absence of pseudochactid taxa from the Southern Hemisphere, remains consistent with the hypothesized Eurasian origin of the family (Loria et al., 2022). It is also possible, however, that Pseudochactidae originated on one of the former Gondwana landmasses on which members of the family have been recorded (i.e., South China, Indochina, Western Cimmeria), later dispersing upon collision with Eurasia. However, without understanding the biogeographical history of the sister family, Chaerilidae, it is difficult to make assumptions about the ancestral range of Pseudochactidae. The analyses presented here indicate that, in the Early Cretaceous, a vicariance event resulted in Pseudochactidae diverging into two lineages: Pseudochactinae in South China + Western Cimmeria + Tajik–North Pamir, and the ancestor of the Southeast Asian subfamilies in Indochina.

Central versus Southeast Asian Subfamilies

The analyses suggest that the ancestor of Pseudochactinae was epigean and widespread across South China + Western Cimmeria + Tajik–North Pamir and began diversifying at the end of the Late Cretaceous (ca. 67 Ma). This Late Cretaceous divergence corresponds to the Cretaceous-Tertiary (KT) mass extinction and perhaps climatic changes caused by this event resulted in habitat fragmentation of Pseudochactinae across its range, ultimately resulting in a divergence between *Qianxie* in South China and *Pseudochactas* in Western Cimmeria/Tajik–North Pamir. By 55 Ma, the Indian subconti-

nent began its initial contact with Eurasia (Ali and Aitchison, 2008), pushing the Tibetan Plateau and the Himalayas upwards. Divergence between *P. mischi* and *P. ovchinnikovi* occurred in the Miocene (ca. 20 Ma), possibly as the result of another vicariance event, uplift of the Hindu Kush Mountains–Central Mountain range in Afghanistan induced by the final push of the Indian subcontinent into Eurasia (35 Ma). However, with molecular sequence data missing for *P. mischi*, this divergence date should be interpreted with caution.

Loria et al. (2022) proposed a "Climate Relict" hypothesis, which suggested that Southeast Asian pseudochactids (i.e., the ancestors of Troglokhammouaninae and Vietbocapinae) survived in subterranean refugia of the Annamite Mountains during Miocene aridification. The phylogenetic position of Chaerilobuthinae and its morphological characters provide additional support for this hypothesis. Troglokhammouaninae and Vietbocapinae include hypogean species that exhibit troglomorphies. The extinct Chaerilobuthinae from 99-million-year-old Burmese amber are also troglomorphic (Xuan et al., 2025). The analyses presented here suggest that, at the time of its diversification, the ancestor of the Southeast Asian pseudochactids was troglomorphic and inhabited Indochina in the Early Cretaceous (ca. 130 Ma). Perhaps this ancestor resembled Chaerilobuthinae and was endogean, inhabiting the leaf litter as proposed by Xuan et al. (2025). A jump dispersal event of this ancestor to the Burma Terrane occurred approximately 117 Ma ago, suggesting that the Burma Terrane was accessible from Indochina at this time. At the end of the Early Cretaceous (ca. 105 Ma), the troglomorphic ancestor of Vietbocapinae diverged into two lineages (genera) on opposite sides of the Annamite Mountains. During the Miocene, aridification caused the extinction of endogean Chaerilobuthinae on the Burma Terrane, whereas hypogean pseudochactids survived in caves of the Annamite Mountains in Indochina.

Implications for the Burma Terrane

The paleogeographical history of the Burma Terrane is contested (Röschmann et al., 2024). Most researchers agree that it rifted from Gondwana, traveled northwards and collided with Eurasia. However, the trajectory of its journey, its connections with other areas, and the timing of these events are poorly understood. Studies on angiosperms (Poinar, 2018), wasps (Jouault et al., 2021), and other arachnid taxa including short-tailed whip-scorpions (De Francesco Magnussen et al., 2022), spiders (Wood and Wunderlich, 2023), ticks (Chitimia-Dobler et al., 2023), and pseudoscorpions (Wriedt et al., 2021; Geißler et al., 2022; Röschmann et al., 2024) preserved in Burmese amber, support a hypothesis of Late Jurassic rifting. According to this hypothesis, the Burma Terrane rifted from Gondwana in the Late Jurassic and only collided with Sundaland in the Late Cretaceous (Heine et al., 2004; Zhang et al., 2017) or the Eocene–Oligocene (Westerweel et al., 2019). A hypothesis of "Early Devonian rifting" (Metcalfe, 2013) suggests that the Burma Terrane rifted from Gondwana in the Early Devonian and traveled with South China, Indochina, West Sumatra and East Malaya as a continent known as Cathaysialand. Collison only occurred at the Late Triassic/Early Jurassic boundary. Johnson et al. (2023) proposed that Permian diversification (Johnson et al., 2022) and Burmese amber inclusions support an Early Devonian rifting hypothesis for the chthoniid pseudoscorpion tribe Tyrannochthoniini Chamberlin, 1962.

In the time stratified analyses with mx = 5 presented here, the DIVALIKE + *j* model recovered an Early Cretaceous (117 Ma) jump dispersal event from Indochina to Burma, interpreted as support for the Early Devonian rifting hypothesis of Metcalfe (2011, 2013). The DIVALIKE model, with the best AICc score, also recovered dispersal to the Burma Terrane but via an anagenic process. Although supporting the Late Jurassic rifting hypothesis, Wood and Wunderlich (2023) found similar dates (ca. 109 Ma) for three dispersal/

range expansion events from the Burma Terrane into the Holarctic in palpimanoid spiders, with the Burma Terrane acting as a biotic ferry bringing taxa to Asia. Similarly, Xing et al. (2018) discovered a species of Burmese amber frogs with morphological affinities to anurans of the Jehol biota (ca. 130–122 Ma). Regardless of when the Burma Terrane rifted from Gondwana, the results presented here, together with previous studies, suggest a pattern of early biotic connection between the Burma Terrane and Asia.

Revised Timeline of Pseudochactid Diversification

Based on the present analysis, the timeline for the origins, dispersal, and diversification of Pseudochactidae provided by Loria et al. (2022) is revised as follows (figs. 4–6): The ancestor of Pseudochactidae was epigean and originated during the Carboniferous although the ancestral range of the family remains unclear. At the Jurassic–Triassic boundary (ca. 200 Ma), the Cimmerian continent, Tajik–North Pamir, South China, Indochina, and other parts of Eurasia collided (Metcalfe, 2011, 2013), permitting biotic exchange between these landmasses. In the Early Cretaceous, Pseudochactidae experienced a vicariance event that separated the Central Asian Pseudochactinae in Western Cimmeria + Tajik–North Pamir + South China, from the common ancestor of the Southeast Asian subfamilies, in Indochina. Connections between the Burma Terrane and Eurasia permitted a jump dispersal event from Indochina in the Early Cretaceous, resulting in subfamily Chaerilobuthinae, coinciding with the divergence of Vietbocapinae in the Annamite Mountains. Divergence between *Pseudochactas* and *Qianxie* occurred at the KT boundary, perhaps the result of habitat fragmentation and extinction caused by climate change. Uplift of the Himalayas, the Tibetan Plateau, and neighboring mountain ranges followed as the Indian subcontinent pushed into Eurasia during the Eocene, causing another vicariance event, which separated the ancestors of *P. mischi* from *P. ovchinnikovi*. Subsequent Miocene aridification resulted in extinction of some lineages (Chaerilobuthinae) whereas others (Troglokhammouaninae, Vietbocapinae) survived in subterranean refugia.

Evolution of Troglomorphism

According to the reconstructions of Loria et al. (2022), the ancestors of Pseudochactidae and Pseudochactinae were epigean, whereas the ancestor of the clade comprising (Troglokhammouaninae + Vietbocapinae) was troglobitic. The inclusion of *Q. solegladi* and Chaerilobuthinae in the present analyses altered some of those findings (figs. 6, 7). The ancestors of Pseudochactidae and Pseudochactinae were again reconstructed as epigean, whereas the ancestor of the clade comprising the Southeast Asian subfamilies, (Troglokhammouaninae (Chaerilobuthinae + Vietbocapinae)), was instead recovered as troglophilic in one analysis but epigean in the others. Troglokhammouaninae and Vietbocapinae were recovered as troglophilic or troglobitic, respectively. The ancestor of Chaerilobuthinae was troglophilic, consistent with the interpretation by Xuan et al. (2025) that these scorpions were endogean. This finding should nevertheless be interpreted with caution because four characters of pigmentation could not be scored for the ensemble index in Chaerilobuthinae.

ACKNOWLEDGMENTS

Aspects of this research were funded by the following awards: National Science Foundation Doctoral Dissertation Improvement grant DEC 1310855 to L.P. and S.F.L.; NSF grants EAR 0228699, DEB 0413453 and DEB 1655050 to L.P.; a grant from the Richard Lounsbery Foundation to L.P.; two Constantine S. Niarchos Expedition grants from the Stavros Niarchos Foundation to L.P.; two grants from the Exploration Fund of the Explorer's Club, one each to S.F.L. and V.L.E.; Young Explorers Grant 9816-15 from the National Geographic

Society to S.F.L.; and scholarship 202404910460 from the China Scholarship Council to Q.X. We acknowledge the following friends and colleagues for assistance with fieldwork and/or donations of material used in the study: Kazakhstan: A.V. Gromov and S. Mozorov; Laos: P. Kanyavong, S.T. Kangnavong, W. Phimmathong, and P.T. Thon Thondet; Uzbekistan: S. Chibutarov, A. and E. Kreuzberg, and S. Shanazarov; Vietnam: D.A. Nguyen, V.A. Dang, H.V. Dương, L. Ngo, D.-S. Pham, and B.Đ. Trần; L. Monod and V. Vignoli for material from Morocco; D.-Y. Huang for collecting Burmese amber; and the following colleagues, institutions and organizations for facilitating permissions to collect and export material: P. Kanyavong and S.T. Kangnavong (Green Discovery, Laos), Lao Ministry of Natural Resources and Environment Permits 91 and 297; A. Kreuzberg (Institute of Zoology, Uzbek Academy of Sciences, Tashkent) and P. Usmanov (Institute of Physiology and Biophysics, Uzbek Academy of Sciences, Tashkent); D.A. Nguyen, A.T.T. Nguyễn, N.V. Sinh, T.Đ. Bình, S.T. Nguyễn, and D.-S. Pham (Institute of Ecology and Biological Resources, Vietnam Academy of Science and Technology, Hanoi), IEBR Permits 72/STTNSV, 73/STTNSV and 74/STTNSV; B.Đ. Trần and H.V. Dương (Phong Nha-Kẻ Bàng National Park), Vietnam Ministry of Agriculture and Rural Development, General Department of Forestry Collecting Permits 110/TCLN-BTTN and 1643/TCLN-ĐDPH; Vietnamese Ministry of Natural Resources and Environment Export Permit 3493/QĐ-BTNMT; D.-Y. Huang, State Key Laboratory of Palaeobiology and Stratigraphy, Nanjing Institute of Geology and Palaeontology, and Center for Excellence in Life and Palaeoenvironment, Chinese Academy of Sciences, Nanjing; M. Judson, C. Rollard, and E.-A. Leguin (MNHN) for access to the scorpion collection during visits by S.F.L. and L.P.; P.A. Colmenares, O. Delgado, P. Horsley, M.M. Locke, and L. Sorkin for logistical support with collections at the AMNH; D. Harms for covering travel expenses for V.L.E. and assistance with the DAAD for S.F.L.; P. Rubi, C. Sain and T. Sharma for generating some of the DNA sequence data used in the study; S. Thurston for assistance with the plates for this contribution; and I. Magalhães and an anonymous reviewer for constructive comments on a previous draft of the manuscript.

REFERENCES

Ali, J.R., and J.C. Aitchison. 2008. Gondwana to Asia: plate tectonics, paleogeography and the biological connectivity of the Indian sub-continent from the Middle Jurassic through latest Eocene (166–35 Ma). Earth-Science Reviews 88: 145–166.

Assmann, T., et al. 2010. The dark side of relict species biology: cave animals as ancient lineages. *In* J.C. Habel and T. Assmann (editors), Relict species: 91–103. Berlin, Heidelberg: Springer.

Barr, T.C. 1968. Cave ecology and the evolution of troglobites. *In* T. Dobzhansky, M.K. Hecht, and W.C. Steere (editors), Evolutionary biology: 35–102. Boston: Springer.

Bouckaert, R., et al. 2019. BEAST 2.5: An advanced software platform for Bayesian evolutionary analysis. PLoS Computational Biology 15: p.e1006650.

Bryson, R.W., Jr., B.R. Riddle, M.R. Graham, B.T. Smith, and L. Prendini. 2013. As old as the hills: montane scorpions in southwestern North America reveal ancient associations between biotic diversification and landscape history. PLoS One 8: e52822.

Bryson, R.W., Jr., L. Prendini, W.E. Savary, and P.B. Pearman. 2014. Caves as microrefugia: Pleistocene phylogeography of the troglophilic North American scorpion *Pseudouroctonus reddelli*. BMC Evolutionary Biology 14: 1–16.

Chitimia-Dobler, L., et al. 2023. Hard ticks in Burmese amber with Australasian affinities. Parasitology 150: 157–171.

Cock, P.J.A., et al. 2009. Biopython: freely available Python tools for computational molecular biology and bioinformatics. Bioinformatics 25: 1422–1423.

Coddington, J.A., G. Giribet, M.S. Harvey, L. Prendini, and D.E. Walter. 2004. Arachnida. *In* J. Cracraft and M. Donoghue (editors), Assembling the Tree of Life: 296–318. Oxford: Oxford University Press.

Collett, S., S.W. Faryad, and A.M. Mosazai. 2015. Polymetamorphic evolution of the granulite-facies Paleoproterozoic basement of the Kabul Block, Afghanistan. Mineralogy and Petrology 109: 463–484.

Darriba, D., G.L. Taboada, R. Doallo, and D. Posada. 2012. jModelTest 2: more models, new heuristics and parallel computing. Nature Methods 9: 772.

De Francesco Magnussen, I., S.P. Müller, J.U. Hammel, U. Kotthoff, and D. Harms. 2022. Diversity of schizomids (Arachnida: Schizomida) revealed by new fossil genera and species from mid-Cretaceous Burmese amber with implications for a Gondwanan origin of the Burma Terrane. Zoological Journal of the Linnean Society 196: 792–844.

Dimitrov, D., et al. 2012. Tangled in a sparse spider web: single origin of orb weavers and their spinning work unravelled by denser taxonomic sampling. Proceedings of the Royal Society of London B, Biological Sciences 279: 1341–1350.

Dimitrov, D., J.J. Astrin, and B.A. Huber. 2013. Pholcid spider molecular systematics revisited, with new insights into the biogeography and the evolution of the group. Cladistics 29: 132–146.

Drummond, A.J., M.A. Suchard, D. Xie, and A. Rambaut. 2012. Bayesian phylogenetics with BEAUti and the BEAST 1.7. Molecular Biology and Evolution 29: 1969–1973.

Du, S.-Y., et al. 2024. A genome-scale phylogeny of scorpions: model comparison and modeling among-site compositional heterogeneity. Palaeoentomology 7: 792–801.

Dunlop, J.A., and D. Penney. 2012. Fossil arachnids, monograph series vol. 2. Manchester, UK: Siri Scientific Press.

Duong, V.-T., et al. 2025. Genetic diversity of scorpions in Thien Duong and Tien Son caves base on mitochondrial COI gene analysis. Vietnam Journal of Biotechnology 23 (3): 403–414.

Fet, V. 2000. Family Pseudochactidae Gromov, 1998. *In* V. Fet, W.D. Sissom, G. Lowe, and M.E. Braunwalder, Catalog of the scorpions of the world (1758–1998): 426. New York: New York Entomological Society.

Fet, V., M.E. Soleglad, and A.V. Gromov. 2004. The platypus of a scorpion: the genus *Pseudochactas* Gromov, 1998 (Scorpiones: Pseudochactidae). Euscorpius 17: 61–68.

Fitch, W.M. 1971. Toward defining the course of evolution: minimum change for a specific tree topology. Systematic Zoology 20: 406–416.

Folmer, O., M.B. Black, W. Hoch, R.A. Lutz, and R.C. Vrijehock. 1994. DNA primers for amplification of mitochondrial Cytochrome *c* Oxidase subunit I from diverse metazoan invertebrates. Molecular Marine Biology and Biotechnology 3: 294–299.

Geißler, C., U. Kotthoff, J.U. Hammel, M.S. Harvey, and D. Harms. 2022 The first fossil of the pseudoscorpion family Ideoroncidae (Arachnida: Pseudoscorpiones): a new taxon from the mid-Cretaceous of northern Myanmar. Cretaceous Research 130: 105030.

Giribet, G., S. Carranza, J. Baguña, M. Riutort, and C. Ribera. 1996. First molecular evidence for the existence of a Tardigrada + Arthropoda clade. Molecular Biology and Evolution 13: 76–84.

Goloboff, P.A. 1993. Estimating character weights during tree search. Cladistics 9: 83–91.

Goloboff, P.A., and M.E. Morales. 2023. TNT version 1.6, with a graphical interface for MacOS and Linux, including new routines in parallel. Cladistics 39: 144–153.

Goloboff, P.A., J.S. Farris, and K.C. Nixon. 2003. TNT: tree analysis using new technology. Computer software and documentation, available online (https://cladistics.org/tnt).

Goloboff, P.A., J.S. Farris, and K.C. Nixon. 2008. TNT, a free program for phylogenetic analysis. Cladistics 24: 774–786.

Gromov, A.V. 1998. [A new family, genus and species of scorpions (Arachnida, Scorpiones) from southern Central Asia]. Zoologicheskii Zhurnal 77: 1003–1008. [in Russian, English summary; English translation: Russian Journal of Zoology 2: 409–413]

Guindon, S., and O. Gascuel. 2003. A simple, fast, and accurate algorithm to estimate large phylogenies by maximum likelihood. Systematic Biology 52: 696–704.

Harrison, R.G., D.M. Rand, and W.C. Wheeler 1987. Mitochondrial DNA variation in field crickets across a narrow hybrid zone. Molecular Biology and Evolution 24: 363–371.

Heine, C., R.D. Müller, and C. Gaina. 2004. Reconstructing the lost eastern Tethys Ocean basin: convergence history of the SE Asian margin and marine gateways. *In* P. Clift, W. Kuhnt, P. Wang, and D. Hayes (editors), Continent-ocean interactions within East Asian marginal seas. Geophysical Monograph Series 149: 37–54.

Howarth, F.G. 1973. The cavernicolous fauna of Hawaiian lava tubes, 1. Introduction. Pacific Insects 15: 139–151.

Ji, Y.-J., D.-X. Zhang, and L.-J. He. 2003. Evolutionary conservation and versatility of a new set of primers for amplifying the ribosomal internal transcribed spacer regions in insects and other invertebrates. Molecular Ecology Notes 3, 581–585.

Johnson, J., S.F. Loria, M.M. Joseph, and D. Harms. 2022. Biogeographical and diversification analyses of Indian pseudoscorpions reveal the Western Ghats as museums of ancient biodiversity. Molecular Phylogenetics and Evolution 175: 107495.

Johnson, J., et al. 2023. First record of the pseudoscorpion tribe Tyrannochthoniini Chamberlin, 1962 from mid-Cretaceous Burmese amber of northern Myanmar (Pseudoscorpiones: Chthoniidae: Chthoniinae). Cretaceous Research 144: 105459.

Jouault, C., V. Perrichot, and A. Nel. 2021. New flat wasps from mid-Cretaceous Burmese amber deposits highlight the bethylid antiquity and paleobiogeography (Hymenoptera: Chrysidoidea). Cretaceous Research 123: 104772.

Juan, C., M.T. Guzik, D. Jaume, and S.J. Cooper. 2010. Evolution in caves: Darwin's 'wrecks of ancient life' in the molecular era. Molecular Ecology 19: 3865–3880.

Katoh, K., and D.M. Standley. 2013. MAFFT multiple sequence alignment software, version 7: improvements in performance and usability. Molecular Biology and Evolution 30: 772–780.

Katoh, K., K. Misawa, K.I. Kuma, and T. Miyata. 2002. MAFFT: a novel method for rapid multiple sequence alignment based on fast Fourier transform. Nucleic Acids Research 30: 3059–3066.

Kocher, T.D., et al. 1989. Dynamics of mitochondrial DNA evolution in animals: amplification and sequencing with conserved primers. Proceedings of the National Academy of Sciences of the United States of America 86: 6196–6200.

Kumar, S., G. Stecher, M. Li, C. Knyaz, and K. Tamura. 2018. MEGA X: molecular evolutionary genetics analysis across computing platforms. Molecular Biology and Evolution 35: 1547–1549.

Lamoral, B.H. 1980. A reappraisal of the suprageneric classification of Recent scorpions and their zoogeography. *In* J. Grube (editor), Verhandlungen 8. Internationaler Arachnologen-Kongress abgehalten an der Universität für Bodenkultur, Wien, 7–12 Juli, 1980: 439–444. Vienna: H. Egermann.

Lewis, P.O. 2001. A likelihood approach to estimating phylogeny from discrete morphological character data. Systematic Biology 50: 913–925.

Li, X., et al. 2023. Reconstruction of the proto-type basin and tectono-paleogeography of Tarim Block in the Mesozoic. Frontiers in Earth Science 11: 1121428.

Li, Y.P., A.C. Robinson, M. Gadoev, and I. Oimuhammadzoda. 2020. Was the Pamir salient built along a Late Paleozoic embayment on the southern Asian margin? Earth and Planetary Science Letters 550: 116554.

Loria, S.F., and L. Prendini. 2020. Out of India, thrice: diversification of Asian forest scorpions reveals three colonizations of Southeast Asia. Scientific Reports 10: 1–19.

Loria, S.F., and L. Prendini. 2021. Burrowing into the forest: phylogeny of the Asian forest scorpions (Scorpionidae: Heterometrinae) and the evolution of ecomorphotypes. Cladistics 37: 109–161

Loria, S.F., V.L. Ehrenthal, D.A. Nguyen, and L. Prendini. 2022. Climate relicts: Asian scorpion family Pseudochactidae survived Miocene aridification in caves of the Annamite Mountains. Insect Systematics and Diversity 6: 3.

Lourenço, W.R. 2000. Panbiogéographie, les familles des scorpions et leur répartition géographique. Biogeographica (Paris) 76: 21–39.

Lourenço, W.R. 2007. First record of the family Pseudochactidae Gromov (Chelicerata, Scorpiones) from Laos and new biogeographic evidence of a Pangaean palaeodistribution. Comptes Rendus Biologies 330: 770–777.

Lourenço, W.R. 2012. The genus *Vietbocap* Lourenço and Pham, 2010 (Scorpiones: Pseudochactidae); proposition of a new subfamily and description of a new species from Laos. Comptes Rendus Biologies 335: 232–237.

Lourenço, W.R. 2015. An unusual new species of *Chaerilobuthus* Lourenço and Beigel, 2011 (Scorpiones: Chaerilobuthidae) from the Cretaceous amber of Myanmar (Burma). Arachnida – Rivista Aracnologica Italiana 5: 44–48.

Lourenço, W.R. 2017. Second record of the genus *Troglokhammouanus* Lourenço, 2007 from Laos, with the description of a new species (Scorpiones: Pseudochactidae). Acta Arachnologica 66: 19–24.

Lourenço, W.R. 2018. Further data on the genus *Chaerilobuthus* Lourenço et Beigel, 2011 (Scorpiones: Chaerilobuthidae) from Cretaceous Burmite and description of a new species. Arachnida – Rivista Aracnologica Italiana 19: 2–13.

Lourenço, W.R., and A. Beigel. 2011. A new scorpion fossil from the Cretaceous amber of Myanmar (Burma). New phylogenetic implications. Comptes Rendus Palevol 10: 635–639.

Lourenço W.R., and D.-S. Pham. 2010. A remarkable new cave scorpion of the family Pseudochactidae Gromov (Chelicerata, Scorpiones) from Vietnam. ZooKeys 71: 1–13.

Lourenço, W.R., and D.-S. Pham. 2012. A second species of *Vietbocap* Lourenço and Pham, 2010 (Scorpiones: Pseudochactidae) from Vietnam. Comptes Rendus Biologies 335: 80–85.

Lourenço, W.R., and J. Velten. 2015. Another new species of *Chaerilobuthus* Lourenço and Beigel, 2011 (Scorpiones: Chaerilobuthidae) from the Cretaceous

amber of Myanmar (Burma). Arachnida – Rivista Aracnologica Italiana 5: 2–8.

Lourenço, W.R., and J. Velten. 2019. One more contribution to the knowledge of Cretaceous Burmese amber scorpions: description of one new species of *Chaerilobuthus* Lourenço et Beigel, 2011 (Scorpiones: Chaerilobuthidae). Arachnida – Rivista Aracnologica Italiana 25: 2–10.

Lourenço, W.R., and J. Velten. 2020. A new contribution to the knowledge of Cretaceous Burmese amber scorpions with the descriptions of two new genera and two new species (Scorpiones: Chaerilobuthidae; Palaeoeuscorpiidae: Archaeoscorpiopinae). Arachnida – Rivista Aracnologica Italiana 28: 34–50.

Lourenço, W.R., and J. Velten. 2021. Early Cretaceous Burmite fossils of the genus *Chaerilobuthus* Lourenço and Beigel, 2011 (Scorpiones: Chaerilobuthidae) and description of a particular new species. Faunitaxys 9: 1–5.

Lourenço, W.R., and J. Velten. 2022. The remarkable variability of the genus *Chaerilobuthus* Lourenço and Beigel, 2011 (Scorpiones: Chaerilobuthidae) and description of a new species from Early Cretaceous Burmite. Faunitaxys 10: 1–6.

Lourenço, W.R., and J. Velten. 2025. Description of a second species for the genus *Serratochaerilobuthus* Lourenço, 2024 (Scorpiones: Chaerilobuthidae). Faunitaxys 13 (10): 1–6.

Lourenço, W.R., D.S. Pham, and T.H. Tran. 2018. The genus *Vietbocap* Lourenço and Pham, 2010 in the Thien Duong cave, Vietnam: a possible case of subterranean speciation in scorpions (Scorpiones: Pseudochactidae). Comptes Rendus Biologies 341: 264–273.

Maddison, W.P., and D.R. Maddison. 2025. Mesquite: a modular system for evolutionary analysis. Version 4.0. Computer software and documentation. Available online (http://www.mesquiteproject.org).

Massana, K.A., J.M. Beaulieu, N.J. Matzke, and B.C. O'Meara. 2015. Non-null effects of the null range in biogeographic models: exploring parameter estimation in the DEC model. BioRxiv: 026914.

Matzke, N.J. 2013a. BioGeoBEARS: Biogeography with Bayesian (and likelihood) evolutionary analysis in R scripts. R Package, version 0.2.1. Available online (http://CRAN.R-project.org/package=BioGeoBEARS).

Matzke, N.J. 2013b. Probabilistic historical biogeography: new models for founder-event speciation, imperfect detection, and fossils allow improved accuracy and model-testing. Frontiers in Biogeography 5: 242–248.

Matzke, N.J. 2014. Model selection in historical biogeography reveals that founder-event speciation is a crucial process in island clades. Systematic Biology 63: 951–970.

Matzke, N.J. 2022. Statistical comparison of DEC and DEC+ J is identical to comparison of two ClaSSE submodels, and is therefore valid. Journal of Biogeography 49: 1805–1824.

Metcalfe, I. 2011. Tectonic framework and Phanerozoic evolution of Sundaland. Gondwana Research 19: 3–21.

Metcalfe, I. 2013. Gondwana dispersion and Asian accretion: tectonic and palaeogeographic evolution of eastern Tethys. Journal of Asian Earth Sciences 66: 1–33.

Miller, M.A., et al. 2015. A RESTful API for access to phylogenetic tools via the CIPRES science gateway. Evolutionary Bioinformatics 11: EBOS21501.

Montenat, C. 2009. The Mesozoic of Afghanistan. GeoArabia 14: 147–210.

Nga, P.T., et al. 2026. Paleoclimate variation during the Cretaceous revealed by geochemical and mineralogical analyses from continental sediments in northern Vietnam. Cretaceous Research 179: 106246.

Niemiller, M.L., B.M. Fitzpatrick, and B.T. Miller. 2008. Recent divergence with gene flow in Tennessee cave salamanders (Plethodontidae: *Gyrinophilus*) inferred from gene genealogies. Molecular Ecology 17: 2258–2275.

Nixon, K.C. 2002. WinClada, ver. 1.00.08. Computer software and documentation. Available online (http://www.diversityoflife.org/winclada).

Nunn, G.B., B.F. Theisen, B. Christensen, and P. Arctander. 1996. Simplicity-correlated size growth of the nuclear 28S ribosomal RNA D3 expansion segment in the crustacean order Isopoda. Journal of Molecular Evolution 42: 211–223.

Oksanen, J., et al. 2020. vegan: community ecology package. R package version 2.5-7. Available online (https://CRAN.R-project.org/package=vegan).

Ojanguren-Affilastro, A.A., et al. 2016. Phylogeny, species delimitation and convergence in the South American bothriurid scorpion genus *Brachistosternus* Pocock 1893: integrating morphology, nuclear and mitochondrial DNA. Molecular Phylogenetics and Evolution 94: 159–170.

Paradis, E., J. Claude, and K. Strimmer. 2004. APE: analyses of phylogenetics and evolution in R language. Bioinformatics 20: 289–290.

Poinar, G. Jr. 2018. Burmese amber: evidence of Gondwanan origin and Cretaceous dispersion. Historical Biology 31: 1304–1309.

Prendini, L. 2000. Phylogeny and classification of the superfamily Scorpionoidea Latreille 1802 (Chelicerata, Scorpiones): an exemplar approach. Cladistics 16: 1–78.

Prendini, L. 2001. Substratum specialization and speciation in southern African scorpions: the Effect Hypothesis revisited. *In* V. Fet and P.A. Selden (editors), Scorpions 2001: in memoriam Gary A. Polis. British Arachnological Society: 113–138. Burnham Beeches, Bucks, U.K.: British Arachnological Society.

Prendini, L. 2004. Systematics of the genus *Pseudolychas* Kraepelin (Scorpiones: Buthidae). Annals of the Entomological Society of America 97: 37–63.

Prendini, L., T.M. Crowe, and W.C. Wheeler. 2003. Systematics and biogeography of the family Scorpionidae (Chelicerata: Scorpiones), with a discussion on phylogenetic methods. Invertebrate Systematics 17: 185–259.

Prendini, L., P. Weygoldt, and W.C. Wheeler. 2005. Systematics of the *Damon variegatus* group of African whip spiders (Chelicerata: Amblypygi): evidence from behaviour, morphology and DNA. Organisms, Diversity and Evolution 5: 203–236.

Prendini, L., E.S. Volschenk, S. Maaliki, and A.V. Gromov. 2006. A 'living fossil' from Central Asia: the morphology of *Pseudochactas ovchinnikovi* Gromov, 1998 (Scorpiones: Pseudochactidae), with comments on its phylogenetic position. Zoologischer Anzeiger 245: 211–248.

Prendini, L., V.L. Ehrenthal, and S.F. Loria. 2021. Systematics of the relictual Asian scorpion family Pseudochactidae Gromov, 1998, with a review of cavernicolous, troglobitic, and troglomorphic scorpions. Bulletin of the American Museum of Natural History 453: 1–149.

R Core Team. 2023. R: a language and environment for statistical computing. R Foundation for Statistical Computing, Vienna, Austria. Available online (https://www.R-project.org).

Rambaut, A., M.A. Suchard, D. Xie, and A.J. Drummond. 2014. Tracer 1.6. Available online (http://beast.bio.ed.ac.uk/tracer).

Ramírez, M.J. and P. Michalik. 2014. Calculating structural complexity in phylogenies using ancestral ontologies. Cladistics 30: 635–649.

Ree, R. H. and I. Sanmartín. 2018. Conceptual and statistical problems with the DEC+ J model of founder-event speciation and its comparison with DEC via model selection. Journal of Biogeography, 45: 741–749.

Revell, L.J. 2012. phytools: an R package for phylogenetic comparative biology (and other things). Methods in Ecology and Evolution 3: 217–223.

Robinson, A.C. 2015. Mesozoic tectonics of the Gondwanan terranes of the Pamir Plateau. Journal of Asian Earth Sciences 102: 170–179.

Romero, A., and S.M. Green. 2005. The end of regressive evolution: examining and interpreting the evidence from cave fishes. Journal of Fish Biology 67: 3–32.

Ronquist, F., and J.P. Huelsenbeck. 2003. MrBayes 3: Bayesian phylogenetic inference under mixed models. Bioinformatics 19: 1572–1574.

Röschmann, L.M., et al. 2024. First fossil species of family Hyidae (Arachnida: Pseudoscorpiones) confirms 99 million years of ecological stasis in a Gondwanan lineage. PeerJ 12: e17515.

Santibáñez-López, C.E., O.F. Francke, and L. Prendini. 2014. Phylogeny of the North American scorpion genus *Diplocentrus* Peters, 1861 (Scorpiones: Diplocentridae) based on morphology, nuclear and mitochondrial DNA. Arthropod Systematics and Phylogeny 72: 257–279.

Santibáñez-López, C.E., E. González-Santillán, L. Monod, and P.P. Sharma. 2019. Phylogenomics facilitates stable scorpion systematics: reassessing the relationships of Vaejovidae and a new higher-level classification of Scorpiones (Arachnida). Molecular Phylogenetics and Evolution 135: 22–30.

Santibáñez-López, C.E., A.A.Ojanguren-Affilastro, M.R. Graham, and P.P. Sharma. 2023. Congruence between ultraconserved element-based matrices and phylotranscriptomic datasets in the scorpion Tree of Life. Cladistics 39 (6): 533–547.

Sharma, P.P., R. Fernández, L.A. Esposito, E. González-Santillán, and L. Monod. 2015a. Phylogenomic resolution of scorpions reveals multilevel discordance with morphological phylogenetic signal. Proceedings of the Royal Society of London B, Biological Sciences 282: 20142953.

Sharma, P.P., M.A. Santiago, E. González-Santillán, L. Monod, and W.C. Wheeler. 2015b. Evidence of duplicated Hox genes in the most recent common ancestor of extant scorpions. Evolution and Development 17: 347–355.

Sharma, P.P., et al. 2018. A revised dated phylogeny of scorpions: phylogenomic support for ancient divergence of the temperate Gondwanan family Bothriuridae. Molecular Phylogenetics and Evolution 122: 37–45.

Siehl, A. 2017. Structural setting and evolution of the Afghan orogenic segment – a review. *In* M.-F. Brunet, T. McCann, E.R. Sobel (editors), Geological evolution of Central Asian basins and the Western

Tien Shan Range: 57–88. London: Geological Society, Special Publication 427.

Simon, C., A. Francke, and A. Martin. 1991. The polymerase chain reaction: DNA extraction and amplification. *In* G. Witt, A. Johnson, and J. Young (editors), Molecular techniques in taxonomy: 329–355. New York: Springer.

Soleglad, M.E., and V. Fet. 2001. Evolution of scorpion orthobothriotaxy – a cladistic approach. Euscorpius 1: 1–38.

Soleglad, M.E., and V. Fet. 2003a. High-level systematics and phylogeny of the extant scorpions (Scorpiones: Orthosterni). Euscorpius 11: ii + 1–175.

Soleglad, M.E., and V. Fet. 2003b. The scorpion sternum: structure and phylogeny (Scorpiones: Orthosterni). Euscorpius 5: 1–34.

Soleglad, M.E., and W.D. Sissom. 2001. Phylogeny of the family Euscorpiidae Laurie, 1896: a major revision. *In* V. Fet and P.A. Selden (editors), Scorpions 2001: in memoriam Gary A. Polis: 25–111. Burnham Beeches, Bucks, U.K.: British Arachnological Society.

Soleglad, M.E., F. Kovařík, and V. Fet. 2012. A new species of *Pseudochactas* from Afghanistan (Scorpiones: Pseudochactidae). Boletín de la Sociedad Entomológica Aragonesa 50: 89–98.

Stamatakis, A. 2006. RAxML-VI-HPC: maximum likelihood-based phylogenetic analyses with thousands of taxa and mixed models. Bioinformatics 22: 2688–2690.

Stamatakis, A. 2014. RaxML version 8: a tool for phylogenetic analysis and post-analysis of large phylogenies. Bioinformatics 30: 1312–1313.

Stecher, G., K. Tamura, and S. Kumar. 2020. Molecular evolutionary genetics analysis (MEGA) for macOS. Molecular Biology and Evolution 37: 1237–1239.

Stockwell, S.A. 1989. Revision of the phylogeny and higher classification of scorpions (Chelicerata). Ph.D. dissertation, University of California, Berkeley.

Tamura, K., G. Stecher, and S. Kumar. 2021. MEGA11: molecular evolutionary genetics analysis, version 11. Molecular Biology and Evolution 38: 3022–3027.

Tamura, K., M. Nei, and S. Kumar. 2004. Prospects for inferring very large phylogenies by using the neighbor-joining method. Proceedings of the National Academy of Sciences of the United States of America 101: 11030–11035.

Tamura, K., G. Stecher, D. Peterson, A. Filipski, and S. Kumar. 2013. MEGA6: molecular evolutionary genetics analysis, version 6.0. Molecular Biology and Evolution 30: 2725–2729.

Tang, V. 2022. A new scorpion genus and species from China, *Qianxie solegladi* gen. et sp. n. (Scorpiones: Pseudochactidae). Euscorpius 351: 1–19.

Valdez-Cruz, N.A., et al. 2004. Biochemical, genetic and physiological characterization of venom components from two species of scorpions: *Centruroides exilicauda* Wood and *Centruroides sculpturatus* Ewing. Biochimie 86: 387–396.

Villesen, P. 2007. FaBox: an online toolbox for fasta sequences. Molecular Ecology Notes 7: 965–968.

Wessel, A., P. Erbe, and H. Hoch. 2007. Pattern and process: evolution of troglomorphy in the cave-planthoppers of Australia and Hawai'i – preliminary observations (Insecta: Hemiptera: Fulgoromorpha: Cixiidae). Acta Carsologica 36: 199–206.

Westerweel, J., et al. 2019. Burma Terrane part of the Trans-Tethyan arc during collision with India according to palaeomagnetic data. Nature Geoscience 12: 863–868.

Wheeler, W.C., P. Cartwright, and C. Hayashi. 1993. Arthropod phylogeny: a combined approach. Cladistics 9: 1–39.

Wickham, H. 2016. ggplot2: elegant graphics for data analysis. New York: Springer.

Wood, H.M., and J. Wunderlich. 2023. Burma Terrane amber fauna shows connections to Gondwana and transported Gondwanan lineages to the Northern Hemisphere (Araneae: Palpimanoidea). Systematic Biology 72: 1233–1246.

Wriedt, A.L., M.S. Harvey, J.U. Hammel, U. Kotthoff, and D. Harms. 2021. The second chthonioid pseudoscorpion (Pseudoscorpiones: Chthoniidae) from mid-Cretaceous Burmese amber: a new genus with unique morphological features and potential Gondwanan affinities. Journal of Arachnology 48: 311–321.

Xing, Lida, E.L. Stanley, M. Bai, and D.C. Blackburn. 2018. The earliest direct evidence of frogs in wet tropical forests from Cretaceous Burmese amber. Scientific Reports 8: 8770.

Xuan, Q., L. Prendini, M.S. Engel, C. Cai, and D. Huang. 2025. Extinct scorpion family Chaerilobuthidae from mid-Cretaceous Burmese amber reinterpreted as subfamily of extant family Pseudochactidae (Chelicerata: Scorpiones). Zoological Journal of the Linnean Society 203: p.zlae169.

Zhang, J.E., et al. 2017. Early Cretaceous wedge extrusion in the Indo-Burma Range accretionary complex: implications for the Mesozoic subduction of Neotethys in SE Asia. International Journal of Earth Sciences (G.R. Geologische Rundschau) 106: 1391–1408.

APPENDIX 1

Terminal taxa, specimens and tissue samples used for phylogenetic analysis of the relictual Asian scorpion family Pseudochactidae Gromov, 1998. Depositories for material examined abbreviated as follows: Alexander V. Gromov Private Collection (AGPC), Almaty, Kazakhstan; American Museum of Natural History (AMNH), New York, including the Ambrose Monell Cryocollection (AMCC); Institute of Ecology and Biological Resources (IEBR), Vietnamese Academy of Sciences, Hanoi; Museum National d'Histoire Naturelle (MNHN), Paris; Nanjing Institute of Geology and Palaeontology (NIGP) at the Chinese Academy of Sciences, Nanjing; Phong Nha-Kẻ Bàng National Park (PNKB), Bố Trạch, Vietnam. Tissue samples deposited in the Ambrose Monell Collection for Molecular and Microbial Research (AMCC) at the AMNH.

Family Buthidae C.L. Koch, 1837

***Buthus atlantis* Pocock, 1889: MOROCCO: Marrakesh-Safi Region:** *Essaouira Prov.*: Essaouira (Mogador), 4 km S, 31°29′21.7″N 09°46′08.2″W, 3 m, 19.ix.2004, V. Vignoli, 1 ♀ (AMCC [LP 3489]), 1 ♀ (AMCC [LP 3559]), 1 ♀ (AMCC [LP 3571]). Road between Oualidia and Essaouira, 31°38′10.5″N 09°39′45.7″W, 9 m, 24.iii.2003, L. Monod and P. Jenkins, 1 juv. (AMCC [LP 2989]). *Tiznit Prov.*: N of Ouglou Plage [29°48′32.7″N 09°49′47.2″W], 20 km W of Tiznit, 17 m, 17.ix.2004, V. Vignoli, 1 ♂ (AMCC [LP 3570]), 1 ♀ (AMCC [LP 3560]).

Family Chaerilidae Pocock, 1893

***Chaerilus sejnai* Kovařík, 2005: MALAYSIA: Pahang:** *Rompin Distr.*: Tioman Island, near Paya, iv.2002, V. Šejna, paratype ♂, paratype ♀ (CAS 9039962), 1 ex. (AMCC [LP 3685]); Pulau Tioman (Tioman Island), trail between Kampung Genting and Kampung Paya, 02°46′25.6″N 104°07′11.9″E, 35 m, 11.vi.2013, L. Prendini and S.F. Loria, primary rainforest close to seashore, moderately open canopy, sparse understorey, moderate leaf litter layer, many large granite boulders, brownish-orange, clayey granitic loam, under fallen palm log near path, among leaf litter, 1 ♂, 1 ♀ (AMNH), 02°46′43.4″N 104°07′08.2″E, 31 m, 12.vi.2013, L. Prendini and S.F. Loria, primary rainforest close to seashore, moderately open canopy, sparse understory, moderate leaf litter layer, many large granite boulders, brownish-orange, clayey granitic loam, under stone on leaf litter-covered slope, 1 ♀ (AMCC [LP 11962]).

Family Pseudochactidae Gromov, 1997

Subfamily †Chaerilobuthinae Lourenço and Beigel, 2011

†*Chaerilobuthus bruckschi* Lourenço, 2015: MYANMAR: Kachin State: Noije Bum near Hukawng Valley [ca. 26°14′51.1″N 96°33′22.5″E], Cretaceous (Cenomanian) burmite: 1 juv. [sex unknown], dextral pedipalp patella and chela absent (NIGP 201161), 1 juv. [sex unknown] (NIGP 201162).

†*Chaerilobuthus complexus* Lourenço and Beigel, 2011: MYANMAR: Kachin State: Noije Bum near Hukawng Valley [ca. 26°14′51.1″N 96°33′22.5″E], Cretaceous (Cenomanian) burmite: 1 juv. [sex unknown], mesosomal segments IV, V and telson absent (NIGP 200655), 1 juv. [sex unknown], sinistral pedipalp absent (NIGP 201160).

†*Chaerilobuthus enigmaticus* Lourenço, 2015: MYANMAR: Kachin State: Noije Bum near Hukawng Valley [ca. 26°14′51.1″N 96°33′22.5″E], Cretaceous (Cenomanian) burmite: 2 juv. [sex unknown] (NIGP 201158, 201159).

†*Chaerilobuthus gigantosternum* Lourenço, 2016: MYANMAR: Kachin State: Noije Bum near Hukawng Valley [ca. 26°14′51.1″N 96°33′22.5″E], Cretaceous (Cenomanian) burmite: first instar juv. [sex unknown] (NIGP 200654).

†***Chaerilobuthus hansgeorgmuelleri*** **Lourenço, 2019: MYANMAR: Kachin State:** Noije Bum near Hukawng Valley [ca. 26°14′51.1″N 96°33′22.5″E], Cretaceous (Cenomanian) burmite: 1 subad. [sex unknown], mesosoma and metasoma absent (NIGP 201164).

†***Chaerilobuthus knodelorum*** **Lourenço, 2018: MYANMAR: Kachin State:** Noije Bum near Hukawng Valley [ca. 26°14′51.1″N 96°33′22.5″E], Cretaceous (Cenomanian) burmite: 1 juv. [♀?], metasomal segment IV and telson absent (NIGP 200657).

†***Chaerilobuthus serratus*** **Lourenço, 2016: MYANMAR: Kachin State:** Noije Bum near Hukawng Valley [ca. 26°14′51.1″N 96°33′22.5″E], Cretaceous (Cenomanian) burmite: 2 juv. [sex unknown] (NIGP 200656, 201163).

Subfamily Pseudochactinae Gromov, 1997

Pseudochactas ovchinnikovi **Gromov, 1998: TAJIKISTAN:** *Leninskii Distr.*: Aruktau Mt. Range, near Gandzhina village [37°58′N 68°34′E], 10.iv.1988, S.L. Zonstein and A.S. Zorkin, paratype ♀ (AGPC). **UZBEKISTAN: Surkhandarya Region:** *Uzun Distr.*: Okmachit [Ak-Mechet], ca. 7 km W–4 km WSW, E slope of Babatag Mt. Range, 38°02′50″N 68°14′22″E–38°01′45″N 68°15′30″E, 760–1010 m, 29.iv–9.v.1994, A.V. Gromov and S.V. Ovchinnikov, 2 ♀, 3 subad. ♂ paratypes (AGPC), 1 ♀, 6 juv. (AGPC); Okmachit, ca. 7 km W, E slope of Babatag Mt. Range, 38°02′50″N 68°14′22″E, ca. 1010 m, 13.v.1995, O.V. Lyakhov, 2 juv. (AGPC); Okmachit, ca. 6.5–7 km W, E slope of Babatag Mt. Range, 38°02′50″N 68°14′22″E–38°02′04″N 68°14′51″E, 905–1010 m, 30.iv–2.v.2002, A.V. Gromov, 6 ♀, 7 subad. ♂, 1 subad. ♀, 26 juv. (AGPC); Okmachit, ca. 5 km WSW, E slope of Babatag Mt. Range, 38°02′26″N 68°14′59″E–38°02′01″N 68°15′08″E, 760–830 m, 3.v.2002, A.V. Gromov, 1 ♀ 10 juv. (AGPC); Okmachit, ca. 5–6 km WSW, E slope of Babatag Mt. Range, 38°02′01″N 68°14′03″E–38°01′36″N 68°15′00″E, 730–870 m, 4.v.2002, A.V. Gromov, 1 ♂, 1 subad. ♂ (AMNH), 3 ♀, 16 subad. ♂, 1 subad. ♀, 67 juv. (AGPC); Dikhana [Dukhana] Canyon, foothills of E slopes of Babatag Mountain Range, ca. 5 km WSW of Akmechet village, 38°01′38.3″N 68°15′11.9″E, 722 m, 20–24.v.2003, L. Prendini and A.V. Gromov, UV detection on earthen walls and rocky slopes along riverbanks and canyon walls through mountains, hard clayey soil, short grass cover with small trees and shrubs, 9 ♀, 9 subad. ♂, 3 subad. ♀, 18 juv. ♂, 10 juv. ♀ (AMNH), 3 juv. ♀ (AMCC 159928 [LP 2303A–C]); Dikhana Canyon, ca. 5.5 km WSW of Okmachit, E slope of Babatag Mt. Range, 38°01′33″N 68°14′26″E, ca. 774 m, 22.v.2003, A.V. Gromov and L. Prendini, 1 juv. (AGPC).

Qianxie solegladi **Tang, 2022: CHINA: Sichuan Prov.:** *Ningnan Co.*: between Hujia Wanzi and Leijiabazi, 27°11′09″N 102°36′56″E, 6.iii.2024, Y. Li, 1 ♀ (AMCC [LP 20856]).

Subfamily Troglokhammouaninae Lourenço, 2007

Troglokhammouanus steineri **Lourenço, 2007: LAOS: Khammouane Prov.:** *Boualapha Distr.*: Hin Namno National Biodiversity Conservation Area: Boualapha, Tham Xe Bangfai [cave], Ban Nong Ping, 17°22′19.8″N 105°40′18.6″E, 14.ii.2007, H. Steiner, mid-section [of cave], on sand, holotype ♀ (MNHN RS 9098); Tham Xe Bang Fai (Xe Bang Fai River Cave), 17°22′23.6″N 105°50′11.8″E, 159 m, left bank of Xe Bang Fai River (coming from downstream entrance): 19.ii.2012, L. Prendini and P. Kanyavong, very steep muddy beach on riverbank, with few cracks and no debris, UV detection, specimen on mud bank, 1 ♂ (AMNH), muddy beach on riverbank, with moderate to steep mud bank with few rocks, UV detection, all specimens on moist mud bank, 2 ♀, 1 subad. ♂, 4 juv. ♂, 1 juv. ♀ (AMNH), rocky beach of riverbank at base of "Stairway to Heaven," with little mud except at base of rocks close to river, UV detection, 1 ♀, several imm. on moist mud, 1 imm. among vegetative debris

caught between rocks, none on dry sand or rocks, 1 ♀, 1 subad. ♀, 3 juv. ♂, 3 juv. ♀, pair of pedipalp chelae (AMNH), 1 juv. ♀ (AMCC [LP 11275]), 19–21.ii.2012, L. Prendini, P. Kanyavong and W. Phimmathong, rocky beach on riverbank, with extensive mud and sand banks in places, UV detection, specimens mostly on mud banks, almost all on moist soil, 5 ♂, 9 ♀, 4 subad. ♂, 9 juv. ♂, 4 juv. ♀, dextral pedipalp femur and patella (AMNH), 1 juv. ♂ (AMCC [LP 11273]), 20.ii.2012, L. Prendini and P. Kanyavong, in twilight zone at cave entrance, muddy beach on riverbank, UV detection at night, specimens sitting on muddy banks (none collected at this site during daylight), 2 ♀ (AMNH), 20–21.ii.2012, L. Prendini, P. Kanyavong and W. Phimmathong, large sandy beach of riverbank, midway through cave [type locality], with muddy bank immediately along river and muddy patches in several depressions further from river edge, UV detection, all specimens collected on moist muddy soil, some among vegetative debris (sticks, etc.) trapped between stones, others sitting in open on mud, one in mud cracks, one below stone, 7 ♀, 1 juv. ♀ (AMNH), 1 juv. ♀ (AMCC [LP 11272]); right bank of Xe Bang Fai River (coming from downstream entrance): 19–20.ii.2012, L. Prendini and P. Kanyavong, muddy beach of riverbank at bottom of "Balcony Passage," ca. 300–500 m from downstream entrance of cave, UV detection during day: specimens very common on moist mud banks, mostly in cracks between drying mud slabs or among sticks and other vegetative debris caught between rocks, all collected on moist soil, none on dry sand banks higher upslope; UV detection at night: several ♂♂ sitting on flowstone rock faces, several ♀♀ and juv. on mud banks and cracked clay, 1 ♂ partly cannibalized by ♀, 2 ♂ (1 ♂ partially predated), 22 ♀, 2 subad. ♂, 4 subad. ♀, 5 juv. ♂, 7 juv. ♀, carapace and sinistral pedipalp chela (AMNH), 1 juv. ♀ (AMCC [LP 11271]), 19–21.ii.2012, L. Prendini, P. Kanyavong, and W. Phimmathong, muddy beach of riverbank between "Balcony Passage" and "Stairway to Heaven," steep and dry with little cracked mud, relatively few rocks with trapped vegetative debris, UV detection, specimens uncommon, mostly on mud close to river edge, few higher upslope against cave walls, near moist flowstone, all specimens collected on moist mud surfaces, none on dry sand, 1 ♂, 7 ♀ (AMNH), 20.ii.2012, L. Prendini and P. Kanyavong, rocky beach of riverbank before second rapids, UV detection, several adult ♀♀ and imm. on mud bank or in rock crevices close to river, none on dry soil higher upslope, 5 ♀, 1 subad. ♀, 1 juv. ♂ (AMNH), 20–21.ii.2012, L. Prendini, P. Kanyavong and W. Phimmathong, rocky/muddy beach of riverbank before "Stairway to Heaven," UV detection, several ♀♀ and imm. on muddy banks or among trapped vegetative debris between rocks, none on dry sand, 1 ♂, 4 ♀, 4 subad. ♂, 1 subad. ♀, 2 juv. ♂, 8 juv. ♀ (AMNH), 1 juv. (AMCC [LP 11274]), 21.ii.2012, L. Prendini and W. Phimmathong, Oxbow Lake, rocky beach on riverbank, UV detection, specimens on rocky shore, 2 ♀, 1 subad. ♂, dextral pedipalp chela (AMNH).

Subfamily Vietbocapinae
Lourenço and Pham, 2010

***Aemngvantom lao* (Lourenço, 2012): LAOS: Khammouane Prov.:** *Gnommalath Distr.*: Grotte Tham Nam Lot au NO de Ban Naden (village) [Ban Naden, Tham Nam Lot (cave)], 17°30′18″N 105°23′08″E, 176 m, 8.xi.2011, L. Deharveng and A. Bedos, 350–450 m from main cave entrance, collected by hand, Lao11-46, 1 juv. ♀ holotype (MNHN RS 9096), 1 juv. ♀ paratype (MNHN RS 9097); Tham Nam Lot (Lod) near Ban Naden village, 17°30′13.8″N 105°23′09.2″E, 260 m, 13–14.vi.2012, L. Prendini, S.F. Loria and P. Kanyavong, limestone cave in primary rainforest at base of limestone mountain, fairly moist cave with pools of water in places, entrances on both sides of mountain, specimens collected with UV light detection ca. midday, uncommon, taken mostly 300–400 m (roughly halfway) from main entrance in dark zone, mostly in moist areas, sitting in crevices in mud walls below flowstone walls, 1 ♀ running on surface, several specimens

(including 1 ♂) in mud walls of side room, 2 ♂, 3 ♀, 1 subad. ♂, 3 subad. ♀, 3 juv. ♂, 7 juv. ♀ (AMNH), 2 juv. ♀ (AMCC [LP 11349, 11350]); Tham Nam Lot (Lod), near Ban Naden Village, inside cave, 17°30′13.8″N 105°23′09.2″E, 260 m, 19.v.2018, S.F. Loria, L. Ngo, S.T. Kangnavong and P.T. Thon Thondet, deep in cave, walking on ground, under stones or in rock cracks, 2 ♀, 1 subad. ♀, 1 juv. ♀ (AMNH), 1 juv. ♂ (AMCC [LP 15570]), [telson] (AMCC [LP 15591]), same data except 20.v.2018, 1 ♂, 1 subad. ♂, 1 subad. ♀, 3 juv. ♀ (AMNH).

Aemngvantom thamnongpaseuam **Prendini et al., 2021: LAOS: Khammouane Prov.:** *Thakhek Distr.*: Phou Hin Boun National Biodiversity Conservation Area: Tham Paseum [Tham Nong Paseum, Tham Nong Pa Seuam, Tham Pa Seuam or Tham Pa Suam], 8.5 km from turn-off to Tham Phanong Pafa [Tham Nong Pa Fa or Tham Pa Fa] or Buddha Cave on main road Thakhek–Gnommalath (4 km E Thakhek), 17°28′18″N 104°51′23.9″E, 141 m, 15.vi.2012, L. Prendini, S.F. Loria and P. Kanyavong, limestone cave in primary rainforest, very wet cave with river running through, specimen taken from dark zone, in large terminal room [pillar room], ca. 500 m from cave entrance, with extensive rubble breakdown, stalactites, stalagmites and flowstone formations, specimen collected with UV light detection, ca. midday, sitting still on side of small stone, holotype ♀ (AMNH/AMCC [LP 11351]).

Vietbocap canhi **Lourenço and Pham, 2010: VIETNAM: Quảng Bình Prov.:** *Bố Trạch Distr.*: Phong Nha-Kẻ Bàng National Park: Tiên Sơn (Cave), 17°32′N 106°16′E, 200 m, 23.ii.2012, L. Prendini and V.A. Dang, dark zone of cave, ca. 200–500 m from entrance, UV detection in moist cave environment with abundant dripstone and flowstone formations, stalactites and stalagmites, specimens usually sitting in rock crevices or under small stones, mostly in moist situations (near areas where water collects from dripstone formations), none found in dry areas of cave, 7 ♀, 2 subad. ♂, 1 subad. ♀, 4 juv. ♂, 4 juv. ♀, pedipalp fragments (AMNH), 3 juv. ♀ (AMCC [LP 11270, 16750, 16751]); Thiên Đường (Cave), 17°18′55″N 106°08′05″E, 200 m, 12.xi.2011, ex P.-D. Sac, cave, No. 1279, 1 juv. ♀ (AMCC [LP 11348]), Động Thiên Đường (Paradise Cave), 17°31′11.1″N 106°13′23″E, 248 m, 12–13.xi.2018, S.F. Loria, V.L. Ehrenthal, B.Đ. Trần and H.V. Dương, blacklight in cave, specimens collected between 1 km and 5 km deep in cave, walking on ground, under rocks or in limestone cracks, 1 ♀ (AMNH), 1 subad. ♂ (IEBR), [leg] (AMCC [LP 16535]), 1 subad. ♀ (AMCC [LP 16536]), 1 subad. ♀ (IEBR), [leg] (AMCC [LP 16533]), 1 juv. ♂ (PNKB), [leg] (AMCC [LP 16534]), 1 juv. ♀ (PNKB), [leg] (AMCC [LP 16537]).

APPENDIX 2

Measurements (mm) and counts of the holotype female (holo.) of *Qianxie solegladi* Tang, 2022, from Tang (2022) and a female specimen deposited in the Ambrose Monell Cryocollection (AMCC [LP 20856]) of the American Museum of Natural History, New York.

	Holo. ♀	AMCC ♀		Holo. ♀	AMCC ♀
Total length	24.7	21.58	Telson width	1.5	1.25
Carapace length	3.1	2.53	Telson height	1.4	1.17
Carapace anterior width	–	1.45	Metasoma + telson length	13.5	11.69
Carapace width	3.2	2.64	Pedipalp length	10.7	8.41
Mesosoma length	8.1	7.36	Pedipalp femur length	2.8	2.3
Tergite VII length	1.7	–	Pedipalp femur width	1.0	0.83
Tergite VII width	2.8	–	Pedipalp patella length	2.9	2.22
Metasomal segment I length	1.1	1.1	Pedipalp patella width	1.2	0.98
Metasomal segment I width	1.6	1.45	Pedipalp chela length	5.0	3.89
Metasomal segment I height	1.3	0.98	Pedipalp chela manus length	1.6	1.83
Metasomal segment II length	1.4	1.24	Pedipalp chela manus width	1.3	1.17
Metasomal segment II width	1.5	1.37	Pedipalp chela manus height	2.4	0.99
Metasomal segment II height	1.3	0.98	Pedipalp chela fixed finger length	2.1	2.06
Metasomal segment III length	1.5	1.38	Pedipalp chela movable finger length	2.6	2.34
Metasomal segment III width	1.4	1.33	Pectinal median lamellae (sinistral)	9	10
Metasomal segment III height	1.3	0.99	Pectinal median lamellae (dextral)	10	10
Metasomal segment IV length	2.0	1.74	Pectine teeth count (sinistral)	10	11
Metasomal segment IV width	1.4	1.34	Pectine teeth count (dextral)	10	11
Metasomal segment IV height	1.3	1.03	Movable finger denticle row (sinistral)	7	7
Metasomal segment V length	3.8	3.08	Movable finger denticle row (dextral)	7	8
Metasomal segment V width	1.4	1.31	Fixed finger denticle row (sinistral)	7	7
Metasomal segment V height	1.3	1.06	Fixed finger denticle row (dextral)	7	7
Telson length	3.7	3.15			

APPENDIX 3

Ratios and counts for females used in nonmetric multidimensional scaling analysis of the relictual Asian scorpion family Pseudochactidae Gromov, 1998.

1. Carapace length : total length
2. Carapace anterior width : length
3. Carapace posterior width : length
4. Pedipalp femur width : length
5. Pedipalp patella width : length
6. Pedipalp chela manus width : chela length
7. Pedipalp chela manus height : width
8. Pedipalp chela movable finger length : chela length
9. Pedipalp chela fixed finger median denticle subrows (sinistral)
10. Pedipalp chela fixed finger median denticle subrows (dextral)
11. Pedipalp chela movable finger median denticle subrows (sinistral)
12. Pedipalp chela movable finger median denticle subrows (dextral)
13. Pectinal median lamellae (sinistral)
14. Pectinal median lamellae (dextral)
15. Pectinal teeth (sinistral)
16. Pectinal teeth (dextral)
17. Metasoma–telson length : total length
18. Metasomal segment I width : length
19. Metasomal segment II width : length
20. Metasomal segment III width : length
21. Metasomal segment IV width : length
22. Metasomal segment V width : length
23. Metasomal segment I length : segment II length
24. Metasomal segment II length : segment III length
25. Metasomal segment III length : segment IV length
26. Metasomal segment IV length : segment V length
27. Metasomal segment V length: telson length
28. Metasomal segment V width : telson vesicle width
29. Telson vesicle width : telson length
30. Telson vesicle height : telson length

APPENDIX 4

Ratios and counts for females used in nonmetric multidimensional scaling analysis of the relictual Asian scorpion family Pseudochactidae Gromov, 1998: *Pseudochactas mischi* Soleglad et al., 2012; *Pseudochactas ovchinnikovi* Gromov, 1998; *Qianxie solegladi* Tang, 2022; *Troglokhammouanus steineri* Lourenço, 2007, and its junior synonym, *Troglokhammouanus louiseanneorum* Lourenço, 2017 (*T. lou*). Ratios for *Q. solegladi* calculated from data in appendix 2; for other taxa from data in Prendini et al. (2021). Ratios and counts in appendix 3. Char. = character; Holo. = holotype.

Char.	*P. mischi*	*P. ovchinnikovi*								*Q. solegladi*		*T. steineri*											
	Holo. subad. ♀	♀	♀	♀	♀	♀	♀	♀	♀	Holo. ♀	♀	Holo. ♀	*T. lou.* Holo. ♀	♀	♀	♀	♀	♀	♀	♀	♀	♀	♀
1	0.15	0.12	0.13	0.12	0.13	0.13	0.13	0.13	0.13	0.13	0.12	0.14	0.17	0.14	0.14	0.14	0.14	0.14	0.14	0.14	0.14	0.14	0.14
2	0.33	0.57	0.56	0.56	0.58	0.58	0.56	0.60	0.55	0.61	0.57	0.57	0.47	0.55	0.45	0.51	0.48	0.45	0.54	0.50	0.53	0.54	0.51
3	0.54	1.00	0.96	0.96	0.92	0.94	0.95	1.03	1.00	1.03	1.04	1.02	0.79	1.01	0.97	0.93	0.96	0.92	0.98	1.01	0.94	0.92	1.01
4	0.33	0.33	0.35	0.33	0.32	0.33	0.33	0.33	0.36	0.36	0.36	0.39	0.41	0.36	0.36	0.33	0.35	0.32	0.37	0.38	0.39	0.36	0.34
5	0.43	0.47	0.50	0.46	0.48	0.47	0.45	0.45	0.46	0.41	0.44	0.38	0.41	0.40	0.38	0.42	0.39	0.38	0.38	0.39	0.40	0.39	0.40
6	0.35	0.34	0.37	0.34	0.36	0.32	0.33	0.34	0.33	0.26	0.30	0.37	0.38	0.37	0.37	0.36	0.39	0.35	0.37	0.35	0.38	0.37	0.39
7	1.04	0.80	0.78	0.83	0.73	0.80	0.79	0.79	0.88	1.85	0.85	0.79	0.80	0.75	0.82	0.84	0.79	0.84	0.79	0.82	0.79	0.78	0.82
8	0.54	0.51	0.55	0.53	0.53	0.53	0.54	0.52	0.56	0.52	0.60	0.57	0.55	0.56	0.57	0.58	0.57	0.62	0.59	0.58	0.59	0.58	0.57
9	7	7	7	7	7	7	7	7	7	7	7	7	7	7	7	7	7	7	7	7	7	7	7
10	7	7	7	7	7	7	7	7	7	7	7	7	7	6	7	7	6	7	7	7	7	7	7
11	7	7	7	7	7	7	7	7	7	7	7	8	7	8	8	7	7	8	8	8	8	8	7
12	7	7	7	7	7	7	7	7	7	7	8	8	7	7	8	7	7	8	8	8	8	7	7
13	9	10	10	9	10	9	10	10	10	9	10	13	13	13	13	12	13	12	14	13	12	13	13
14	8	9	10	10	9	10	9	9	9	10	10	14	14	12	13	13	13	13	14	13	12	14	13
15	10	11	11	10	11	10	11	11	11	10	11	14	14	14	15	13	14	13	15	14	13	14	15
16	9	10	11	11	10	11	10	10	10	10	11	14	14	13	14	14	14	14	15	14	13	15	14
17	0.59	0.57	0.56	0.54	0.57	0.55	0.56	0.53	0.54	0.55	0.54	0.58	0.61	0.55	0.54	0.54	0.55	0.53	0.55	0.54	0.54	0.55	0.55
18	1.56	1.29	1.57	1.67	1.69	1.35	1.42	1.65	1.41	1.45	1.32	1.45	1.53	1.56	1.30	1.24	1.30	1.30	1.32	1.50	1.36	1.40	1.31
19	1.24	1.00	1.06	1.09	1.12	1.14	1.07	1.21	1.08	1.07	1.10	1.18	1.09	1.06	1.02	0.96	1.02	1.05	1.06	1.09	1.17	1.08	1.04
20	1.13	0.86	0.95	0.89	0.95	1.00	0.91	0.93	0.93	0.93	0.96	1.00	0.96	0.98	0.89	0.96	0.91	0.89	0.93	0.96	0.98	0.89	0.88
21	0.89	0.65	0.76	0.71	0.68	0.73	0.70	0.75	0.74	0.70	0.77	0.74	0.68	0.64	0.68	0.71	0.69	0.65	0.70	0.71	0.64	0.69	0.67
22	0.46	0.38	0.43	0.38	0.37	0.39	0.38	0.38	0.37	0.37	0.43	0.39	0.38	0.35	0.35	0.34	0.38	0.35	0.36	0.39	0.35	0.35	0.37
23	0.86	0.89	0.78	0.75	0.76	0.93	0.86	0.83	0.85	0.79	0.89	0.91	0.83	0.75	0.83	0.80	0.85	0.83	0.84	0.79	0.89	0.82	0.80
24	0.95	0.86	0.90	0.84	0.85	0.93	0.88	0.80	0.93	0.93	0.90	0.88	0.88	0.95	0.88	1.00	0.92	0.90	0.92	0.92	0.86	0.87	0.89
25	0.82	0.81	0.80	0.79	0.80	0.75	0.80	0.83	0.82	0.75	0.79	0.81	0.76	0.70	0.81	0.79	0.78	0.74	0.78	0.76	0.71	0.79	0.77
26	0.52	0.59	0.58	0.57	0.58	0.57	0.56	0.53	0.55	0.53	0.56	0.53	0.54	0.58	0.53	0.49	0.56	0.56	0.51	0.56	0.56	0.53	0.56
27	0.90	0.89	0.86	0.85	0.84	0.83	0.88	0.87	0.89	1.03	0.98	0.86	0.93	0.91	0.88	0.92	0.93	0.89	0.87	0.86	0.91	0.96	0.89
28	0.96	0.88	0.88	0.84	0.80	0.90	0.84	0.87	0.88	0.93	1.05	0.88	0.96	1.02	0.86	0.85	0.93	0.93	0.91	0.97	0.98	0.98	1.03
29	0.43	0.39	0.42	0.38	0.39	0.36	0.39	0.38	0.37	0.41	0.40	0.38	0.37	0.32	0.35	0.36	0.38	0.34	0.34	0.34	0.33	0.34	0.32
30	0.35	0.35	0.37	0.32	0.36	0.33	0.37	0.33	0.31	0.38	0.37	0.33	0.31	0.31	0.28	0.28	0.30	0.29	0.28	0.27	0.28	0.30	0.27

APPENDIX 5

Ratios and counts for females used in nonmetric multidimensional scaling analysis of the relictual Asian scorpion family Pseudochactidae Gromov, 1998: *Aemngvantom lao* (Lourenço, 2012); *Aemngvantom thamnongpaseuam* Prendini et al., 2021 (*A. tham.*); *Vietbocap canhi* Lourenço and Pham, 2010, and its junior synonyms, *Vietbocap aurantiacus* Lourenço et al., 2018 (*V. aur.*) and *Vietbocap quinquemilia* Lourenço et al., 2018 (*V. qui.*). Ratios calculated from data in Prendini et al. (2021). Ratios and counts in appendix 3.
Char. = character; Holo. = holotype; Para. = paratype.

Char.	*A. lao*						*A. tham.*	*V. canhi*												
	Holo. ♀	♀	♀	♀	♀	♀	Holo. ♀	♀	♀	♀	♀	♀	♀	♀	♀	*V. aur.* Holo. ♀	subad. ♀	Para. juv. ♀	*V. qui.* Para. juv. ♀
1	0.14	0.13	0.13	0.13	0.13	0.12	0.13	0.12	0.12	0.12	0.12	0.12	0.12	0.12	0.13	0.13	0.13	0.13	0.12	
2	0.69	0.48	0.48	0.48	0.49	0.44	0.53	0.54	0.54	0.56	0.52	0.47	0.48	0.47	0.49	0.60	0.67	0.64	0.72	
3	0.97	0.86	0.87	0.92	0.85	0.89	0.99	1.02	1.04	1.05	1.04	0.98	0.96	0.90	1.01	1.07	1.07	1.04	1.08	
4	0.24	0.22	0.20	0.19	0.22	0.22	0.24	0.22	0.21	0.20	0.20	0.18	0.19	0.18	0.20	0.22	0.25	0.23	0.28	
5	0.22	0.24	0.21	0.21	0.24	0.23	0.29	0.28	0.29	0.30	0.29	0.28	0.28	0.29	0.28	0.29	0.32	0.28	0.29	
6	0.18	0.16	0.14	0.15	0.17	0.16	0.21	0.14	0.16	0.14	0.14	0.15	0.15	0.15	0.13	0.16	0.16	0.17	0.18	
7	0.92	0.89	0.99	0.90	0.95	0.96	0.84	1.16	1.01	1.07	1.04	1.04	1.04	0.97	1.07	0.94	1.00	0.90	0.90	
8	0.66	0.66	0.67	0.65	0.66	0.66	0.62	0.61	0.59	0.60	0.58	0.63	0.61	0.57	0.59	0.59	0.59	0.67	0.60	
9	10	10	10	10	10	10	10	8	8	8	8	8	8	8	7	7	7	8	7	
10	10	10	10	10	10	10	10	8	8	8	8	8	8	8	7	7	7	8	7	
11	10	10	10	10	10	10	10	8	8	8	8	8	8	8	7	7	7	8	7	
12	10	10	10	10	10	10	10	8	8	8	8	8	8	8	7	7	7	8	7	
13	12	13	12	12	12	12	12	7	7	7	7	7	7	7	6	7	6	7	7	
14	12	13	12	11	12	12	11	7	7	7	7	7	7	6	5	8	7	7	8	
15	13	14	13	13	13	13	13	8	8	8	8	8	8	8	7	7	7	7	7	
16	13	14	13	12	13	13	13	8	8	8	8	9	8	8	6	7	7	7	7	
17	0.65	0.54	0.59	0.55	0.57	0.58	0.56	0.55	0.56	0.55	0.57	0.56	0.56	0.56	0.59	0.64	0.64	0.57	0.57	
18	1.00	1.08	1.15	1.03	1.02	1.06	1.15	1.02	1.04	0.98	1.01	1.01	0.97	0.95	0.98	1.16	1.25	1.20	1.20	
19	0.87	0.71	0.77	0.78	0.76	0.75	0.89	0.83	0.77	0.81	0.70	0.75	0.73	0.74	0.68	0.86	0.86	0.83	0.83	
20	0.81	0.63	0.58	0.72	0.67	0.67	0.77	0.72	0.64	0.65	0.63	0.63	0.59	0.61	0.63	0.72	0.65	0.64	0.69	
21	0.55	0.50	0.44	0.52	0.50	0.47	0.52	0.51	0.51	0.51	0.48	0.47	0.46	0.45	0.44	0.53	0.50	0.47	0.50	
22	0.32	0.26	0.23	0.26	0.27	0.25	0.29	0.25	0.23	0.25	0.21	0.24	0.24	0.23	0.20	0.25	0.23	0.25	0.25	
23	0.93	0.79	0.78	0.84	0.81	0.89	0.87	0.91	0.85	0.93	0.80	0.87	0.88	0.87	0.87	0.86	0.86	0.83	0.83	
24	0.94	0.91	0.87	0.93	0.89	0.94	0.89	0.89	0.87	0.85	0.92	0.87	0.82	0.94	0.95	0.88	0.82	0.86	0.92	
25	0.73	0.79	0.79	0.73	0.78	0.74	0.73	0.74	0.81	0.79	0.76	0.79	0.80	0.75	0.78	0.78	0.77	0.82	0.81	
26	0.54	0.54	0.53	0.50	0.54	0.53	0.57	0.51	0.48	0.50	0.50	0.52	0.53	0.52	0.47	0.51	0.51	0.53	0.50	
27	0.91	0.98	0.94	0.98	0.93	0.97	0.88	0.90	0.96	0.92	0.94	0.92	0.94	0.94	1.00	0.93	0.93	0.89	0.97	
28	0.93	0.86	0.79	0.88	0.85	0.82	0.83	0.76	0.73	0.77	0.69	0.81	0.83	0.81	0.69	0.73	0.71	0.80	0.73	
29	0.31	0.30	0.27	0.29	0.29	0.29	0.31	0.29	0.30	0.30	0.29	0.28	0.27	0.27	0.30	0.32	0.30	0.28	0.33	
30	0.27	0.26	0.23	0.27	0.27	0.28	0.27	0.27	0.24	0.26	0.24	0.25	0.26	0.25	0.27	0.28	0.26	0.25	0.27	

APPENDIX 6

Morphological characters and character states used for phylogenetic analysis of the relictual Asian scorpion family Pseudochactidae Gromov, 1998. Character states scored 0–5, inapplicable (-) or unknown (?). Terminology, including trichobothrial homology, follows Prendini et al. (2006). Characters corresponding to lists of Lamoral (1980), Stockwell (1989), Prendini (2000), Soleglad and Sissom (2001), Soleglad and Fet (2001), Soleglad and Fet (2003b: table 4), Soleglad and Fet (2003b, table 5), Prendini (2004), Prendini et al. (2021, appendices 2 and 3), Xuan et al. (2025) denoted, respectively, by abbreviations L80, S89, P00, S&S01, S&F01, S&F03.4, S&F03.5, P04, PEA21 and XEA25, followed by the corresponding number. Character matrix in table 2.

Coloration and Infuscation

1. Tegument base coloration: **0,** yellowish; **1,** brown; **?,** unknown. [PEA21/1, XEA25/1]
2. Carapace infuscation: **0,** absent (immaculate); **1,** present; **?,** unknown. [PEA21/2, XEA25/2]
3. Mesosomal tergites infuscation: **0,** absent (immaculate); **1,** median stripe and pair of lateral bands; **2,** paired submedian and sublateral stripes; **3,** entirely or mostly (anterior two-thirds) infuscate; **?,** unknown. [PEA21/3, XEA25/3]
4. Legs, femoral and patellar surfaces, infuscation: **0,** prolateral and retrolateral surfaces infuscate; **1,** prolateral surfaces infuscate, retrolateral surfaces immaculate; **2,** prolateral and retrolateral surfaces immaculate; **?,** unknown. [PEA21/4, XEA25/4] Original character (PEA21/1) revised to the current version (XEA25/4).

Chelicerae

5. Cheliceral fixed finger, ventral surface, teeth or denticles: **0,** two major teeth; **1,** four or five small denticles (ventral accessory denticles); **?,** unknown. [S&S01/8, S&F03.5/45, P04/1, PEA21/5, XEA25/5]
6. Cheliceral fixed finger, median and basal teeth, fusion: **0,** fused into bicuspid ("conjoined on trunk"); **1,** separate; **?,** unknown. [S&S01⁄9, S&F03.5⁄44, PEA21/6, XEA25/6]
7. Cheliceral movable finger, dorsal margin, basal teeth: **0,** absent; **1,** one; **2,** two; **?,** unknown. [S89/33, S&S01/2, S&F03.5/40, PEA21/7, XEA25/7]
8. Cheliceral movable finger, ventral margin, teeth or denticles: **0,** two large, subequal median teeth; **1,** four or five ventral accessory denticles (crenulate margin); **?,** unknown. [S89/34–36, S&S01/4, S&F03.5/42, 43, PEA21/8, XEA25/8]
9. Cheliceral movable finger, ventral margin, serrula: **0,** absent; **1,** present; **?,** unknown. [S89/34–36, S&S01/4, S&F03.5/42, 43, PEA21/9, XEA25/9]

Carapace

10. Carapace posterior width, relative to length: **0,** posterior width greater than length; **1,** posterior width similar to or less than length; **?,** unknown. [PEA21/10, XEA25/10]
11. Carapace anteromedian margin, alignment relative to anterolateral margins: **0,** anteromedian margin recessed, posterior to anterolateral margins; **1,** anteromedian margin aligned with anterolateral margins; **2,** anteromedian margin protruding, anterior to anterolateral margins; **?,** unknown. [PEA21/11, XEA25/11]
12. Carapace anteromedian margin, curvature: **0,** sublinear; **1,** convex (procurved); **2,** shallowly concave (recurved); **?,** unknown. [PEA21/12, XEA25/12]
13. Carapace anterolateral margins: **0,** entire; **1,** with pronounced incision lateral to lateral ocelli (rostrolateral incision); **?,** unknown. [PEA21/13, XEA25/13]
14. Carapace anteromedian depression, dimensions: **0,** broad, deep; **1,** narrow, shallow; **2,**

narrow, deep; **?,** unknown. [PEA21/14, XEA25/14]

15. Carapace anterosubmedial depressions, medial to lateral ocelli: **0,** absent; **1,** vestigial; **2,** well developed; **?,** unknown. [PEA21/15, XEA25/15]
16. Carapace anterosubmedial lyriform carinae, vertical development and macrosculpture: **0,** absent; **1,** obsolete, granular; **2,** pronounced, costate-granular; **?,** unknown. [PEA21/16, XEA25/16]
17. Carapace median ocular tubercle (or eyeless surface representing ocular tubercle), distance from anterior margin relative to carapace length: **0,** medial; **1,** anteromedial; **?,** unknown. [PEA21/17, XEA25/17]
18. Carapace median ocelli: **0,** present; **1,** absent; **?,** unknown. [PEA21/18, XEA25/18]
19. Carapace interocular sulcus (regardless of presence or absence of median ocelli), depth: **0,** deep; **1,** shallow; **?,** unknown. [PEA21/19, XEA25/19]
20. Carapace circumocular sutures: **0,** absent; **1,** present; **?,** unknown. [PEA21/20, XEA25/20]
21. Carapace circumocular sutures, development: **0,** complete, connected posteriorly (post-ocular); **1,** complete, disconnected posteriorly; **2,** partial (disconnected); **?,** unknown; **-,** inapplicable. [PEA21/21, XEA25/21]
22. Carapace circumocular triangle (regardless of presence or absence of median ocelli), shape: **0,** subtriangular (broad V-shape), median ocellar curvatures present; **1,** parallel-sided (U-shape), median ocellar curvatures absent; **?,** unknown; **-,** inapplicable. [PEA21/22, XEA25/22]
23. Carapace circumocular sulci, posterior margin, distance from anterior margin relative to carapace length: **0,** anteromedial; **1,** medial; **2,** posteromedial; **?,** unknown; **-,** inapplicable. [PEA21/23, XEA25/23]
24. Carapace lateral ocelli, anterolateral major (ALMa) ocelli: **0,** present; **1,** absent; **?,** unknown. [PEA21/24, XEA25/24]
25. Carapace lateral ocelli, mediolateral major (MLMa) ocelli: **0,** present; **1,** absent; **?,** unknown. [PEA21/25, XEA25/25]
26. Carapace lateral ocelli, posterolateral major (PLMa) ocelli: **0,** present; **1,** absent; **?,** unknown. [PEA21/26, XEA25/26]
27. Carapace lateral ocelli, posterolateral major (PLMa) ocelli, size: **0,** small; **1,** large; **?,** unknown. This new character was added in the present study.
28. Carapace lateral ocelli, anterodorsal minor (ADMi) ocelli: **0,** present; **1,** absent; **?,** unknown. [PEA21/27, XEA25/27]
29. Carapace lateral ocelli, posterodorsal minor (PDMi) ocelli: **0,** present; **1,** absent; **?,** unknown. [PEA21/28, XEA25/28]
30. Carapace lateral eyespot: **0,** absent; **1,** present; **?,** unknown. [PEA21/29, XEA25/29]
31. Carapace circumocular surfaces: **0,** mostly granular; **1,** mostly smooth except for sparse granulation near anterior carapace margin; **2,** entirely smooth; **?,** unknown. [PEA21/30, XEA25/30] Original character (PEA21/30) split to create XEA25/30 and 31 and state 2 added for fossil taxa.
32. Carapace anterolateral and posteromedian surfaces: **0,** mostly granular; **1,** smooth; **?,** unknown. [PEA21/30, XEA25/31] Original character (PEA21/30) split to create XEA25/30 and 31.
33. Carapace mediolateral surfaces, macrosculpture: **0,** granular; **1,** smooth; **?,** unknown. [PEA21/31, XEA25/32]
34. Carapace posterolateral margins, curvature: **0,** gently curved; **1,** angular, slanting; **?,** unknown. [PEA21/32, XEA25/33]
35. Carapace posteromedian margin, curvature: **0,** shallowly concave (recurved); **2,** sublinear to shallowly convex (procurved); **?,** unknown. [PEA21/33, XEA25/34]

Pedipalps

36. Pedipalps shape: **0,** segments very robust, chela manus incrassate; **1,** segments moderately robust, chela manus globose; **2,** segments gracile, chela manus globose; **3,** segments gracile, chela manus elongate; **?,** unknown. [PEA21/34, XEA25/35]

37. Pedipalp femur trichobothrium i_2: **0,** absent; **1,** present; **?,** unknown. [Prendini et al. (2006) preferred hypothesis, PEA21/35, XEA25/36]
38. Pedipalp femur petite trichobothrium i_3: **0,** absent; **1,** present; **?,** unknown. [Prendini et al. (2006) preferred hypothesis, PEA21/36, XEA25/37]
39. Pedipalp femur petite trichobothrium i_4: **0,** absent; **1,** present; **?,** unknown. [Prendini et al. (2006) preferred hypothesis, PEA21/37, XEA25/38]
40. Pedipalp femur prodorsal carina, longitudinal development: **0,** complete; **1,** partial; **?,** unknown. [PEA21/38, XEA25/39]
41. Pedipalp femur trichobothrium d_1, size: **0,** petite; **1,** full size; **?,** unknown. [Prendini et al. (2006) preferred hypothesis, PEA21/39, XEA25/40]
42. Pedipalp femur trichobothria d_1 and $i_{1–4}$, relative alignment: **0,** d_1 aligned with or distal to $i_{1–4}$; **1,** d_1 proximal to $i_{1–4}$; **?,** unknown. [S&S01/38, S&F03.5/5, PEA21/40, XEA25/41]
43. Pedipalp femur petite trichobothrium d_2: **0,** absent; **1,** present; **?,** unknown. [Prendini et al. (2006) preferred hypothesis, PEA21/41, XEA25/42]
44. Pedipalp femur trichobothrium d_3, size: **0,** petite; **1,** full size; **?,** unknown. [Prendini et al. (2006) preferred hypothesis, PEA21/42, XEA25/43]
45. Pedipalp femur trichobothrium d_4, size: **0,** absent; **1,** petite; **2,** full size; **?,** unknown. [Prendini et al. (2006) preferred hypothesis, PEA21/43, XEA25/44]. States 1 and 2 accidentally swapped in the original character (PEA21/43). Corrected to the current version (XEA25/44).
46. Pedipalp femur trichobothrium d_5: **0,** absent; **1,** present; **?,** unknown. [Prendini et al. (2006) preferred hypothesis, PEA21/44, XEA25/45]
47. Pedipalp femur trichobothrium d_6, size: **0,** petite; **1,** full size; **?,** unknown. [Prendini et al. (2006) preferred hypothesis, PEA21/45, XEA25/46]
48. Pedipalp femur trichobothria d_3 and d_4 alignment relative to retrodorsal carina: **0,** d_4 prolateral to d_3 such that d_3–d_4 directed away from retrodorsal carina (beta configuration); **1,** d_3 and d_4 in same axis, such that d_3–d_4 parallel to retrodorsal carina; **2,** d_4 retrolateral to d_3 such that d_3–d_4 directed toward retrodorsal carina (alpha configuration); **?,** unknown. [S&F03.5/3, P04/11, PEA21/46, XEA25/47]
49. Pedipalp femur retrodorsal carina, vertical development: **0,** absent or obsolete; **1,** present, distinct; **?,** unknown. [PEA21/47, XEA25/48]
50. Pedipalp femur trichobothrium e_3: **0,** absent; **1,** present; **?,** unknown. [Prendini et al. (2006) preferred hypothesis, PEA21/48, XEA25/49]
51. Pedipalp femur trichobothrium e_4: **0,** absent; **1,** present; **?,** unknown. [S&F01/62, S&F03.4/62, PEA21/49, XEA25/50]
52. Pedipalp patella promedian carina ("dorsal patellar spur carina"): **0,** present; **1,** absent; **?,** unknown. [S&F03.5/94 (part), PEA21/50, XEA25/51]
53. Pedipalp patella prolateral surface, dorsoventral projection ("anterior process"): **0,** absent; **1,** moderate; **2,** pronounced; **?,** unknown. [P00/18, S&S01/16,17, S&F03.5/97, 98, PEA21/51, XEA25/52]
54. Pedipalp patella prolateral surface, dorsoventral projection, pair of spiniform granules proximally (dorsal and ventral "patellar spurs" situated proximally on dorsal and ventral prolateral carinae, respectively): **0,** present; **1,** absent; **?,** unknown. [P00/18, S&S01/16,17, S&F03.5/97, 98, PEA21/52, XEA25/53]
55. Pedipalp patella trichobothrium i_2: **0,** absent; **1,** present; **?,** unknown. [S&F01/28, S&F03.4/28, PEA21/53, XEA25/54]
56. Pedipalp patella dorsomedian carina: **0,** present; **1,** absent; **?,** unknown. [S&F03.5/95, PEA21/54, XEA25/55]
57. Pedipalp patella trichobothium d_3: **0,** absent; **1,** present; **?,** unknown. [S&F01/31, S&F03.4/31, PEA21/55, XEA25/56]
58. Pedipalp patella trichobothium d_4: **0,** absent; **1,** present; **?,** unknown. [S&F01/32, S&F03.4/32, PEA21/56, XEA25/57]

59. Pedipalp patella petite trichobothium d_5: **0,** absent; **1,** present; **?,** unknown. [S&F01/33, S&F03.4/33, PEA21/57, XEA25/58]
60. Pedipalp patella retromedian carina: **0,** present; **1,** absent; **?,** unknown. [PEA21/58, XEA25/59]
61. Pedipalp patella trichobothium em_1: **0,** absent; **1,** present; **?,** unknown. [S&F01/41, S&F03.4/41, PEA21/59, XEA25/60]
62. Pedipalp patella trichobothium *est*, size: **0,** petite; **1,** full size; **?,** unknown. [S&F01/43, S&F03.4/43, PEA21/60, XEA25/61]
63. Pedipalp patella ventromedian carina: **0,** present; **1,** absent; **?,** unknown. [PEA21/61, XEA25/62]
64. Pedipalp patella trichobothria v_1, v_2 and v_3: **0,** absent; **1,** present; **?,** unknown. [S&F01/47–49, S&F03.4/47–49, PEA21/62, XEA25/63]
65. Pedipalp chela manus prolateral dorsal carina (♂), longitudinal development: **0,** absent or obsolete; **1,** complete; **?,** unknown. [PEA21/63, XEA25/64]
66. Pedipalp chela manus prolateral ventral carina (♂, ♀), longitudinal development: **0,** absent or obsolete; **1,** complete; **?,** unknown. [PEA21/64, XEA25/65]
67. Pedipalp chela manus trichobothrium ib_1: **0,** absent; **1,** present; **?,** unknown. [S&F01/1, S&F03.4/1, PEA21/65, XEA25/66]
68. Pedipalp chela manus petite trichobothrium ib_2: **0,** absent; **1,** present; **?,** unknown. [Prendini et al. (2006) preferred hypothesis, PEA21/66, XEA25/67]
69. Pedipalp chela fixed finger trichobothrium it_1 (*it* situated at base of fixed finger): **0,** absent; **1,** present; **?,** unknown. [S89/70–72, P00/47, S&S01/40, S&F03.5/11, 14, PEA21/67, XEA25/68]
70. Pedipalp chela fixed finger trichobothrium it_2 (*it* situated in proximal third of fixed finger): **0,** absent; **1,** present; **?,** unknown. [S89/70–72, P00/47, S&S01/40, S&F03.5/11, 14, PEA21/68, XEA25/69]
71. Pedipalp chela fixed finger trichobothrium it_3 (*it* situated distally on finger): **0,** absent; **1,** present; **?,** unknown. [S89/70–72, P00/47, S&S01/40, S&F03.5/11, 14, PEA21/69, XEA25/70]
72. Pedipalp chela manus dorsomedian carina, longitudinal development: **0,** absent or obsolete; **1,** vestigial; **2,** complete; **?,** unknown. [PEA21/70, XEA25/71]
73. Pedipalp chela manus dorsal secondary and subdigital carinae, longitudinal development: **0,** absent or obsolete; **1,** vestigial; **2,** complete; **?,** unknown. [PEA21/71, XEA25/72]
74. Pedipalp chela manus digital carina, longitudinal development: **0,** absent or obsolete; **1,** complete; **?,** unknown. [PEA21/72, XEA25/73]
75. Pedipalp chela manus retromedian carina, longitudinal development: **0,** absent or obsolete; **1,** partial; **2,** complete; **?,** unknown. [PEA21/73, XEA25/74]
76. Pedipalp chela manus secondary accessory and retroventral carinae, fusion: **0,** entire; **1,** incomplete, slight disjunction evident in proximal third; **?,** unknown. [PEA21/74, XEA25/75]
77. Pedipalp chela manus trichobothrium Eb_1: **0,** present; **1,** absent; **?,** unknown. This character was newly added in the present study.
78. Pedipalp chela manus trichobothrium Eb_3, size: **0,** petite; **1,** full size; **?,** unknown. [Prendini et al. (2006) preferred hypothesis, PEA21/75, XEA25/76]
79. Pedipalp chela manus trichobothrium Est_1 (*Est* situated distal on chela manus): **0,** absent; **1,** present; **?,** unknown. [S89/86, PEA21/76, XEA25/77]
80. Pedipalp chela manus trichobothrium Est_2 (*Est* situated proximal to movable finger condyle): **0,** absent; **1,** present; **?,** unknown. [S89/86, PEA21/77, XEA25/78]
81. Pedipalp chela manus/fixed finger trichobothrium Et_1 (in Pseudochactidae, and positionally homologous trichobothrium *eb* in Buthidae and Chaerilidae), position: **0,** situated proximally on fixed finger; **1,** situated on fixed finger, slightly distal to movable finger condyle; **2,** situated distally on manus, aligned with or proximal to movable finger condyle; **?,** unknown. [PEA21/78, XEA25/79]

82. Pedipalp chela manus petite trichobothrium Et_4: **0,** absent; **1,** present; **?,** unknown. [S&F01/21, S&F03.4/21, PEA21/79, XEA25/80]
83. Pedipalp chela trichobothrium *eb* (not positionally homologous with *eb* in Buthidae and Chaerilidae), position: **0,** absent; **1,** present, situated on fixed finger, slightly distal to movable finger condyle; **2,** present, situated in proximal third of fixed finger, distal to basalmost retrolateral denticle of median denticle row; **?,** unknown. [PEA21/80, XEA25/81]
84. Pedipalp chela fixed finger petite trichobothrium esb_1 (*esb* situated in proximal quarter of fixed finger, between second and third most proximal retrolateral denticles of median denticle row): **0,** absent; **1,** present; **?,** unknown. [Prendini et al. (2006) preferred hypothesis, PEA21/81, XEA25/82]
85. Pedipalp chela fixed finger trichobothrium esb_2 (in Pseudochactidae, not positionally homologous with *esb* in Buthidae and Chaerilidae), position: **0,** absent; **1,** situated in proximal third of fixed finger, approximately aligned with proximal retrolateral denticle of median denticle row; **2,** situated in proximal third of fixed finger, between first and second most proximal retrolateral denticles of median denticle row; **3,** situated approximately midway on fixed finger, between second and third most proximal retrolateral denticles of median denticle row; **?,** unknown. [PEA21/82, XEA25/83]
86. Pedipalp chela fixed finger trichobothria *est* and *et*, position: **0,** absent; **1,** situated medially on finger; **2,** situated distally on finger; **?,** unknown. [Prendini et al. (2006) preferred hypothesis, PEA21/83, XEA25/84]
87. Pedipalp chela manus ventromedian carina, longitudinal development: **0,** absent or obsolete; **1,** vestigial; **2,** partial; **?,** unknown. [PEA21/84, XEA25/85]
88. Pedipalp chela manus V_1: **0,** absent; **1,** present; **?,** unknown. [Prendini et al. (2006) preferred hypothesis, PEA21/85, XEA25/86]
89. Pedipalp chela manus V_2: **0,** absent; **1,** present; **?,** unknown. [Prendini et al. (2006) preferred hypothesis, PEA21/86, XEA25/87]
90. Pedipalp chela manus V_2, position: **0,** medial; **1,** near retroventral carina; **?,** unknown; **-,** inapplicable. [XEA25/88]
91. Pedipalp chela fixed and movable fingers, shape lateral aspect (adult ♂): **0,** sublinear, similar to adult ♀; **1,** sinuous, sexually dimorphic; **?,** unknown. [PEA21/87, XEA25/89]
92. Pedipalp chela fixed finger, median denticle rows, number of subrows: **0,** 11; **1,** 10; **2,** 8; **3,** 7; **?,** unknown. [PEA21/88, XEA25/90]
93. Pedipalp chela movable finger, median denticle rows, number of subrows: **0,** 11 or 12; **1,** 10; **2,** 8; **3,** 7; **?,** unknown. [PEA21/89, XEA25/91]
94. Pedipalp chela fixed finger, median denticle rows, number of prolateral denticles: **0,** 11; **1,** 10; **2,** 8; **3,** 7; **4,** 6; **?,** unknown. [PEA21/90, XEA25/92]
95. Pedipalp chela movable finger, median denticle rows, number of prolateral denticles: **0,** 11 or 12; **1,** 10; **2,** 8; **3,** 7; **?,** unknown. [PEA21/91, XEA25/93]
96. Pedipalp chela fixed finger, median denticle rows, number of retrolateral denticles: **0,** 11 or 12; **1,** 9; **2,** 7; **3,** 6; **?,** unknown. [PEA21/92, XEA25/94]
97. Pedipalp chela movable finger, median denticle rows, number of retrolateral denticles: **0,** 12; **1,** 9; **2,** 7; **3,** 6; **?,** unknown. [PEA21/93, XEA25/95]

Coxosternum

98. Leg I, maxillary lobes (coxapophyses), distal edges, shape: **0,** unexpanded (non-spatulate); **1,** distinctly expanded (spatulate); **?,** unknown. [L80/5, S&S01/68, S&F03.5/70, PEA21/94, XEA25/96]
99. Leg I, maxillary lobes (coxapophyses), anterior margins, serrula: **0,** absent; **1,** vestigial, few serrations restricted to anterolateral margins; **2,** distinct, extensive serrations along

anterior and lateral margins; **?,** unknown. [XEA25/97]

100. Sternum shape: **0,** pentagonal; **1,** subtriangular; **?,** unknown. [L80/3, 18, S89/28, P00/9, S&S01/69, S&F03.5/64, PEA21/95, XEA25/98]
101. Sternum lateral margins, curvature: **0,** curved medially; **1,** sublinear; **?,** unknown; **-,** inapplicable. [PEA21/96, XEA25/99]
102. Sternum ventral surface: **0,** flat/planar ("no concave region, minimal outer ridge"); **1,** shallowly concave ("marginal concave region, minimal outer ridge"); **2,** markedly concave ("well-developed concave region and outer ridge"); **?,** unknown. [L80/3, 18, S89/28, P00/9, S&S01/69, S&F03.5/64, PEA21/97, XEA25/100]

Legs

103. Legs III and IV, tibial spurs: **0,** present; **1,** absent; **?,** unknown. [S89/89, S&F03.5/59, P04/15, PEA21/98, XEA25/101]
104. Legs I–IV basitarsi and telotarsi, spinules: **0,** absent; **1,** short; **2,** long; **?,** unknown. [PEA21/99, XEA25/102]
105. Legs I–IV telotarsi, spinule rows: **0,** single ventromedian row; **1,** paired ventrosubmedian rows; **?,** unknown; **-,** inapplicable. [L80/9, S89/93, 94, 97, P00/68, 70, S&S01/83, 84, 88, 89, S&F03.5/57, 58, PEA21/100, XEA25/103]
106. Legs I–IV telotarsi, paired ventrosubmedian rows of spinules: **0,** regular; **1,** slightly irregular; **?,** unknown; **-,** inapplicable. [PEA21/101, XEA25/104]
107. Legs I–IV telotarsi, ventrosubmedian rows of (socketed) macrosetae: **0,** present; **1,** absent; **?,** unknown. [L80/9, S89/93, 94, 97, P00/68, 70, S&S01/83, 84, 88, 89, S&F03.5/57, 58, PEA21/102, XEA25/105]

Genital Operculum

108. Genital papillae (♂), length relative to genital opercula: **0,** inconspicuous; **1,** conspicuously visible along length of opercula; **?,** unknown. [S&S01/72, S&F03.5/81, PEA21/103, XEA25/106]

Reproductive Anatomy

109. Paraxial organ, accessory glands: **0,** absent; **1,** present; **?,** unknown. [S89/113, PEA21/104, XEA25/107]
110. Hemispermatophore, basal lobe: **0,** present; **1,** absent; **?,** unknown. [S89/112, PEA21/105, XEA25/108]
111. Hemispermatophore, *pars recta*: **0,** absent (Chaerilidae, Pseudochactidae); **1,** present (Buthidae); **?,** unknown. [L80/2 (part), S89/110, 111, P00/82, S&S01/74, S&F03.5/73, PEA21/106, XEA25/109]
112. Ovariuterus, number of "cells" in ovariuterine net (reticulate mesh): **0,** six; **1,** eight; **?,** unknown. [S89/102, S&F03.5/100, PEA21/107, XEA25/110]

Pectines

113. Pectines, marginal lamellae, fusion: **0,** three; **1,** two (fusion of proximal and medial marginal lamellae); **?,** unknown. [PEA21/108, XEA25/111]
114. Pectines, marginal and median lamellae, fusion: **0,** separate, longitudinal suture between marginal and median lamellae present; **1,** fused, longitudinal suture between marginal and median lamellae absent; **?,** unknown. [PEA21/109, XEA25/112]
115. Pectines, median lamellae, fusion and number: **0,** variously fused, many fewer than pectinal teeth; **1,** separate, similar number to pectinal teeth; **?,** unknown; **-,** inapplicable. [PEA21/110, XEA25/113]
116. Pectines, proximal median lamella (scape), angle (♂): **0,** acute; **1,** obtuse; **?,** unknown. [PEA21/111, XEA25/114]
117. Pectines, fulcra: **0,** moderate to large; **1,** small; **2,** very small (vestigial); **?,** unknown. [PEA21/112, XEA25/115]
118. Pectines, median lamellae, count: **0,** 4; **1,** 5–8; **2,** 9–10; **3,** 11–15; **?,** unknown; **-,** inapplicable. [PEA21/113, 114, XEA25/116] Original male and female characters (PEA21/113, 114) fused into single unisex character

(XEA25/116) to minimize the effect of missing entries.

119. Pectines, tooth count: **0,** >20; **1,** 13–16; **2,** 9–12; **3,** 7 or 8; **4,** 5 or 6; **5,** 3 or 4; **?,** unknown. [PEA21/115, 116, XEA25/117] Original male and female characters (PEA21/115, 116) fused into single unisex character (XEA25/117) to minimize the effect of missing entries.
120. Pectinal teeth, peg sensillae, sockets: **0,** papillate; **1,** smooth; **?,** unknown. [PEA21/117, XEA25/118]
121. Pectinal teeth, peg sensillae, length and shape: **0,** short, barely protruding from sensilla socket, stout, subcylindrical basally, flattened and truncate distally; **1,** intermediate, protruding from sensillla socket stout, flattened and truncate distally; **2,** long, protruding from sensilla socket, cylindrical, tubular or bottle-shaped, and rounded distally; **?,** unknown. [PEA21/118, XEA25/119]
122. Pectinal teeth, peg sensilla, laterodistal processes: **0,** absent; **1,** present; **?,** unknown. [PEA21/119, XEA25/120]

Tergites

123. Post-tergites I–VI surfaces, macrosculpture: **0,** granular; **1,** smooth or nearly so; **?,** unknown. [PEA21/120, XEA25/121]

Sternites

124. Sternites VI and VII, ventral surface, macrosculpture (♂): **0,** smooth; **1,** granular; **?,** unknown [PEA21/121, XEA25/122]
125. Sternite VII, ventral surface, ventrosubmedian and ventrolateral carinae (adult ♂): **0,** well developed, costate; **1,** obsolete, granular; **2,** absent; **?,** unknown. [PEA21/122, XEA25/123]
126. Sternites III–VI, respiratory spiracles (stigmata), shape: **0,** long, slit-like; **1,** small, circular or oval; **?,** unknown. [L80/20 (part), S&F03.5/101, PEA21/123, XEA25/124]

Metasoma

127. Metasomal segments I–IV, dorsosubmedian and dorsolateral carinae, posterior granules size relative to preceding granules: **0,** similar; **1,** markedly larger and spiniform; **?,** unknown. [PEA21/124, XEA25/125]
128. Metasomal segment V, dorsolateral carinae, vertical development: **0,** distinct; **1,** obsolete; **?,** unknown. [PEA21/125, XEA25/126]
129. Metasomal segments I and II, median lateral carinae, longitudinal development: **0,** absent or obsolete (segments I and II); **1,** complete (segment I), partial, becoming obsolete anteriorly (segment II); **2,** complete (segments I and II); **?,** unknown. [PEA21/126, XEA25/127] The states in previous versions of this character were revised to accommodate a third state observed in the fossil taxa.
130. Metasomal segments III and IV, median lateral carinae, longitudinal development: **0,** absent or obsolete (segments III and IV); **1,** partial, becoming obsolete anteriorly (segment III), vestigial or absent (segment IV); **2,** complete (segments III and IV); **?,** unknown. [PEA21/127, XEA25/128] The states in previous versions of this character were revised to accommodate a third state observed in the fossil taxa.
131. Metasomal segment V, median lateral carinae, longitudinal development: **0,** absent or obsolete; **1,** partial; **2,** complete; **?,** unknown. [S&F03.5/86, PEA21/128, XEA25/129]
132. Metasomal segment I, ventrosubmedian carinae (♂): **0,** distinct; **1,** absent or obsolete; **?,** unknown. [PEA21/129, XEA25/130]
133. Metasomal segment I, ventrosubmedian carinae, vertical development: **0,** distinct; **1,** absent or obsolete; **?,** unknown. [PEA21/130, XEA25/131]
134. Metasomal segments II–IV, ventrosubmedian carinae, vertical development: **0,** distinct; **1,** absent or obsolete; **?,** unknown. [PEA21/131, XEA25/132]
135. Metasomal segment V, ventrosubmedian carinae, longitudinal development: **0,** com-

plete; **1,** partial; **2,** absent; **?,** unknown. [S&F03.5/84, PEA21/132, XEA25/133]

136. Metasomal segment V, ventrosubmedian carinae, posterior orientation: **0,** diverging; **1,** converging; **?,** unknown; **-,** inapplicable. [S&F03.5/84, PEA21/133, XEA25/134]
137. Metasomal segment V, ventromedian carina, vertical development: **0,** absent or obsolete; **1,** distinct; **?,** unknown. [PEA21/134, XEA25/135]

Telson

138. Telson vesicle, shape: **0,** globose; **1,** elongate; **?,** unknown. [PEA21/135, XEA25/136]
139. Telson vesicle surfaces, macrosculpture (♂): **0,** lateral and ventral surfaces with granular carinae; **1,** lateral and ventral surfaces smooth or nearly so; **?,** unknown. [PEA21/136, XEA25/137]
140. Telson vesicle surfaces, macrosculpture (♀): **0,** lateral and ventral surfaces with granular carinae; **1,** lateral and ventral surfaces smooth or nearly so; **?,** unknown. [PEA21/137, XEA25/138]
141. Telson vesicle, venom gland epithelium walls, folding: **0,** simple, unfolded; **1,** complex, folded; **?,** unknown. [S89/137, P00/113, S&S01/14, S&F03.5/99, PEA21/138, XEA25/139]
142. Telson subaculear tubercle: **0,** absent; **1,** obsolete, very small bump; **?,** unknown. [PEA21/139, XEA25/140]
143. Telson aculeus, length and shape: **0,** long, deeply curved; **1,** short, shallowly curved; **?,** unknown. [PEA21/140, XEA25/141]

APPENDIX 7

Primers used to generate DNA sequences from the 18S rDNA (18S), Internal Transcribed Spacer (ITS2), 28S rDNA (28S), 12S rDNA (12S), 16S rDNA (16S), and Cytochrome *c* Oxidase Subunit I (COI) loci for phylogenetic analysis of the relictual Asian scorpion family Pseudochactidae Gromov, 1998.

Primer	Sequence (5′–3′)	Other Name	Citation
18S			
18S1F	TACCTGGTTGATCCTGCCAGTAG		Giribet et al. (1996)
18S5R	CTTGGCAAATGCTTTCGC		Giribet et al. (1996)
18S3F	GTTCGATTCCGGAGAGGGA		Giribet et al. (1996)
18Sbi	GAGTCTCGTTCGTTATCGGA		Wheeler et al. (1993)
18Sa2.0	ATGGTTGCAAAGCTGAAAC		Wheeler et al. (1993)
18S9R	GATCCTTCCGCAGGTTCACCTAC		Giribet et al. (1996)
ITS2			
CAS18sF1	TACACACCGCCCGTCGCTACTA		Ji et al. (2003)
CAS5p8sB1d	ATGTGCGTTCRAAATGTCGATGTTCA		Ji et al. (2003)
CAS5p8dFc	TGAACATCGACATTTYGAACGCACAT		Ji et al. (2003)
CAS28sB1d-spid	TTCTTTTCCTCCGCTTATTTATATGCTTAA		Ji et al. (2003)
28S			
28S-RD1A	CCCSCGTAAYTTAGGCATAT		Nunn et al. (1996)
28S-RD4B	CCTTGGTCCGTGTTTCAAGAC		Nunn et al. (1996)
28S-RD3.2A	AGTACGTGAAACCGTTCASGGGT		Nunn et al. (1996)
28SB	TCGGAAGGAACCAGCTAC	D3B	Nunn et al. (1996)
28SA	GACCCGTCTTGAAGCACG	D3A	Nunn et al. (1996)
28SBout	CCCACAGCGCCAGTTCTGCTTACC		Prendini et al. (2005)
28S-RD4.5A	AAGTTTCCCTCAGGATAGCTG		Nunn et al. (1996)
28S-RD4.8A	ACCTATTCTCAAACTTTAAATGG		Nunn et al. (1996)
28S-RD7B1	GACTTCCCTTACCTACAT		Nunn et al. (1996)
12S			
12Sai	AAACTAGGATTAGATACCCTATTAT	SR-N-14588	Kocher et al. (1989)
12Sbi	AAGAGCGACGGGCGATGTGT	SR-J-14233	Kocher et al. (1989)
16S			
16Sa	CTCCGGTTTGAACTCAGATCA	LR-N-13398	Simon et al. (1991)
16Sb	CGCCTGTTTATCAAAAACAT	LR-J-12887	Simon et al. (1991)
COI			
LCO	GGTCAACAAATCATAAAGATATTGG	LCO1490-J-1514	Folmer et al. (1994)
COImodF	ATCATAAGGATATTGGGACTATGT		Bryson et al. (2013)
Nancy	CCCGGTAAAATTAAAATATAAACTTC	C1-N-2191	Harrison et al. (1987)
HCO	TAAACTTCAGGGTGACCAAAAAATCA	HCO2198-N-2175	Folmer et al. (1994)
HCOoutout	GTAAATATATGRTGDGCTC		Prendini et al. (2003)
CruzR	CATACCCAAAGARCCAAAAGG		Valdez-Cruz et al. (2004)
CI-J01718-spider	GGNGGATTTGGAAATTGRTTRGTTCC	C1-J-1718	Harrison et al. (1987)
CI-N02776-spider	GGATAATCAGAATANCGNCGAGG		Simon et al. (1991)
EXTB	CCTATTGAWARAACATARTGAAAATG		Simon et al. (1991)
EXTA	GAAGTTTATATTTTAATTTTACCTGG		Simon et al. (1991)

APPENDIX 8

Dispersal multiplier matrix, areas adjacent matrix, and areas allowed matrix used in BioGeoBEARS analysis of the relictual Asian scorpion family Pseudochactidae Gromov, 1998, indicating probability of dispersal events between areas (1, highest dispersal; 0.5, intermediate dispersal; and 0.0000001, little to no dispersal) and adjacent (1) and nonadjacent (0) areas, across two time periods. Letters correspond to five biogeographical regions: South China (A); Western Cimmeria, including only the Farah, Helmand, South-Central Pamirs, Karakorum and Band-e Bayan blocks (present-day Afghanistan and northern Pakistan) (B); Tajik and North Pamir blocks (northern Afghanistan and southern China, Uzbekistan and Tajikistan) (C); the Indochina block (D); Burma Terrane (E).

Dispersal	Time Period 1		A	B	C	D	E
Multiplier	0–55 Ma	A	1	0.0000001	0.0000001	1	0.5
Matrx		B	0.0000001	1	0.0000001	0.0000001	0.0000001
		C	0.0000001	0.0000001	1	0.0000001	0.0000001
		D	1	0.0000001	0.0000001	1	0.5
		E	0.5	0.0000001	0.0000001	0.5	1
	Time Period 2		A	B	C	D	E
	55–153 Ma	A	1	0.0000001	0.0000001	1	0.5
		B	0.0000001	1	1	0.0000001	0.0000001
		C	0.0000001	1	1	0.0000001	0.0000001
		D	1	0.0000001	0.0000001	1	0.5
		E	0.5	0.0000001	0.0000001	0.5	1
Areas	Time Period 1		A	B	C	D	E
Adjacent	0–55 Ma	A	1	0	0	1	1
Matrix		B	0	1	1	0	0
		C	0	1	1	0	0
		D	1	0	0	1	1
		E	1	0	0	1	1
	Time Period 2		A	B	C	D	E
	55–153 Ma	A	1	1	1	1	1
		B	1	1	1	1	1
		C	1	1	1	1	1
		D	1	1	1	1	1
		E	1	1	1	1	1
Areas	Time Period 1		A	B	C	D	E
Allowed	0–55 Ma	A	1	1	1	1	1
Matrix		B	1	1	1	1	1
		C	1	1	1	1	1
		D	1	1	1	1	1
		F	1	1	1	1	1
	Time Period 2		A	B	C	D	E
	55–153 Ma	A	1	1	1	1	1
		B	1	1	1	1	1
		C	1	1	1	1	1
		D	1	1	1	1	1
		F	1	1	1	1	1

All issues of *Novitates* and *Bulletin* are available on the web (https://digitallibrary.amnh.org/handle/2246/5). Order printed copies on the web from:

https://shop.amnh.org/books/scientific-publications.html

or via standard mail from:

American Museum of Natural History—Scientific Publications
Central Park West at 79th Street
New York, NY 10024

♾ This paper meets the requirements of ANSI/NISO Z39.48-1992 (permanence of paper).